

การสังเคราะห์แอนไอออนเซ็นเซอร์ที่มีสีย้อมอินทรีย์เป็นองค์ประกอบชนิดให้สัญญาณเคมีไฟฟ้า
และแสง



นายสมชาย แก้ววังชัย

สถาบันวิทยบริการ
จุฬาลงกรณ์มหาวิทยาลัย

วิทยานิพนธ์นี้เป็นส่วนหนึ่งของการศึกษาตามหลักสูตรปริญญาวิทยาศาสตรดุษฎีบัณฑิต

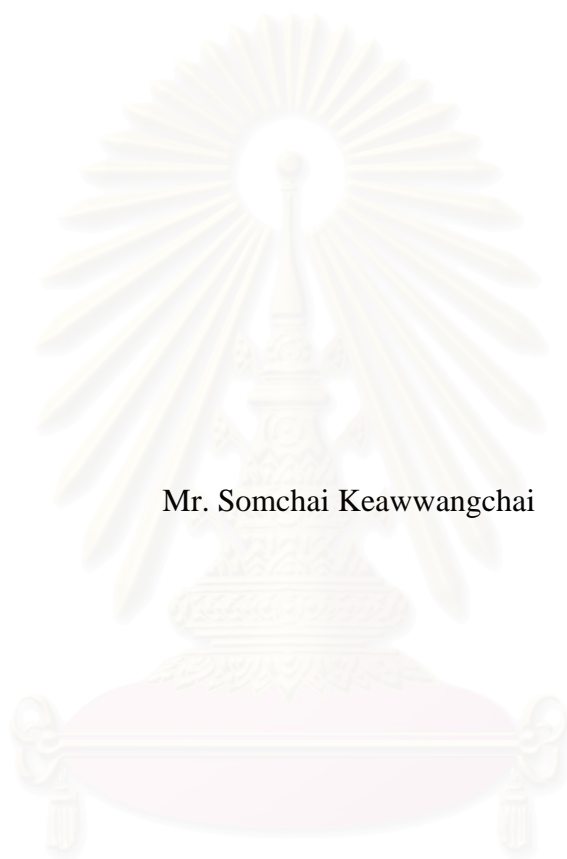
สาขาวิชาเคมี ภาควิชาเคมี

คณะวิทยาศาสตร์ จุฬาลงกรณ์มหาวิทยาลัย

ปีการศึกษา 2549

ลิขสิทธิ์ของจุฬาลงกรณ์มหาวิทยาลัย

SYNTHESIS OF ELECTROCHEMICAL AND OPTICAL ANION SENSORS
CONTAINING ORGANIC DYES



Mr. Somchai Keawwangchai

สถาบันวิทยบริการ
จุฬาลงกรณ์มหาวิทยาลัย

A Dissertation Submitted in Partial Fulfillment of the Requirements
for the Degree of Doctor of Philosophy Program in Chemistry

Department of Chemistry

Faculty of Science

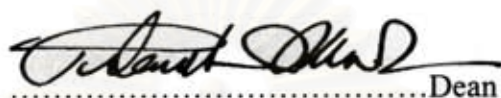
Chulalongkorn University

Academic Year 2006


Copyright of Chulalongkorn University

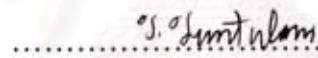
Thesis title SYNTHESIS OF ELECTROCHEMICAL AND OPTICAL
ANION SENSORS CONTAINING ORGANIC DYES
By Mr. Somchai Keawwangchai
Field of Study Chemistry
Thesis Advisor Associate Professor Thawatchai Tuntulani, Ph.D.

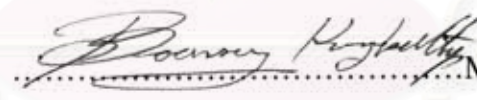
Accepted by the Faculty of Science, Chulalongkorn University in Partial
Fulfillment of the Requirements for the Doctoral Degree


.....Dean of the Faculty of Science
(Professor Piamsak Menasveta, Ph.D.)

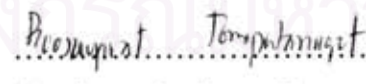
DISSERTATION COMMITTEE


.....Chairman
(Professor Sophon Reengsumran, Ph.D.)


..... Thesis Advisor
(Associate Professor Thawatchai Tuntulani, Ph.D.)


.....Member
(Associate Professor Boonsong Kongkathip, Ph.D.)


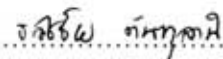

.....Member
(Associate Professor Orawon Chailapakul, Ph.D.)


.....Member
(Assistant Professor Boosayarat Tomapatanaget, Ph.D.)


.....Member
(Oravan Sanguanruang, Ph.D.)

นายสมชาย แก้ววงษ์ชัย : การสังเคราะห์แอนไอออนเซ็นเซอร์ที่มีสีย้อมอินทรีย์เป็นองค์ประกอบ ชนิดให้สัญญาณเคมีไฟฟ้าและแสง. (SYNTHESIS OF ELECTROCHEMICAL AND OPTICAL ANION SENSORS CONTAINING ORGANIC DYES) อ. ที่ปรึกษา : รศ. ดร. ธวัชชัย ตันกุลธานี, 132 หน้า.

งานวิจัยนี้ได้ทำการสังเคราะห์เซ็นเซอร์ระดับไมโครสตรักเจอร์ขึ้นจำนวนทั้งสิ้น 6 ตัว สำหรับตรวจการเกิดสารประกอบเชิงซ้อนแอนไอออนชนิดต่างๆ โดยใช้อนุพันธ์ของแอนทราซีนเป็นตัวให้สัญญาณและหมู่ไธโอยูเรียเป็นตัวรับแอนไอออน จากการศึกษาความจำเพาะของการเกิดสารประกอบเชิงซ้อนกับไดคาร์บอกซิเลตแอนไอออนชนิดต่างๆ โดยการไทเทรตด้วยเทคนิคโปรตอนนิวเคลียร์แมกเนติกเรโซแนนซ์ ที่ความเข้มข้น 10 มิลลิโมลาร์ในไดเมทิลซัลโฟลไซด์ พบว่าสารทั้งหมดเกิดสารประกอบเชิงซ้อนกับแอนไอออนในอัตราส่วน 1:1 โดยสาร L1 และ L4 เกิดสารประกอบเชิงซ้อนได้ดีที่สุดกับพิมิเลต สาร L3 และ L5 เกิดสารประกอบเชิงซ้อนกับกลูตาเรตได้ดีที่สุด และสาร L2 เกิดสารประกอบเชิงซ้อนกับซัคซิเนตได้ดีที่สุด นอกจากนี้ยังพบว่าสารทั้งหมดเกิดสารประกอบเชิงซ้อนกับมาโลเนตได้น้อยที่สุด ซึ่งสามารถสรุปได้ว่าค่าคงที่การรวมตัวขึ้นอยู่กับความยาวของไดคาร์บอกซิเลตแอนไอออน และระยะห่างระหว่างหมู่ไธโอยูเรีย และได้ทำการศึกษาผลของการเปลี่ยนแปลงสีจากการเกิดสารประกอบเชิงซ้อนกับไดคาร์บอกซิเลตแอนไอออนชนิดต่างๆ โดยการไทเทรตด้วยเทคนิคยูวีวิสิเบิลสเปกโตรโฟโตเมทรี พบว่าเมื่อเกิดสารประกอบเชิงซ้อนของลิแกนด์ทั้งหมด (0.02 มิลลิโมลาร์) กับไดคาร์บอกซิเลตแอนไอออนในตัวทำละลายไดเมทิลซัลโฟลไซด์ จะทำให้สีของสายละลายจางลงและค่าการดูดกลืนแสงของสารละลายลดลง จากนั้นนำไปคำนวณค่าคงที่การรวมตัวของสาร L1 กับแอนไอออนต่างๆ พบว่าเกิดสารประกอบเชิงซ้อนได้ดีที่สุดกับ อะดิเปต สาร L5 นั้นเกิดสารประกอบเชิงซ้อนกับออกซาเลตและพิมิเลตได้ดีพอกัน ขณะที่สาร L2, L3 และ L4 ไม่มีความจำเพาะกับแอนไอออนใดๆ นอกจากนี้ได้ทำการศึกษาการเกิดสารประกอบเชิงซ้อนของสาร L1, L3 และ L5 กับแอนไอออนต่างๆ โดยการไทเทรตด้วยเทคนิคฟลูออเรสเซนซ์ ซึ่งพบว่าการเติมแอนไอออนจะทำให้ค่าความเข้มของการฟลูออเรสเซนซ์ลดลง การศึกษาสมบัติทางเคมีไฟฟ้าของสาร L2 และ L4 โดยใช้เทคนิคไซคลิกโวลแทมเมทรี สามารถยืนยันได้ถึงผลของการเกิดสารประกอบเชิงซ้อน โดยพบว่าสารประกอบเชิงซ้อนของสาร L2 กับซัคซิเนต และสาร L4 กับอะดิเปตจะทำให้เกิดการเปลี่ยนแปลงของไซคลิกโวลแทมโมแกรมมากที่สุดนอกจากนี้ยังทำการศึกษาทางทฤษฎี ด้วยการคำนวณทางคอมพิวเตอร์ เพื่อหาโครงสร้างที่เสถียรและสมบัติต่างๆของสารและสารประกอบเชิงซ้อนกับแอนไอออนซึ่งสามารถนำมาใช้อธิบายและเปรียบเทียบผลที่เกิดขึ้นจากการทดลอง

ภาควิชา.....เคมี..... ลายมือชื่อนิสิต..... .....
 สาขาวิชา.....เคมี..... ลายมือชื่ออาจารย์ที่ปรึกษา..... .....
 ปีการศึกษา2549.....

4373840223 : MAJOR CHEMISTRY

KEY WORD: ANION SENSOR, THIOUREA, ANTHRACENE, DFT, NAKED EYE SENSOR, ONIOM, MP2

SOMCHAI KEAWWANGCHAI: SYNTHESIS OF ELECTROCHEMICAL AND OPTICAL ANION SENSORS CONTAINING ORGANIC DYES. THESIS ADVISOR: ASSOC. PROF. THAWATCHAI TUNTULANI, Ph.D., 132 pp.

Six chromo- and fluorogenic anion sensors have been synthesized by coupling the appropriate dithioisocyanate of anthracene derivatives with hexylamine in dichloromethane. The anthracene moieties acted as signaling units and thiourea moieties as binding sites. Anions binding properties of synthetic sensors have been studied by $^1\text{H-NMR}$ titration (10 mM in $\text{DMSO-}d_6$) and the 1:1 complexations were confirmed by Job's plots. Compounds L1 and L4 formed the most stable complexes with pimelate. Compounds L3 and L5 formed the most stable complexes with glutarate. Compound L2 formed the most stable complexes with succinate. Binding constants were, therefore, found to be strongly dependent on the chain length of dicarboxylate anions and the distance between thiourea groups. UV-vis titrations of all compounds (0.02 mM in DMSO) showed decreasing of maxima absorption intensity when successive addition of dicarboxylate anions. The $\log\beta_1$ results indicated that compounds L1 formed the most stable complex with adipate. Compound L5 showed strongest binding abilities with oxalate as well as pimelate. However, compounds L2, L3, and L4 did not show much difference in binding abilities toward any anion. The complexation between compounds L1, L3 and L5 and anions were also studied by fluorescence titration and showed the decreasing of fluorescence emission upon successive addition of anions. The electrochemical studies of compounds L2 and L4 by cyclic voltammetry confirmed the occurring of complexation. The electrochemistry of compound L2 changed dramatically in the presence of succinate. The complexation between compound L4 and adipate showed the most significant change in cyclic voltammograms. Optimized structures of all conformers of the synthesized compounds and anion binding structures were obtained using density functional theory (DFT) and ONIOM methods.

Department.....CHEMISTRY.....Student's signature.....*Somchai*

Field of study.....CHEMISTRY.....Advisor's signature.....*อ. ทวี ตันตูลานี*

Academic year2006.....

ACKNOWLEDGEMENTS

The accomplishment of this thesis can be attributed to the extensive support and assistance from my advisor, Associate Professor Dr. Thawatchai Tuntulani. I am grateful for his suggestions, assistance, encouragement, kindness, and personal friendship throughout my PhD career. Particular thanks are given to Dr. Philip A. Gale for offering the chance to do some part of my thesis at University of Southampton. I would like to thank Associate Professor Dr. Vithaya Ruangpornvisuti for his trainings, expert guidance and assistance in computation studies. I also thank Associate Professor Dr. Orawon Chailapakul, the Head of Electroanalytical Chemistry Research Group for offering excellent physical devices and ensuring that our synthesized compounds can find their practical use. In addition, I would like to thank Professor Dr. Sophon Roengsumran, Associate Professor Dr. Boonsong Kongkathip, Assistant Professor Dr. Boosayarat Tomapatanaget and Dr. Oravan Sanguanruang for their input, interest, valuable suggestions, comments and acting as thesis examiners.

This thesis would not be successful without kindness and helps of a number of people. First, I am grateful to the school of chemistry, Southampton University for my research experience and for allowing me to use some equipment such as an NMR machine. I would like to acknowledge the grant and funding supports provided by Mahasarakham University, the Royal Golden Jubilee (RGJ) grant from The Thailand Research Fund (PHD0090/2544).

I would like to express my appreciation to the former and the current staffs in Supramolecular Chemistry Research unit. I am also grateful to Dr. Sauwarux Fuangsawadi for her advice and precious suggestions in using SIRKO program for UV-vis titration experiments, Assistant Professor Dr. Boosayarat Tamapatanaget, Assistant Professor Dr. Nongnit Morakot, Mr. Neramit Morakot, Mr. Banchob Wannoo for valuable idea to solve problems arisen in my experiments.

My appreciation would be expressed to all of my friends and colleagues for their helps and encouragement throughout my study.

Finally, my love and thanks go to my family, especially my father, my mother my wife and my pretty daughter for their love, care, encouragement, kindness, financial support and other assistances throughout my life.

CONTENTS

	Page
ABSTARCT INTHAL.....	iv
ABSTRACT IN ENGLISH.....	v
ACKNOWLEDGEMENTS.....	vi
LIST OF ABBREVIATIONS AND SIGNS.....	xi
LIST OF FIGURES.....	xiii
LIST OF TABLES.....	xvi
LIST OF SCHEMES.....	xviii
CHAPTER I INTRODUCTION.....	1
1.1 Supramolecular chemistry.....	1
1.2 Anion Recognition.....	4
1.3 Neutral Hydrogen Bonding Receptors for Anions	6
1.4 Thiourea-Based Anion Receptor	7
1.5 Anion Sensors	8
1.6 Biological Process of dicarboxylate anions	9
1.7 Determination of Binding Constant by ¹ H NMR titration	9
1.8 Cyclic Voltammetry	11
1.9 Computational chemistry	13
1.9.1 Ab initio methods	15
1.9.2 Semiempirical methods	16
1.9.3 ONIOM method	17
1.9.4 Basis sets	17
1.9.5 Molecular properties	19
1.10 Literature Review	24
1.11 Scope of this research.....	29
CHAPTER II EXPERIMENTAL SECTION.....	30
2.1 General Procedures.....	30
2.1.1 Analytical Instrument.....	30
2.1.2 Materials.....	30

	Page
2.2 Synthesis.....	31
2.2.1 Preparation of 3,6-diisothiocyanatoacridine (2).....	31
2.2.2 Preparation of 3,6-di(hexylthioureido)acridine (L1).....	32
2.2.3 Preparation of 3,6-di(hexylthioureido)acridinium trifate (HL1).....	33
2.2.4 Preparation of 1,8-Diaminoanthracene-9,10-dione, (4).....	34
2.2.5 Preparation of 1,8-diisothiocyanatoanthracene-9,10-dione (5)...	35
2.2.6 Preparation of 1,8-Diaminoanthracene (6).	36
2.2.7 Preparation of 1,8-diisothiocyanatoanthracene (7).	37
2.2.8 Preparation of 1,8-di(hexylthioureido)anthracene-9,10-dione (L2)	38
2.2.9 Preparation of 1,8-di(hexylthioureido)anthracene (L3).	39
2.2.10 Preparation of 2,7-Dinitroanthracene-9,10-dione (9).....	40
2.2.11 Preparation of 2,7-Diaminoanthracene-9,10-dione (10).	41
2.2.12 Preparation of 2,7-diisothiocyanatoanthracene-9,10-dione (11)	42
2.2.13 Preparation of 2,7-Diaminoanthracene (12).	43
2.2.14 Preparation of 2,7-diisothiocyanatoanthracene (13).	44
2.2.15 Preparation of 1,8-di(hexylthioureido)anthracene-9,10-dione (L4).	45
2.2.16 Preparation of 1,8-di(hexylthioureido)anthracene (L5).	46
2.3 Preparation of tetrabutylammonium salts.....	47
2.4 Complexation studies.....	47
2.4.1 ¹ H-NMR titration studies for complexes of compound L1-L5 with anion guests	47
2.4.2 UV-vis titration studies for complexes of compound L1-L5 with anion guests	47
2.4.3 Anion complexation studies of compound L1-L5 by fluorescence titrations.....	48
2.5 Electrochemical studies.....	49
2.5.1 Apparatus.....	49
2.5.2 Cleaning procedure for electrode	50
2.5.3 Preparation of the main solution.....	51
2.5.4 CV measurements.....	51

	Page
2.6 Computations.....	51
CHAPTER III RESULTS AND DISSCUSSION.....	53
3.1 Synthesis of dihexylthiourea anthracene sensors.....	53
3.1.1 Synthesis and Characterization of compound L1 and HL1	53
3.1.2 Synthesis and Characterization of compound L2 and L3	55
3.1.3 Synthesis and Characterization of compound L4 and L5	58
3.2 Theoretical studies of synthetic compounds	59
3.2.1 Conformer, stability and protonation of compound L1 and HL1	59
3.2.2 Conformational and stability of compound L2 and L3	62
3.2.3 Conformational and stability of compound L4 and L5	63
3.2.4 Electronic structure of compound L1 and HL1	65
3.2.5 ¹ H NMR chemical shifts of compound L1 and HL1 species	68
3.2.6 FT-IR spectra of compound L1 and HL1 species	71
3.3 Investigation of binding ability	73
3.3.1 The complexation studies of synthetic compounds with various dicarboxylate anions by using ¹ H-NMR titrations	73
3.3.2 The complexation studies of synthetic compounds with various dicarboxylate anions by using UV-Vis titrations	87
3.3.3 The complexation studies of synthetic compounds with various anions by using fluorometric titrations	93
3.4 Electrochemical studies	96
3.4.1 Cyclic voltammograms of compound L2 in DMF	97
3.4.2 Electrochemical studies of compound L2 with various anions ...	99
3.4.3 Cyclic voltammograms of compound L4 in DMF	101
3.4.4 Electrochemical studies of compound L2 with various anions ...	102
CHAPTER IV CONCLUSION.....	105
REFERENCES.....	108
APPENDIX.....	114

VITAE.....	Page
	132



สถาบันวิทยบริการ
จุฬาลงกรณ์มหาวิทยาลัย

LIST OF ABBREVIATIONS AND SIGNS

°	Degree
δ	Chemical shift
°C	Degree Celsius
Δ	Delta
Å	Angstrom
au	Atomic unit
CV	Cyclic voltammetry
DFT	Density functional theory
E	Energy
eV	Electron Volt
equiv.	Equivalent
g	Gram
G	Gibbs free energy
¹ H-NMR	Proton Nuclear Magnetic Resonance
H	Enthalpy
HOMO	Highest Occupied Molecular Orbital
Hz	Hertz
<i>J</i>	Coupling constant
K	Kelvin
K _a	Association constant
kcal	Kilocalorie
LUMO	Lowest Unoccupied Molecular Orbital
M	Molar
mL	Milliliter
mmol	Millimole
mol	Mole
mp	Melting point
ONIOM	Our Own <i>N</i> -Layered Integrated Molecular Orbital and Molecular Mechanics
ppm	Part per million
RT	Room temperature
s, d, t, m	Splitting patterns of ¹ H-NMR (singlet, doublet, triplet and multiplet)

LIST OF FIGURES

Figure	Page
1.1 From molecular to supramolecular chemistry: molecules, supermolecules, molecular and supramolecular devices.....	1
1.2 Electrostatic interactions.....	2
1.3 π - π Stacking interactions.	2
1.4 Hydrophobic binding of organic guests in aqueous solution.....	4
1.5 Formation of hydrogen bonding in carboxylate bound urea or thiourea.....	7
1.6 Action of anionic sensor	8
1.7 The citric acid cycle	9
1.8 Cyclic voltammetry of a reversible process. Aqueous solution, 1.0 mol/m ³ Cd(II) in 100 mol/m ³ KCl, HMDE. Curve A, 20 mV/s; curve B, 50 mV/s; curve C, 100 mV/s; curve D, 200 mV/s. Initial scan cathodic .	12
1.9 Cyclic voltammetry. (A) Excitation signal; (B) response is obtained for a single reversible reduction when the voltage-time excitation signal extends considerably on both sides of the E^o for the reversible process..	12
1.10 Target molecule structures of anthracene derivatives containing thiourea (L1-L5).....	29
3.1 B3LYP/6-31G(d)-optimized structures of 3,9-di (hexylthioureido) acridine conformers (a) L1a , (b) L1b and (c) L1c , and their protonated forms (d) HL1a ⁺ , (e) HL1b ⁺ and (f) HL1c ⁺ left and right figures are front and top views of their molecular structures, respectively	60
3.2 B3LYP/6-31G(d)-optimized structures of L2 and L3 conformer (a) L2 and (b) L3 Left and right figures are front and top views of their molecular structures, respectively	62
3.3 B3LYP/6-31G(d)-optimized structures of 2,7-di(hexylthioureido) anthracene-9,10-dione (L4) conformers (a) L4a , (b) L4b and (c) L4c . Left and right figures are front and top views of their molecular structures, respectively	64

Figure	Page
3.4 B3LYP/6-31G(d)-optimized structures of 2,7-di(hexylthioureido) anthracene conformers (a) L5a , (b) L5b and (c) L5c left and right figures are front and top views of their molecular structures, respectively	65
3.5 Atomic labeling of the 3,9-di(hexylthioureido)acridine	66
3.6 The B3LYP/6-31G(d)-computed molecular orbitals contoured at an iso-surface value of 0.05 a.u. for LUMO and HOMO of conformers (a) L1a , (b) L1b , (c) L1c , (d) HL1a ⁺ , (e) HL1b ⁺ and (f) HL1c ⁺	67
3.7 Electronic potential surface (in a.u.) presented over electronic isodensity $\rho = 0.05 \text{ eA}^{-3}$ for (a) L1a , $V_s=31.5436$, (b) L1b , $V_s=87.5226$, (c) L1c , $V_s=63.9896$, (d) HL1a ⁺ , $V_s=18.3433$, (e) HL1b ⁺ , $V_s=45.3886$ and (f) HL1c ⁺ , $V_s=101.865$	68
3.8 Proton chemical shifts of the measured and B3LYP/6-31G(d)-computed ¹ H-NMR (in parenthesis) of the most stable structure of (a) the neutral and (b) protonated forms of 3,9-di (hexylthioureido) acridine conformers. The chemical shifts are in ppm referenced to the TMS standard	70
3.9 FT-IR spectra of the (a) neutral and (b) protonated forms of L1 Top and bottom are the measured and computed infrared spectra, respectively. The computed IR spectra are of the most stable species, L1a and HL1c ⁺	71
3.10 ¹ H-NMR spectra of L1 and glutarate in DMSO- <i>d</i> ₆ with 400 MHz.	76
3.11 Titration curves between L1 (NH _A) with various dicarboxylate anions in DMSO- <i>d</i> ₆	78
3.12 Titration curves between L1 (NH _B) with various dicarboxylate anions in DMSO- <i>d</i> ₆	79
3.13 Titration curves between L2 (NH _A) with various dicarboxylate anions in DMSO- <i>d</i> ₆	79
3.14 Titration curves between L2 (NH _B) with various dicarboxylate anions in DMSO- <i>d</i> ₆	80
3.15 Titration curves between L3 (NH _A) with various dicarboxylate anions in DMSO- <i>d</i> ₆	80

Figure	Page
3.16 Titration curves between L3 (NH_B) with various dicarboxylate anions in DMSO- d_6	81
3.17 Titration curves between L4 (NH_A) with various dicarboxylate anions in DMSO- d_6	81
3.18 Titration curves between L4 (NH_B) with various dicarboxylate anions in DMSO- d_6	82
3.19 Titration curves between L5 (NH_A) with various dicarboxylate anions in DMSO- d_6	82
3.20 Titration curves between L5 (NH_B) with various dicarboxylate anions in DMSO- d_6	83
3.21 The Job's plot of compound L2 (NH_A) with succinate.....	83
3.22 B3LYP/6-31G(d)-optimized structures for the complex between L1 and L4 with pimelate.	85
3.23 B3LYP/6-31G(d)-optimized structures for the complex between L5 with adipate (a) and malonate (b).....	87
3.24 UV-vis titration spectra of compound L1 with Oxalate in DMSO ($[L1] = 2.0 \times 10^{-5} M$, $[oxalate] = 0-30$ equiv.). Insert show the mole ratio plot.....	88
3.25 UV-vis titration spectra of compound L2 with Oxalate in DMSO ($[L2] = 2.0 \times 10^{-5} M$, $[oxalate] = 0-30$ equiv.). Insert show the mole ratio plot.....	88
3.26 UV-vis titration spectra of compound L3 with Oxalate in DMSO ($[L3] = 2.0 \times 10^{-5} M$, $[oxalate] = 0-30$ equiv.). Insert show the mole ratio plot.....	89
3.27 UV-vis titration spectra of compound L4 with Oxalate in DMSO ($[L4] = 2.0 \times 10^{-5} M$, $[oxalate] = 0-30$ equiv.). Insert show the mole ratio plot.....	90
3.28 UV-vis titration spectra of compound L5 with Oxalate in DMSO ($[L5] = 2.0 \times 10^{-5} M$, $[oxalate] = 0-30$ equiv.). Insert show the mole ratio plot.....	90
3.29 The selectivity of synthetic compounds toward anions	93

Figure	Page
3.30 The absorption and the emission spectra of fluoroionophore L1 in DMSO	94
3.31 mission spectra of L1 ($2 \times 10^{-5} \text{M}$) was quenched by HSO_4^- ($\lambda_{\text{ex}} = 322 \text{ nm}$) in DMSO	94
3.32 The absorption and the emission spectra of fluoroionophore L3 in DMSO	95
3.33 The absorption and the emission spectra of fluoroionophore L5 in DMSO	95
3.34 Cyclic voltammograms of compound L2 with various scan rates	97
3.35 Plots of currents and square root of scan rates ($v^{1/2}$) for L2	98
3.36 Cyclic voltammograms of compound L2 upon addition 2 equiv. of dicarboxylate anions	100
3.37 Cyclic voltammograms of compound L2 upon addition of succinate	101
3.38 Cyclic voltammograms of compound L4 with various scan rates	102
3.39 Plots of currents and square root of scan rates ($v^{1/2}$) for L4	103
3.40 Cyclic voltammograms of compound L4 upon addition 2 equiv. of dicarboxylate anions	104
3.41 Cyclic voltammograms of compound L2 upon addition of succinate	105

LIST OF TABLES

Table	Page
1.1 Properties of hydrogen bonded interactions.....	3
1.2 Comparison of the radius (Å) of anions and cations.....	5
2.1 Amounts of tetrabutylammonium salts that used in anion complexation studies by UV-Vis titrations.....	48
2.2 The concentration of anions that used in anion complexation studies by UV-Vis titrations.....	49
2.3 The concentration of anions that used in anion complexation studies with ligand L3 and L5 for fluorescence titrations.....	50
3.1 Relative energies of 3,9-di(hexylthioureido)acridine conformers and their protonated conformers computed at various levels of theory	61
3.2 Reaction energies and thermodynamic properties of the protonation of compound L1 conformers computed at two different levels of theory	62
3.3 Reaction energies of compound L4 and L5 conformers computed at two different levels of theory	64
3.4 The E_{HOMO} , E_{LUMO} and frontier molecular orbital energy gap, $\Delta E_{\text{HOMO-LUMO}}$ of the 3,9-di(hexylthioureido)acridine conformers and their corresponding protonated forms computed at the B3LYP/6- 31G(d) level of theory	66
3.5 ^1H NMR chemical shifts for the 3,9-di(hexylthioureido)acridine conformers and their corresponding protonated forms	69
3.6 Selected wave numbers (cm^{-1}) and their corresponding intensities of the B3LYP/6-31G(d)-computed and observed IR vibration modes for the neutral and protonated species of 3,9-di(hexylthioureido)acridine. The computed IR vibration frequencies were scaled by 0.9614	72
3.7 Donor numbers determined calorimetrically in dilute 1,2- dichloroethane solution at room temperature	74
3.8 Acceptor numbers which are determined ^{31}P -NMR spectroscopically at 25 °C	75

Table	Page
3.9 $^1\text{H-NMR}$ chemical shifts (ppm) for all compounds (in $\text{DMSO-}d_6$) in the absence and presence of 1 equiv. of dicarboxylate anions	77
3.10 Binding constants of compounds L1-L5 [0.01 M] toward various dicarboxylate anions calculated from thiourea NH proton chemical shifts by WinEQNMR program	84
3.11 Average binding constants of compounds L1-L5 [0.01 M] toward various dicarboxylate anions	84
3.12 Binding constants of synthetic compounds toward various dicarboxylate anions calculated from UV-vis titration by SPECFIT32 program	92
3.13 The characteristic values of compounds L2 and L4	103



สถาบันวิทยบริการ
จุฬาลงกรณ์มหาวิทยาลัย

LIST OF SCHEMES

Scheme		Page
3.1	Possible synthetic pathways of 3,6-di(hexylthiouredo)acridine (L1)... .	54
3.2	Synthetic pathways of 3,6-di(hexylthiouredo)acridine (L1) and protonate form HL1	54
3.3	Synthetic pathways of sensor L2 and sensor L3	56
3.4	Synthetic pathways of sensor L4 and sensor L5	58
3.5	The reduction of anthraquinone processes	96



สถาบันวิทยบริการ
จุฬาลงกรณ์มหาวิทยาลัย

CHAPTER I

INTRODUCTION

1.1 Supramolecular Chemistry

Supramolecular chemistry is a multi-disciplinary field. The concept and the term of supramolecular chemistry were introduced in 1978 as a development and generalization of earlier work.⁽¹⁻³⁾ The field of supramolecular chemistry has been defined in words 'Just as there is a field of *molecular chemistry* based on the covalent bond, there is a field of *supramolecular chemistry*, the chemistry of molecular assemblies and of the intermolecular bond' also as 'chemistry beyond the molecule' by Jean-Marie Lehn (Figure 1.1).⁽⁴⁻⁵⁾

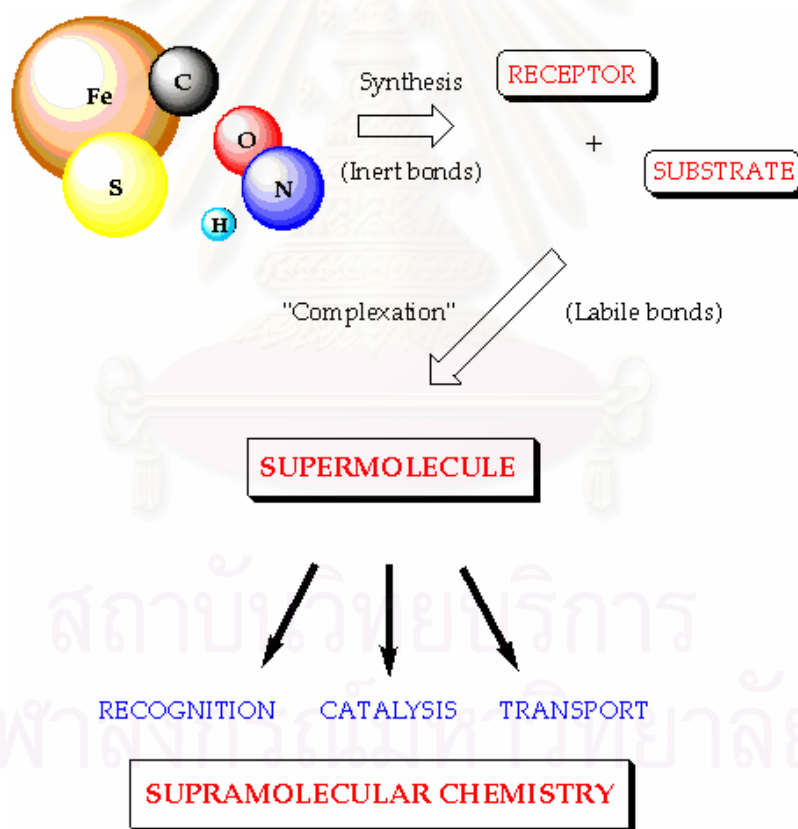


Figure 1.1 From molecular to supramolecular chemistry: molecules, supermolecules, molecular and supramolecular devices.

This field involves investigating new molecular systems in which the most important feature is that the compounds are held together reversibly by intermolecular forces, not by covalent bonds. These non-covalent interactions include⁽⁶⁾

I) Electrostatic interactions (ion-ion, ion-dipole and dipole-dipole) which are based on the Coulombic attraction between opposite charges (Figure 1.2). Bond energy are in the ranges $100\text{-}350\text{ kJ mol}^{-1}$, $50\text{-}200\text{ kJ mol}^{-1}$ and $5\text{-}50\text{ kJ mol}^{-1}$ for ion-ion, ion-dipole and dipole-dipole interactions respectively.

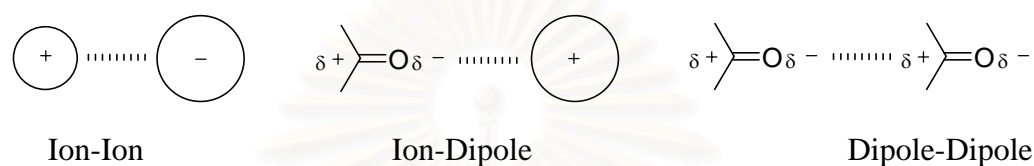


Figure 1.2: Electrostatic interactions.

II) Hydrogen bonds ($4\text{-}120\text{ kJ mol}^{-1}$) which may be regarded as a particular kind of dipole-dipole interaction in which hydrogen atom attached to an electronegative atom (or electron withdrawing group) interacts with a neighbouring dipole on an adjacent molecule or functional group. Because of its relatively strong and highly directional nature, hydrogen bonding has been described as the ‘masterkey interaction in supramolecular chemistry’.⁽⁷⁾ Some general parameters of the hydrogen bond interaction are shown in Table 1.1.

III) π - π Stacking interactions ($0\text{-}50\text{ kJ mol}^{-1}$) occur between aromatic rings, often in situations where one is relatively electron rich and one is electron poor. There are two general types of π -stacking: face-to-face and edge-to-face (Figure 1.3), although a wide variety of intermediate geometries are known.

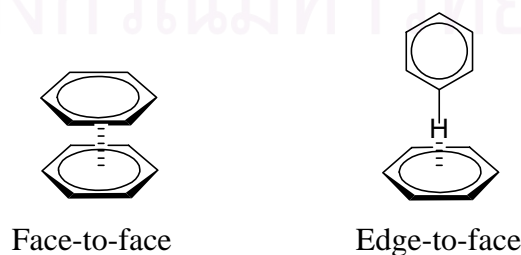


Figure 1.3: π - π Stacking interactions.

Table 1.1 Properties of hydrogen bonded interactions.

	Strong	Moderate	Weak
A-H...B interaction	Mainly covalent	Mainly electrostatic	Electrostatic
Bond energy (kJ.mol ⁻¹)	60-120	16-60	<12
Bond lengths (Å)			
H...B	1.2-1.5	1.5-2.2	2.2-3.2
A...B	2.2-2.5	2.5-3.2	3.2-4.0
Bond angles (°)	175-180	130-180	90-150
Relative IR vibration shift (stretching symmetrical mode, cm ⁻¹)	25%	10-25%	<10%
¹ H NMR chemical shift downfield (ppm)	14-22	<14	?
Example	Gas phase dimers with strong acid/bases HF complexes	Acids Biological molecules	O-H...π hydrogen bonds C-H hydrogen bonds

IV) Dispersion and induction forces (van der Waals forces) occur from the polarisation of an electron cloud by the proximity of an adjacent nucleus, resulting in a weak electrostatic attraction (<5 kJ mol⁻¹).

V) Hydrophobic (or solvatophobic) effects are the specific driving force for the association of non-polar hosts and guests in aqueous solution and may be divided into two energetic components: enthalpic and entropic. The enthalpic hydrophobic effect involves the stabilisation of water molecules that are driven from a host cavity upon guest binding. Because the host's cavities are often hydrophobic, intracavity water does not interact strongly with the cavity wall and is therefore of high energy. Upon release into the bulk solvent, it is stabilised by interactions with other water molecules. The entropic hydrophobic effect arises from the fact that presence of two (often organic) molecules in solution (host and guest) creates two 'holes' in the structure of bulk water. Combining

host and guest to form a complex results in less disruption to the solvent structure and increasing an entropic (resulting in a lowering of overall free energy) as shown in Figure 1.4.⁽⁸⁾

These forces from above can be used individually, but they normally are used in concert to maximize the selectivity and tunability of the new receptor and also increase the strength of the complex formed.

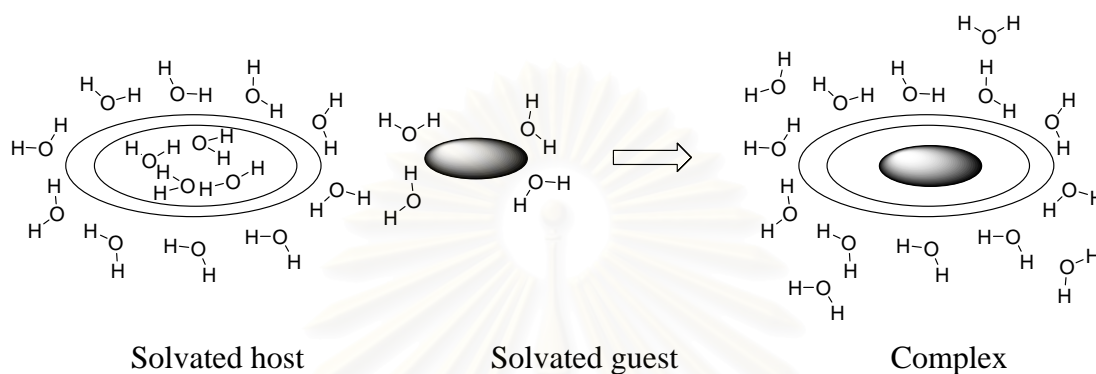


Figure 1.4: Hydrophobic binding of organic guests in aqueous solution.

1.2 Anion Recognition

Anion recognition is classified as a sub-set of supramolecular chemistry. The design of anion receptors is particularly challenging.⁽⁹⁾ There are a number of reasons for this. Anions are relatively large and therefore have lower charge densities than isoelectronic cations. For example, F^- is larger than Na^+ (Table 1.2).⁽¹⁰⁾ Hence electrostatic interactions are weaker.

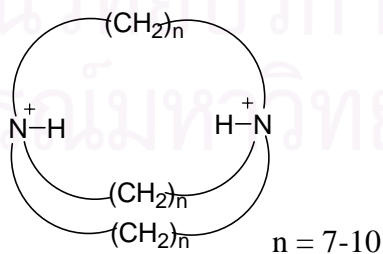
Anions may be sensitive to pH (becoming protonated at low pH and so losing their negative charge). Thus receptors must function within the optimum pH range of their target anion. Anions exhibit a wide range of geometries such as spherical (halides), linear (N_3^- , CN^- , SCN^- , OH^-), trigonal planar (CO_3^{2-} , NO_3^-), tetrahedral (PO_4^{3-} , VO_4^{3-} , SO_4^{2-} , MnO_4^{2-} , SeO_4^{2-} , MnO_4^-), octahedral [$Fe(CN)_6$] $^{3-}$, [$Co(CN)_6$] $^{3-}$) as well as more complex shapes as in the case of biologically important anions. Therefore, a higher degree of design may be required to make receptors complementary to their anionic guest. Solvation is another factor to consider. Electrostatic interactions generally dominate in anion solvation, and hydroxylic solvents in particular can form strong hydrogen bonds with anions. A potential anion receptor must therefore effectively compete with the solvent environment in which the anion-recognition event takes place.

The Hofmeister series,⁽¹¹⁾ which orders anions by their hydrophobicity, shows that hydrophobic anions are generally bound more strongly in hydrophobic binding sites.

Table 1.2 Comparison of the radius (Å) of anions and cations.

Anion	Radius (Å)	Cation	Radius (Å)
F ⁻	1.33	Li ⁺	0.69
Cl ⁻	1.81	Na ⁺	1.02
Br ⁻	1.95	K ⁺	1.38
I ⁻	2.16	Cs ⁺	1.70
SO ₄ ²⁻	2.30	Ca ²⁺	1.00
PO ₄ ³⁻	2.38	Zn ²⁺	0.75
H ₂ PO ₄ ⁻	2.00	Al ³⁺	0.53
Na ⁻	2.2	La ³⁺	1.05
Cs ⁻	3.5	NH ₄ ⁺	1.48

By contrast with supramolecular cation coordination chemistry which was first realized through the pioneering work of Pedersen⁽¹²⁾ on crown ethers and work of Lehn⁽¹³⁾ on cryptands, three-dimensional cation receptors, in the late 1960s, the coordination chemistry of anions has historically received little attention (with a few notable exceptions) after Park and Simmons reported the first synthetic organic ligands of the bicyclic diammonium type **1**, named ‘katapinate’, displaying halide complexation.⁽¹⁴⁾



It has only been in the last twenty five years that sustained effort has been applied to the problems inherent in binding anions.⁽¹⁵⁾ However, recent developments in the area of anion coordination have produced a variety of new selective complexation agents for

anionic guests.⁽¹⁶⁻¹⁸⁾ The great variety of anionic species and their importance in several areas such as biology,⁽¹⁹⁻²⁰⁾ the environment,⁽²¹⁾ catalysis⁽²²⁾ and in potential medical applications⁽²³⁾ is responsible for the fact that interest in anion coordination has becoming more widespread.

1.3 Neutral Hydrogen Bonding Receptors for Anions

The design and synthesis of neutral anion receptors have been a subject of current interest in host-guest chemistry due to their possible applications to ion sensors such as ion-selective electrodes and optodes. The synthetic anion receptors can be actually divided into two classes: positively charged and uncharged receptors.⁽²⁴⁾ Many receptors for anion substrates reported in the first period are charged molecules for example polyammonium receptors, guanidinium based receptors, cobalticinium and ferrocinium based receptors. The particularly important anion receptor is neutral hydrogen bonding receptors, which show higher selectivity, although they are able to operate only in apolar non-competing media. Furthermore, the neutral receptor must compete with solution ion-pairing of guest leading to the lower sensitivity.

In nature, neutral anion binding proteins are known to bind anions only *via* hydrogen bonding interactions⁽²⁵⁻²⁶⁾ which are the most important of all noncovalent bond types in biochemistry. Hydrogen bonds play an essential role in the formation of biological macromolecules such as the globular proteins and the DNA double helix and in the mechanism of enzyme-substrate recognition. Additionally, phosphate or sulfate binding proteins are naturally known examples that bind anions strongly and selectively *via* neutral proton-donor groups using the main chain protein *NH*-groups. Therefore, the formation of hydrogen bonds as a driving force of the molecular recognition has also been widely used in artificial receptors.⁽²⁷⁾

Hydrogen bonds are in general significantly weaker than electrostatic interactions when the corresponding carboxylate anions are involved. The former interaction may become a dominating force in the association process if several hydrogen bond donor and acceptor sites act concertedly; for instance, the carboxylate binding pocket of the vancomycin group antibiotics in nature.⁽²⁸⁻²⁹⁾ This implies that hydrogen bonding is one of the most important recognition elements in anion sensing. Thus, the design and synthesis of hydrogen bonding receptors for biologically and/or chemically important anions are of current interest.⁽³⁰⁻³¹⁾

The relatively strong hydrogen bonding of urea and thiourea groups has been used in the development of neutral anion receptors, because the hydrogen bond is directional in character, and correct orientation of the hydrogen bond donors can provide selective anion recognition. Urea and thiourea are particularly good hydrogen bond donors and are excellent receptors for anions such as carboxylate *via* the formation of two hydrogen bonds (Figure 1.5).



Figure 1.5. Formation of hydrogen bonding in carboxylate bound urea or thiourea.

In general, thiourea derivatives show stronger anion binding ability due to stronger hydrogen-bond donor capability than that of the corresponding ureas because of the higher acidity of the former.⁽³²⁾ The higher acidity of the thiourea hydrogens dominates the weaker hydrogen bond accepting ability of sulfur as compare to oxygen, unlikely to interfere in conformational or complexing studies involving other strong acceptor centers.⁽³³⁻³⁴⁾

1.4 Thiourea-Based Anion Receptor

In recent years, a number of molecules possessing thiourea functional groups have been designed as neutral receptors for various anions. Molecular recognition is achieved by establishing multiple hydrogen bonds with the relatively acidic *NH*- protons of these groups which are located in a well-defined position and direction with complementary acceptor groups in a specific and predictable manner. The potential for establishing highly ordered hydrogen bond networks with these functional groups is also used to construct supramolecular structures both in solution⁽³⁵⁻³⁶⁾ and in solid state.⁽³⁷⁻³⁸⁾ Several receptors contain thiourea functional groups with suitable spacers such as benzene and cyclohexene are particularly useful in the construction of neutral hydrogen bonding receptors.

1.5 Anion Sensors

The field of molecular recognition association with signaling of reversible anion binding using synthetic sensors has witnessed increasing popularity in recent years.⁽³⁹⁾ Such systems generally contain some combination of substrate recognition functionality (receptor) and signaling unit, either directly linked or appropriately associated in a noncovalent manner. The most common modes of signal transduction typically involve electrochemical or optical changes in the sensor incurred by association of the analyte with the receptor. Figure 1.6 illustrates the mechanism of anion sensor.



Figure 1.6 Action of anionic sensor

Electrochemical-based sensing has proved a popular method of signaling analyte recognition. The majority of electrochemical-based sensors employ transition metals or Lanthanides for both analyte binding and electrochemical signaling through changes in metal redox potentials upon anion-receptor complexation.⁽⁴⁰⁾

Optical signal of anion recognition typically involves quenching or enhancing of a chromophore's absorption⁽⁴¹⁾ or a fluorophore's fluorescence emission⁽⁴²⁻⁴⁵⁾ upon proximal association of the analyte. While the utilities of these approaches are becoming increasingly appreciated in terms of both qualitative and quantitative analysis, the number of optical signaling sensors available at present for anionic substrates remains quite limited. Of particular interest in this regard are "colorimetric anion sensors" species that would allow the so-called "naked-eye" detection of anions without resort to any spectroscopy instrumentation.

1.6 Biological Process of dicarboxylate anions

In a living cell, dicarboxylates are essential components of numerous metabolic processes, including for instance, the citric acid cycle⁽⁴⁶⁾ (known as Krebs cycle). Dicarboxylates such as succinate, fumarate, oxaloacetate, α -ketoglutarate and malate are importance intermediates for generating ATP⁴⁰ (adenosine triphosphate) in the citric acid cycle.

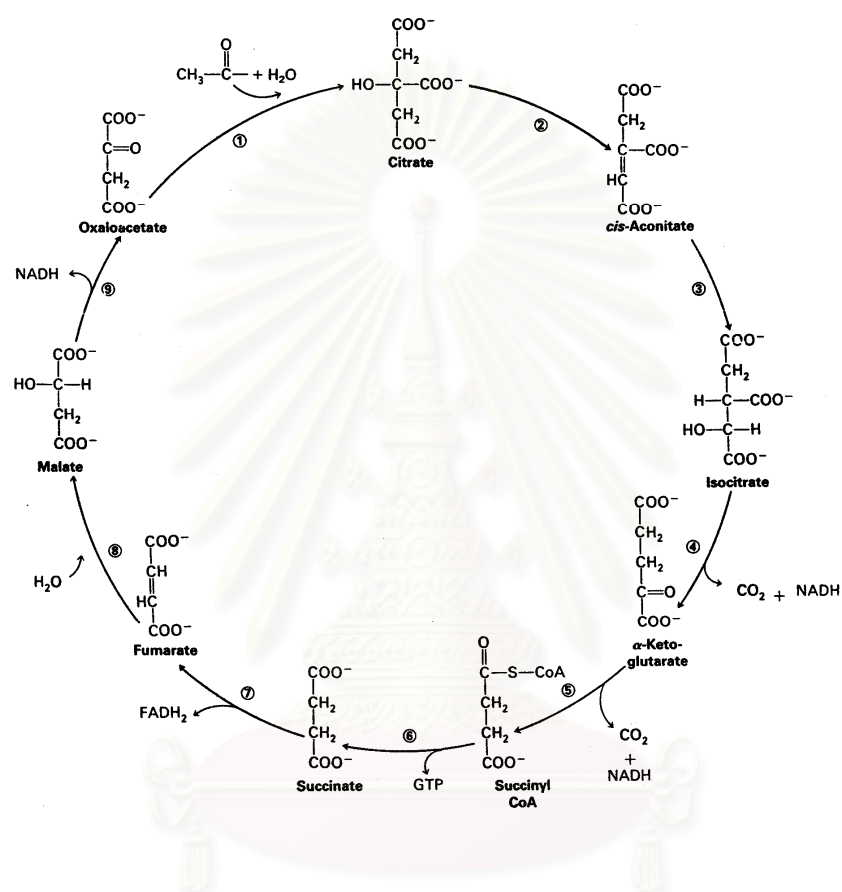


Figure 1.7 The citric acid cycle.

1.7 Determination of Binding Constant by ^1H NMR Titration⁽⁴⁷⁻⁴⁸⁾

In the viewpoint of molecular recognition systems, the weak chemical interaction is amplified, integrated and converted to physical signal that can readily read out and record. This data are related to complexation process. There are several methodologies to determine binding constant such as UV-VIS spectroscopy, NMR spectroscopy, bomb calorimeter, electrochemical instrument and fluorescence depending on the molecular design.

^1H -NMR titration is one of the most useful techniques available to chemists for the investigation of dynamic molecular processes. Appeared NMR spectra are basically treated to display a qualitative description of reversible dynamic processes. This topic is often introduced with a discussion of simple two-site exchange systems; slow and fast exchange. It is stated that the spectrum consists of two signals under “*slow-exchange*” conditions. The binding constant can be evaluated by ratio of integration of the NMR signals for free and bound hosts. The bound and free molecules give rise to discrete NMR signals that can be integrated to determine $[\text{G}]$ and $[\text{HG}]$ directly and association constant (β_i) finally. Occasionally, observation of slow chemical exchange is classified as a moderately tightly bound host-guest system ($\beta_i \approx 10^3$). The exchange rate of ligand does not necessarily correlate with the binding constant. There is just one signal at the population-averages chemical shift under “*fast-exchange*” conditions. Most of the host-guest equilibria are fast on the NMR time scale. Basically, the association constant (β_i) of either slow or fast exchange process is represented by the following equation.

$$\beta_i = [\text{H}\cdot\text{G}_i]/[\text{H}][\text{G}]^i$$

Generally, the Job’s plot of chemical induced shift based on a series of solution containing both host and guest in varying proportions is essential to perform before any determination of β_i . The total concentration in each solution ($[\text{H}]_0 + [\text{G}]_0$) is constant in this continuous variation analysis. Mole ratios between a host and a guest are in the range of $0 > [\text{H}]_0/([\text{H}]_0 + [\text{G}]_0) < 1$.

In a typical fast exchange NMR titration experiment, a small aliquot of a guest may be added to a known concentration solution of a host in a deuterated solvent and the NMR spectrum is monitored as a function of the guest concentration or a host to guest ratio. Commonly, changes in chemical shift ($\Delta\delta$) are noted for various atomic nuclei attributed to the influence of guest binding on their magnetic environments. As a result, two kinds of information are gained. Firstly, the location of nuclei most affected may give qualitative information about the selectivity of guest binding. More importantly, the shape of the titration curve plot of chemical induced shift (δ or $\Delta\delta$) against added guest concentration gives quantitative information about the binding constant. Such titration curves are often analyzed by modern curve fitting procedure; for instance, EQNMR, EMUL/MULTIFIT or NMRTIT. Although several methods have been developed to determine the association constant, curve fitting approaches are more widely used. Clear

advantages of curve fitting treatments are that the experimental conditions are less constrained and more complex binding models (non 1:1 stoichiometry) can be accommodated. NMR based determinations of β_i are usually only reliable for association constants in the range of 10 - 10^4 M^{-1} . To maximize the reliability of NMR titration data, the experiment needs to be designed. The binding curve should cover a large range of percentage bound (ideally from 20 to 80%). For $\beta_i \approx 1$ - 5 M^{-1} , $\Delta\delta_{\max}$ cannot be accurately measured. On the other hand, the graph of $\Delta\delta$ against $[H]_0/[G]_0$ become too steep to determine within convenient measurement times in the case of $\beta_i \approx 10^5$ M^{-1} . A more dilution condition probing by a more sensitive NMR will slightly extend the range of measurable association constants.

1.8 Cyclic Voltammetry⁽⁴⁹⁻⁵⁰⁾

Cyclic voltammetry is the most widely use technique for acquiring qualitative information about electrochemical reactions. The power of cyclic voltammetry results from its ability to rapidly provide considerable information on the thermodynamics of redox processes and the kinetics of heterogeneous electron transfer reactions, and on coupled chemical reactions or adsorption processes. Cyclic voltammetry is often the first experiment performed in an electroanalytical study. In particular, it offers a rapid location of redox potentials of the electroactive species, and convenient evaluation of the effect of media upon the redox process.

Rapid-voltage-scan technique in which the direction of voltage scan is reversed are called cyclic technique. In this technique, a ramp is applied over the full voltage-scan range and then reversed so that a descending ramp returns, almost invariably to the original potential. The scan rate in the forward and reverse directions is normally the same, so that the excitation waveform is actually an isosceles triangle. (Figure 1.8) Cyclic voltammetry can be used in single-cycle (Figure 1.9) or in multicycle modes, depending upon the electrode, the reaction in question, and the information sought. In most cases the first and later scans are not identical.

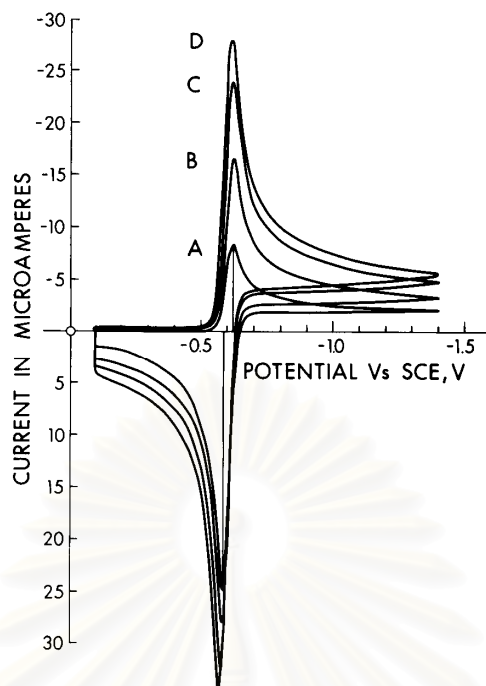


Figure 1.8: Cyclic voltammetry of a quasi-reversible process. Aqueous solution, $1.0 \text{ mol/m}^3 \text{ Cd(II)}$ in $100 \text{ mol/m}^3 \text{ KCl}$, HMDE. Curve A, 20 mV/s ; curve B, 50 mV/s ; curve C, 100 mV/s ; curve D, 200 mV/s . Initial scan cathodic

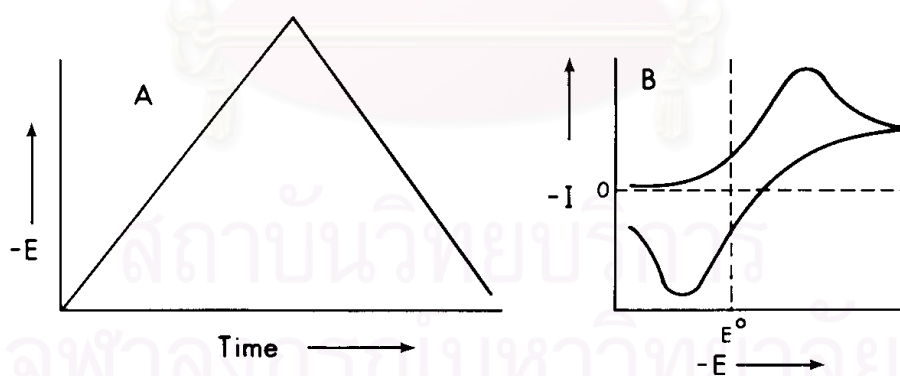


Figure 1.9: Cyclic voltammetry. (A) Excitation signal; (B) response is obtained for a single reversible reduction when the voltage-time excitation signal extends considerably on both sides of the E^o for the reversible process.

The important parameters of a cyclic voltammogram are: anodic peak current (i_{pa}) and anodic peak potential (E_{pa}) taken from the peak position of anodic current and the respective parameters i_{pc} and E_{pc} from the peak position of cathodic current. If the redox couple is reversible the half-wave potential is centered between E_{pa} and E_{pc} .

$$E_{1/2} = (E_{pa} + E_{pc}) / 2$$

Frequently $E_{1/2}$ calculated in this way is considered simply as the formal potential because the diffusion coefficients have a small effect. The difference between peak potentials is related with the number of electrons transferred in the electrode reaction.³⁶

$$\Delta E_p = E_{pa} - E_{pc} = 0.059 / n$$

Electrochemical ‘reversibility’ means that the electrode reaction is fast enough to maintain the surface concentrations of the oxidized and reduced forms at equilibrium with each other, which is an indispensable condition for the validity of the Nernst equation.

1.9 Computational Chemistry⁽⁵¹⁻⁵⁵⁾

Computational chemistry is a branch of chemistry that uses the results of theoretical chemistry incorporated into efficient computer programs to calculate the structures and properties of molecules and solids, applying these programs to real chemical problems. Examples of such properties are structure (i.e. the expected positions of the constituent atoms), energy and interaction energy, charges, dipoles and higher multipole moments, vibrational frequencies, reactivity or other spectroscopic quantities, and cross sections for collision with other particles. The term computational chemistry is also sometimes used to cover any of the areas of science that overlap between computer science and chemistry. Electronic configuration theory is the largest sub-discipline of computational chemistry. The main theoretical methods available belong to five broad classes as described below.

Molecular mechanics (MM) methods represent the simplest computational approaches and may be found in a large array of computational software suites. The general technique assumes that atoms are hard spheres and are attached to each other by

elastic bonds that obey Hook's Law. Molecular mechanics is based on a model of a molecule as a collection of balls (atoms) held together by springs (bonds). If we know the normal spring lengths and the angles between them, and how much energy it takes to stretch and bend the springs, we can calculate the energy of a given collection of balls and springs i.e., of a given molecule; changing the geometry until the lowest energy is found enable us to do a geometry optimization, i.e., to calculate a geometry for the molecule. Molecular mechanics is fast: a fairly large molecule like calix[4]arene [C₂₈H₂₈O₄] can be optimized in seconds on a powerful desktop computer.

Ab initio calculations (also called *ab initio* quantum mechanics: *ab initio* is from the Latin: "from the first principle") are based on the Schrödinger equation. This is one of the fundamental equations of modern physics and describes, among other things, how the electrons in molecule behave. The *ab initio* method solved the Schrödinger equation for a molecule and gives us the molecule's energy and wave function. The wave function is a mathematic function that can be used to calculate the electron distribution (and, in theory at least, any things else about the molecule). From the electron distribution we can tell things like how polar the molecule is, and which parts of it are likely to be attracted by nucleophiles or electrophiles. The Schrödinger equation cannot be solved exactly for any molecule with more than one electron. Thus approximations are used.

Semiempirical (SE) calculations are, like *ab initio*, based on the Schrödinger equation. However, more approximation are made in solving it and the very complicated integrals that must be calculated in the *ab initio* method are not actually evaluated in SE calculations: instead, the program draws on a kind of library of integrals that was compiled by finding the best fit of some calculated entity like geometry or energy (heat of formation) to the experimental values. This plugging of experimental values into a mathematical procedure to get the best calculation values is called parameterization (or parametrization). It is the mixing of the theory and experiment that makes the method "semiempirical": It is based on the Schrödinger equation, but parameterized with experimental values (empirical means experimental). Semiempirical calculations are slower than MM but much faster than *ab initio* calculations.

Density functional calculations (often called Density functional theory (DFT) calculations) are, like *ab initio* and SE calculations, based on the Schrödinger equation. However, unlike the other two methods, the DFT does not calculate a wave function, but rather derives the electron distribution (electron density function) directly. A functional

is a mathematical entity related to a function. Density functional calculations are usually faster than *ab initio*, but slower than SE.

Molecular dynamics (MD) calculations apply the laws of motion to the molecules. Thus one can simulate the motion of an enzyme as it changes shape on binding to the substrate, or the motion of a swarm of water molecules around a molecule of solute. This section provides an introduction of the theoretical method used in this study.

1.9.1 Ab Initio Methods

Ab initio calculations are so called because they assume nothing about the expected outcome of the experiment. No ideal bond lengths, angles or other parameters are supplied. The calculations rely solely on the solution of the Schrodinger equation for the molecular orbital, usually in the ground state, from which geometry and charge distribution are calculated. It is also possible to determine alternative molecular orbitals, such as excited states, and unusual spin states. The main problem with the ab initio technique is that the Schrodinger equation can only be solved accurately for H₂ and that solutions for molecules of any great complexity, particularly those involved in supramolecular chemistry, require that a large number of mathematical shortcuts are taken. Even then the calculations are computationally intensive. In the Hartree-Fock model, the most common method encountered, each atomic orbital is described in terms of a number of overlapping Gaussian functions that average to give a 'true' representation of the Schrodinger solution. The speed and accuracy of the overall calculation depends on how many Gaussian functions are invoked to describe s, p, d and f electrons. In addition to Hartree-Fock treatments other ab initio approaches, such as density functional methods, are also becoming popular due to more efficient calculation protocols that speed up simulations. At present the useful limit for ab initio calculations is around 200 atoms for commercial software running on a desktop computer. Coupled to this is the difficulty in guaranteeing that a molecular geometry derived using this approach is accurate. Fortunately it is usually possible to generate substantially accurate molecular geometries through a combination of conformational analysis and molecular mechanics. An ab initio interrogation of the resultant structure, a so-called single point energy calculation, can save vast amounts of computational resources as no high level iterative geometric calculations are required: the desired information (heat of formation, electron density

dispersion, shape and disposition of the highest occupied and lowest unoccupied molecular orbitals) is calculated for just one geometry.

1.9.2 Semiempirical Methods

As discussed above, calculations that employ the solutions to complex mathematical equations involving all the electrons in the system require no structural parameters to be supplied. These ab initio methods rely upon the correct interpretation of solutions to the Schrodinger wave equation to generate molecular orbitals that in turn predict properties such as equilibrium geometries, heats of formation and so on. The levels of complexity to which these calculations can now be undertaken are quite staggering yet there are two main drawbacks. First, the chemist has to have a good working knowledge of the mathematics behind the (often costly) software in order to use the most appropriate model and to correctly interpret the results. Second, and of greater relevance to supramolecular chemists, is the limit to the number of electrons that may be considered by this method. This leads to the limit of 200 atoms or so that can be considered present and, on this scale, it is only useful for the simplest supramolecular systems. Without access to a supercomputer or a large parallel system this scale of simulation becomes the de facto limit of most chemists and equates to a calculation involving calixarene dimmers or explicitly solvated crown ether complexes. While this may be a useful way to investigate the likely interactions of small guest molecules with small or medium sized hosts it rules out most multicomponent systems and solvated models. How can we obtain quantum mechanical information, without which we cannot probe electron densities, transition states or an array of other properties, for supramolecular complexes? The answer is to consider semiempirical methods.

The main time-saving attribute of semiempirical methods is that they only consider valence electrons and assume localized atomic orbitals. This is the so-called Neglect of Diatomic Differential Overlap (NDDO) approximation. Under the NDDO approximation the number of electron-electron interactions scale as N^2 rather than N^4 where N is the number of mathematical functions used in the calculation. Other parameters derived from experiment, as used extensively in molecular mechanics methods, are incorporated to give further time-saving approximations. Despite these shortcuts it is still possible to generate well-founded models but, more importantly, the limit to semiempirical calculations on a desktop computer is increased to the order of 300

atoms. As with an *ab initio* method it is often wise to assume that a good molecular mechanic method will generate a suitably accurate structure for which a single-point energy calculation can be calculated. Other useful thermodynamic data can be determined using a combination of matrices calculated during the mechanics and energy phases of the simulation. These in turn can be used to generate atomic partial charges (useful in determining charge complementarity between host and guest), molecular orbitals, potential hydrogen bonds and the like.

1.9.3 ONIOM Method

ONIOM (Our *N*-layer Integrated molecular Orbital + molecular Mechanics) is the hybrid method of Morokuma and co-workers that enables different levels of theory to be applied to different parts of a molecule/system and combined to produce a consistent energy expression. The objective is to perform a high-level calculation on just a small part of the system and to include the effects of the remainder at lower levels of theory, with the end result being of similar accuracy to a high-level calculation on the full system.

1.9.4 Basis Sets

In general, a basis set is an assortment of mathematical functions used to solve a differential equation. In quantum chemical calculations, the term ‘basis set’ which applied to a collection of contracted Gaussians representing atomic orbitals, are optimized to reproduce the desired chemical properties of a system.

Standard *ab initio* software packages generally provide a choice of basis sets that vary both in size and in their description of the electrons in different atomic orbitals. Larger basis sets include more and a greater range of basis functions. Therefore, larger basis sets can better refine the approximation to the ‘true’ molecular wave function, but require correspondingly more computer resources. Alternatively, accurate wave functions may be obtained from different treatments of electrons in atoms. For instance, molecules containing large atoms ($Z > 30$) are often modeled using basis sets incorporating approximate treatments of inner-shell electrons which account for relativistic phenomena.

‘Minimal’ basis sets contain the minimum number of AO basis functions needed to describe each atom (*e.g.*, 1s for H and He; 1s, 2s, 2px, 2py, 2pz for Li to Ne). An example of a minimal basis sets is STO-3G, which uses three Gaussian-type functions

(3G) per basis function to approximate the atomic Slater-type orbitals. Although minimal basis sets are not recommended for consistent and accurate predictions of molecular energies, their simple structure provides a good tool for visualizing qualitative aspects of chemical bonding.

1.9.4.1 Split valence basis sets

In split valence basis sets, additional basis functions (one contracted Gaussian plus some primitive Gaussians) are allocated to each valence atomic orbital. The resultant linear combination allows the atomic orbitals to adjust independently for a given molecular environment. Split valence basis sets are characterized by the number of functions assigned to valence orbitals. 'Double zeta' basis sets use two basis functions to describe valence electrons, 'triple zeta' use three functions, and so forth. Basis sets developed by Pople and coworkers are denoted by the number of Gaussian functions used to describe inner and outer shell electron. Thus '6-31G' describes an inner shell atomic orbital with a contracted Gaussian composed of six primitive Gaussians, an inner valence shell with a contracted Gaussian composed of three primitives, and an outer valence shell with one primitive. Other split-valence sets include 3-21G, 4-31G, and 6-31G.

1.9.4.2 Polarized basis sets

Polarization functions can be added to basis sets to allow for non-uniform displacement of charge away from atomic nuclei, thereby improving descriptions of chemical bonding. Polarization functions describe orbitals of higher angular momentum quantum number than those required for the isolated atom (*e.g.*, *p*-type functions for H and He, and *d*-type functions for atoms with $Z > 2$), and are added to the valence electron shells. For example, the 6-31G(d) basis set is constructed by adding six *d*-type Gaussian primitives to the 6-31G description of each non-hydrogen atom. The 6-31G(d,p) is identical to 6-31G(d) for heavy atoms, but adds a set of Gaussian *p*-type functions to hydrogen and helium atoms. The addition of *p*-orbitals to hydrogen is particularly important in systems where hydrogen is bridging atom.

1.9.4.3 Diffuse basis sets

Species with significant electron density far removed from the nuclear centers (*e.g.*, anions, lone pairs and excited states) require diffuse functions to account for the outermost weakly bound electrons. Diffuse basis sets are recommended for calculations of electron affinities, proton affinities, inversion barriers and bond angles in anions. The addition of diffuse *s*- and *p*-type Gaussian functions to non-hydrogen atoms is denoted by a plus sign-as in '3-21+G'. Further addition of diffuse functions to both hydrogen and larger atoms is indicated by a double plus.

1.9.5 Molecular Properties

In theoretical chemistry, chemists, physicists and mathematicians develop algorithms and computer programs to predict atomic and molecular properties and reaction paths for chemical reactions. Computational chemists, in contrast, may simply apply existing computer programs and methodologies to specific chemical questions. There are two different aspects to computational chemistry:

- Computational studies can be carried out in order to find a starting point for a laboratory synthesis, or to assist in understanding experimental data, such as the position and source of spectroscopic peaks.
- Computational studies can be used to predict the possibility of so far entirely unknown molecules or to explore reaction mechanisms that are not readily studied by experimental means.

Thus computational chemistry can assist the experimental chemist or it can challenge the experimental chemist to find entirely new chemical objects. Several major areas may be distinguished within computational chemistry:

- The prediction of the molecular structure of molecules by the use of the simulation of forces to find stationary points on the energy hypersurface as the position of the nuclei is varied.
- Storing and searching for data on chemical entities (see chemical databases).
- Identifying correlations between chemical structures and properties (see QSPR and QSAR).

- Computational approaches to help in the efficient synthesis of compounds.
- Computational approaches to design molecules that interact in specific ways with other molecules (e.g. drug design).

1.9.5.1 Geometry optimization

Geometry optimization is used to find minima on the potential energy surface, with these minimum energy structures representing equilibrium structures. Optimization also is used to locate transition structures, which are represented by saddle points on the potential energy surface. Optimization to minima is also referred to as energy minimization. During minimization, the energy of molecules is reduced by adjusting atomic coordinates. It is applied to model-built structures as well as to those derived from coordinate data banks. Energy minimization is done when using either molecular mechanics or quantum mechanics methods, and it must precede any computational analyses in which these methods are applied. For example, geometry optimization can be used to

- a. characterize a potential energy surface
- b. obtain a structure for a single-point quantum mechanical calculation, which provides a large set of structural and electronic properties
- c. prepare a structure for molecular dynamics simulation - if the forces on atoms are too large, the integration algorithm may fail.

The energy obtained from the potential energy function at the optimized geometry is sometimes called a steric or conformational energy. These energies can be used to calculate differences between stereoisomers and between isologous molecules (i.e., those differing in connectivity but having the same number of each type of functional group). These energies apply to molecules in a hypothetical motionless state at 0 Kelvin. Additional information is needed to calculate enthalpies (e.g., thermal energies of translation, vibration, and rotation) and free energies (i.e., entropy). Programs such as Gaussian provide the information needed for calculating free energies of small molecules. Free energy simulations for macromolecules also are possible.

1.9.5.2 Normal mode analysis or frequency calculation

By definition the Hessian matrix is the matrix of force constants. When expressed in terms of internal coordinates, its elements are the harmonic force constants for the $3N-6$ ($3N-5$) internal degrees of freedom of the molecule of interest. These determine the molecule's harmonic vibrational frequencies. The latter, by definition, correspond to the normal vibrational modes; these can be determined by a unitary transformation of the Hessian such that the classical potential (V) and kinetic (T) energies of the system are in a diagonal representation. In the Cartesian representation V and T are given by:

$$V = X^+ H X$$

$$T = \frac{1}{2} \dot{X}^+ M \dot{X}$$

where H is the Hessian matrix, M is the (diagonal) matrix of atomic masses and X is the vector of Cartesian displacements of the atoms with time derivative, \dot{X} .

The normal modes, Q , are related to X via a linear transformation:

$$X = A Q$$

In the normal mode representation V and T are therefore given as:

$$V = Q^+ A^+ H A Q$$

$$T = \frac{1}{2} \dot{Q}^+ A^+ M A \dot{Q}$$

Thus, if A satisfies the generalized eigenvalue equations

$$H A = M A \Lambda$$

where Λ is the diagonal matrix of eigenvalues, one obtains:

$$V = Q^+ \Lambda Q$$

$$T = \frac{1}{2} \dot{Q}^+ \dot{Q}$$

The normal mode frequencies are simply proportional to the square roots of the elements of Λ . If the geometry of interest corresponds to a minimum on the PES, H is positive definite and thus all diagonal elements of Λ will be positive and all frequencies will be real. If the geometry is a transition state or higher order saddle point, one or several of the elements of Λ will be negative and will thus return imaginary frequencies.

The total zero-point energy (ZPE) of the molecular system in the harmonic approximation can be readily obtained from the vibrational frequencies by summing over the zero-point energies of all modes:

$$ZPE = \frac{1}{2} \sum_i h\nu_i$$

where h is Planck's constant.

In reality the harmonic approximation does not provide a true representation of the vibrational modes since bond stretches are much better represented by Morse type potentials and bending/torsional modes are periodic. Nevertheless, so long as the vibrational amplitudes are small, the harmonic approximation can be demonstrated to be valid for at least the lowest energy vibrations. An anharmonic treatment or at least anharmonic corrections need to be applied in situations where this harmonic approximation fails, such as in the computation of vibrational overtones.

1.9.5.3 Thermochemistry

The calculation of theoretical heats of formation is essential for many of the applications of quantum chemistry, in particular for aiding in the interpretation of experimental results and for the prediction of reaction kinetics. Unfortunately, however, this requires the computation of the reaction enthalpy for the formation of a molecule relative to the standard states of its constituent elements; in many cases these standard states are liquids or solids for which direct calculation of the energy is not feasible. [45] Given that accurate experimental values are available for the enthalpies of formation of free atoms, a practical alternative is to use these in conjunction with a theoretical prediction of the atomization energy, $\sum D_0$, to predict the heat of formation for the molecule of interest. Thus, given an atomization energy at 0K,

$$\sum D_0 = \sum_{atoms} E_{atom} - E_{molecule}$$

(where the total molecular energy includes the zero-point vibrational energy), Hess' law can be applied to obtain the $\Delta_f H_0^0$:

$$\Delta_f H_0^0(molecule) = \sum_{atoms} \Delta_f H_0^0(atom) - \sum D_0$$

Heats of formation at other temperatures ($\Delta_f H_T^0$) as well as entropies (S_T^0) and Gibbs free energies of formation ($\Delta_f G_T^0$) can then be calculated using the standard methods of statistical mechanics.

1.9.5.4 Thermodynamic properties

The thermal contributions to thermodynamic properties such as enthalpy, entropy, free energy, heat capacity, etc. are all derived from the molecular partition functions. For a system of N molecules the internal energy (relative to internal energy at 0 K) is given by

$$U_T^0 - U_0^0 = -N \left(\frac{\partial \ln q}{\partial \beta} \right)$$

where the derivative is taken at constant volume. The enthalpy is therefore

$$\begin{aligned} H_T^0 - H_0^0 &= (U_T^0 - U_0^0) + p\Delta V \\ &= (U_T^0 - U_0^0) + Nk_B T \end{aligned}$$

The entropy of the system is given by

$$S^0 = \frac{(U_T^0 - U_0^0)}{T} + Nk_B \ln q$$

so that the change in Gibbs free energy is

$$\begin{aligned} (G_T^0 - G_0^0) &= (H_T^0 - H_0^0) - TS^0 \\ &= Nk_B T - Nk_B T \ln q \end{aligned}$$

The Gibbs free energy change for a reaction is, of course, related to the equilibrium constant for the reaction:

$$\Delta_r G^0 = -Nk_B T \ln K_{eq}$$

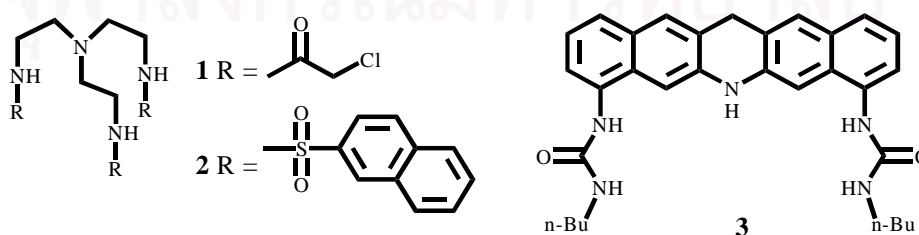
1.9.5.5 Polarizable continuum solvent model

In a polarizable continuum model (PCM), the molecule is surrounded by a dielectric medium, the polarizable continuum, with a given dielectric constant, ϵ . This medium is polarized in response to the charge distribution (nuclei and electrons) that it

experiences and produces an electric field, called a reaction field, which in turn polarizes the molecule. The resulting slightly changed charge distribution alters the reaction field somewhat, which again leads to further polarization of the molecule. This process continues until equilibrium is reached. In the PCM implemented in the Gaussian program, the reaction field is represented through charges located on the surface of the molecular cavity. [48] The molecular cavity can be created in several ways, but is generally based on interlocking van der Waals-spheres centered at atomic positions. The surface of this cavity is smoothed (for numerical reasons) and in the PCM model approximated by many small planar surface elements of given area. Charges are then placed on each of the surface elements to represent the reaction field of the dielectric medium. The extent which the medium can be polarized and hence the ultimate strength of the reaction field is controlled by the magnitude of the dielectric constant.

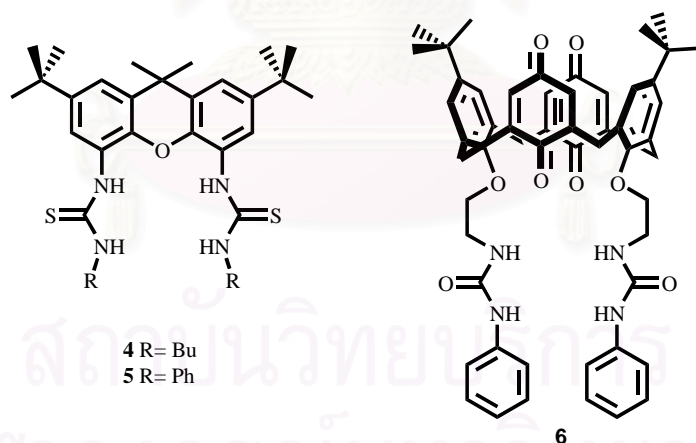
1.10 Literature Review

Anion plays an important role in chemical and biochemical processes and their recognition by artificial receptor has been a focus of interest for chemists in the past decades. In an attempt to mimic nature in its high binding selectivity, several anion receptors have been developed with three dimensional arrangements of hydrogen bond donating moieties. In 1993 Reinhoudt and co-workers produced a series of acyclic tripodal receptors containing amide groups (**1-2**).⁽⁵⁶⁾ Receptor **1** bind H_2PO_4^- with an association constant of $6.1 \times 10^3 \text{M}^{-1}$ in acetonitrile. The increase electrophilicity of sulfonamide NH moieties in receptor **2**, in combination with preorganization of the binding site by π -stacking, enhances the H_2PO_4^- binding with receptor **2** ($k_{\text{as}} = 1.4 \times 10^4 \text{M}^{-1}$).



In 1994, Kelly and Kim reported the synthesis of 4,8-bis[*n*-butylamino)carbonyl]amino]dibenz[*b,i*]acridan (**3**).⁽⁵⁷⁾ The relative rigidity, prevent self-association of urea/thiourea substituents, and preorganization of receptor **3** was expected to confer selectivity and foster strong binding. The binding with the various anions in DMSO-*d*₆ was examined by ¹H-NMR and found that the association constant for isophthalate is high ($6.3 \times 10^5 \text{ M}^{-1}$) because of the potential to form four hydrogen bonds.

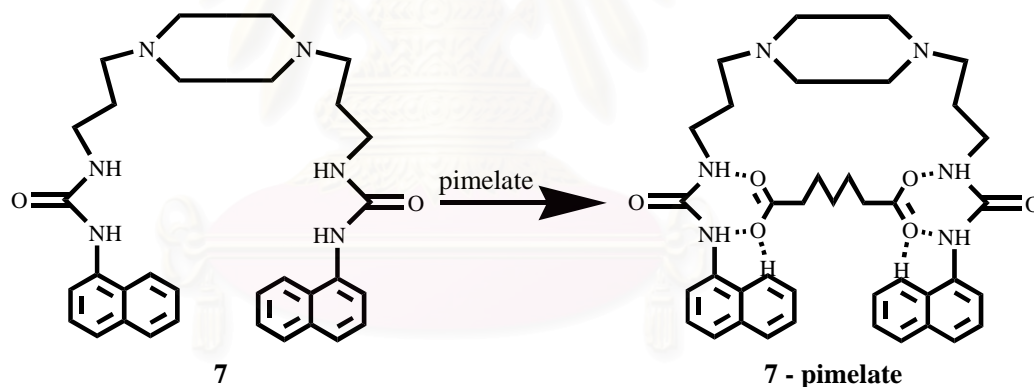
Recently Umezawa and coworkers have produced a series of acyclic thiourea cleft molecules including some highly preorganized systems containing a xanthene spacer.⁽⁵⁸⁾ Receptor **4** and receptor **5** were obtained coupling 2,7-di-*tert*-butyl-9,9-dimethyl-4,5-xanthenediamine with thioisocyanates. Association constants were measured by ¹H-NMR titration with DMSO-*d*₆ as solvent. A Job's plot showed 1:1 complex stoichiometry and titration gave association constant up to $5.5 \times 10^4 \text{ M}^{-1}$ for receptor **4** with H_2PO_4^- ion, while $1.95 \times 10^5 \text{ M}^{-1}$ for receptor **5**. The phenyl substituent leads to much stronger complex stabilities because electron withdrawing effect of phenyl groups increase the acidity of the thiourea. The selectivity for H_2PO_4^- ion can be attributed to the complementary hydrogen bonding array presenting in these clefts that can form four hydrogen bonds to each H_2PO_4^- .



The development of anion sensor for distribution and concentration of organic and inorganic anion is of particular interest in supramolecular chemistry. The common modes of signal transduction are electrochemical and optical changes. In the case of electrochemical sensor, quinone-based ligand and aromatic nitro are the well-known sensing units especially for cation sensors but relative rare for anion sensors. For instance, urea-functionalized calix[4]diquinone-based anion sensor (**6**) has been synthesized and studied for its binding properties with anions by Jeong and coworkers.⁽⁵⁹⁾ The redox

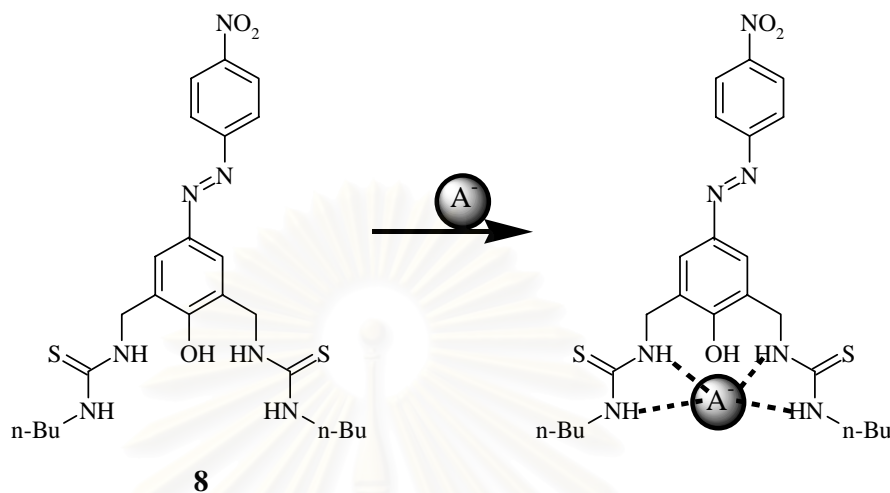
chemistry was investigated in MeCN, CH₂Cl₂, and DMF with BuNPF₆ as a supporting electrolyte under an argon atmosphere. The binding with HSO₄⁻ causes a large negative shift of the electrode potentials of calix[4]diquinone. This neutral anion receptor binds anion through hydrogen bonding and shows high selectivity for HSO₄⁻ over H₂PO₄⁻, Cl⁻ and CH₃CO₂⁻ because of shape and size selectivity.

One of the most appealing approaches in this context involves constructions of optical sensors, which may be fluorescent or colorimetric sensors. A further efficient fluorescent sensor of dicarboxylate anion has been realized by Mei and Wu.⁽⁶⁰⁾ The fluorescence quenching and a new emission of compound **7** through photoinduced electron transfer (PET) process by different dicarboxylate anions has been studied. Its sensitivity for recognition depends strongly on the chain length of dicarboxylate anions and the distance between urea units. ¹H-NMR spectra indicate that a 1:1 complex is formed between compound **7** and dicarboxylate anions through hydrogen bonding interactions. Results also indicate that multiple hydrogen bonding interactions may effect the stability of complex and play an important role in molecular recognition.



In 2001, Hong and co-workers have reported the synthesis of colorimetric azophenol base anion sensor containing thiourea units as hydrogen bonding donor (**8**).⁽⁶¹⁾ Association constants for anion binding were determined by ¹H NMR and UV-Vis titration techniques. Selectivity trends of anion-induced color change for **8** were determined to be F⁻ ~ H₂PO₄⁻ ~ AcO⁻ >> HSO₄⁻ ~ Cl⁻ > Br⁻ ~ I⁻. Upon addition of H₂PO₄⁻ to a solution of **8**, the color of solution changes from light yellow to deep red. This may be due to the electronic excitation occurs through a charge transfer from oxygen donor of the phenol to acceptor substituent (-NO₂) of the chromophore. The excited state would be more stabilized by anion binding, resulting in a bathochromic shift in the absorption maxima as well as the color change. Clear isobestic points were observed,

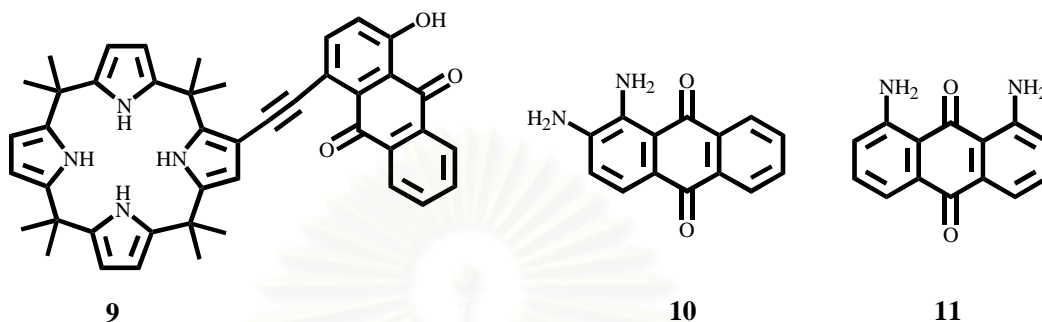
which shows the existence of two states of a 1:1 complex. These results indicated that color changes of **8** was suitable for the “naked-eye” monitoring of selected anions such as H_2PO_4^- and AcO^- .



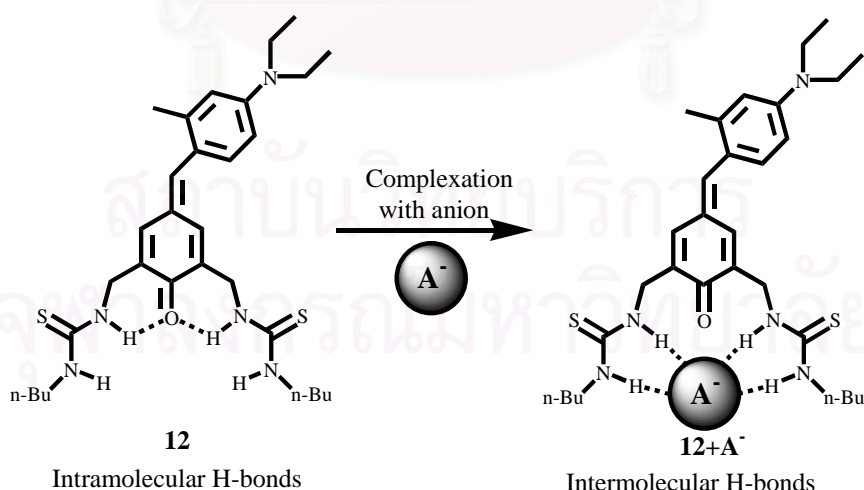
The interest in a colorimetric anion sensor is the ability to sense anions qualitatively by the naked-eyes. However, few such systems exist at present. For instance, a colorimetric anion sensor based on calix[4]pyrrole attaching anthraquinone (**9**) has been used for detecting F^- , Cl^- and H_2PO_4^- in dichloromethane.⁽⁶²⁾ The anthraquinone-functionalized system that bears an appended chromophore directly linked to the calix[4]pyrrole skeleton through a conjugating C-C triple bond. Compound **9** itself is red and displays an absorption maximum at 526 nm. Upon addition of fluoride ion, the absorption maximum is shifted to 613 nm with the net result that the solution turns blue. The dramatic color change tentatively ascribed to a charge transfer interaction between the electron-rich, calix[4]pyrrole-bound anions and the electron deficient anthraquinone moiety.

Sessler and Miyaji have reported many naked eye anion sensors such as 1,2-diaminoanthraquinone (**10**) and 1,8-diaminoanthraquinone (**11**).⁽⁶³⁾ Significant bathochromic shifts in the absorption spectra were also observed for **10** and **11** in dichloromethane in the presence of chloride, bromide, and phosphate ions. These spectral changes were particularly dramatic in the case of **10**. Specifically, it was found that the solution of **10**, initially yellow in color ($\lambda_{\text{max}} = 487 \text{ nm}$), became dark purple ($\lambda_{\text{max}} = 555 \text{ nm}$), red ($\lambda_{\text{max}} = 519 \text{ nm}$), reddish orange ($\lambda_{\text{max}} = 513 \text{ nm}$), orange ($\lambda_{\text{max}} = 499 \text{ nm}$), purple ($\lambda_{\text{max}} = 548 \text{ nm}$), and orange ($\lambda_{\text{max}} = 493 \text{ nm}$), when exposed to fluoride, chloride,

bromide, iodide, phosphate, and sulfate ions, respectively. The solutions of **11** in dichloromethane (1×10^{-4} M) were also found to change color when exposed to these anions, albeit to a lesser extent. For example the color was changed from orange ($\lambda_{\max} = 487$ nm) to red ($\lambda_{\max} = 503$ nm) upon the addition of 500 equivalents of fluoride ion.



Recently, Hong and coworker synthesized an indoaniline-thiourea-based sensor **12** to recognize and sense anions.⁽⁶⁴⁾ In the absence of anions, indoaniline chromophore has intramolecular hydrogen bonding between the carbonyl oxygen of indoaniline unit and the adjacent thiourea NHs. Upon addition of anions, the thiourea NHs are forced to participate in binding anion, hence the contribution of NHs to the hydrogen bonding with the indoaniline C=O group decrease. This structural disturbance is reflected in the observed spectral blue shift of the complexes. This system allows selective colorimetric detection of tetrahedral oxoanions (H_2PO_4^- , HSO_4^- over F^-).



1.11 Scope of This Research

This project has been focused on the synthesis of both electrochemical and optical anion sensors shown in Figure 1.10. Target sensors are designed to contain thiourea moieties as anion binding sites. Different sensing units are directly linked to receptor units that were designed to have various distances for different anions. Binding constants of the complexes between receptors and anions are calculated by ^1H NMR and UV-vis titration. The computer optimizations and calculation are used to investigate the geometrical structures of typical conformers of synthetic compounds, their proton affinities, relative stabilities, and the relative energies using the density functional theory (DFT) and ONIOM two layer methods. The HOMO–LUMO molecular orbital energy gaps of all compounds have been determined. Geometrical structures of the complexes between synthesized compounds and anions are also calculated. The experimental and computational results are compared. Sensing abilities of the synthesized compounds are investigated by fluorescence spectrophotometer and cyclic voltammetry.

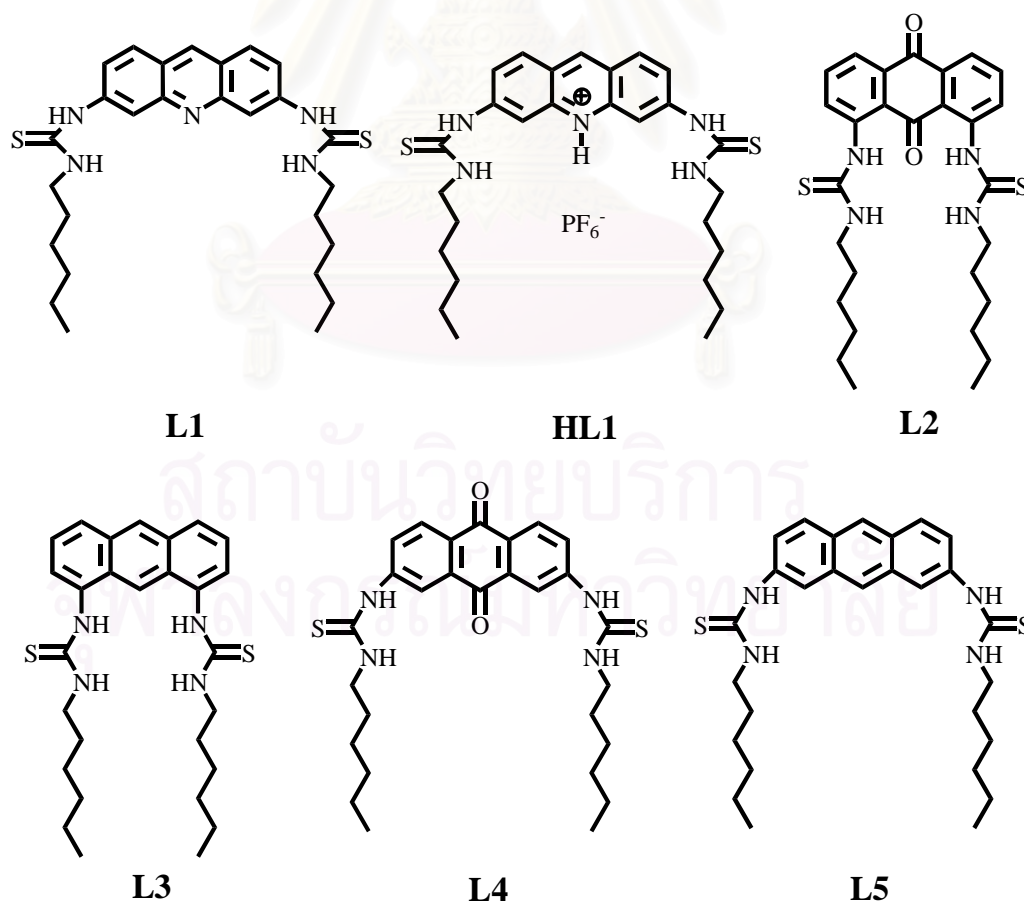


Figure 1.10 Target molecule structures of anthracene derivatives containing thiourea (L1-L5).

CHAPTER II

EXPERIMENTAL SECTION

2.1 General Procedures

2.1.1 Analytical Measurement

Nuclear Magnetic Resonance (NMR) spectra were recorded on Varian 400 MHz nuclear magnetic resonance spectrometers. In all cases, ligands were dissolved in deuterated dimethylsulfoxide (DMSO- d_6). Elemental analysis was carried out on CHNS/O analyzer (Perkin Elmer PE2400 series II). Electrospray mass spectra were determined on a Micromass Platform quadrupole mass analyser (HP1050) with an electrospray ion source using acetonitrile as solvent. Infrared spectra were obtained on a Nicolet Impact 410 using KBr pellet. All melting points were obtained on an Electrothermal 9100 apparatus and uncorrected. Absorption spectra were measured by a Varian Cary 50 UV-vis spectrophotometer. UV-Vis titration spectra were measured by a Perkin Elmer Lambda 25 spectrophotometer at 25 °C. Fluorescence spectra were recorded by Perkin Elmer SL50B fluorescence spectrophotometer.

2.1.2 Materials

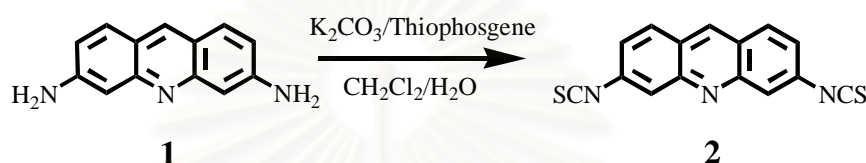
Unless otherwise specified, the solvent and all materials were reagent grades purchased from Fluka, BHD, Aldrich, Carlo Erba, Merck or J.T. Baker and were used without further purification. Commercial grade solvents such as acetone, dichloromethane, hexane, methanol and ethylacetate were purified by distillation before used. Acetonitrile and dichloromethane for set up the reaction were dried over calcium hydride and freshly distilled under nitrogen atmosphere prior to use.

Column chromatographies were carried out on silica gel (Kieselgel 60, 0.063-0.200 nm, Merck). Thin layer chromatography (TLC) were performed on silica gel plates (Kieselgel 60, F₂₅₄, 1mm, Merck). Compound on TLC plates were detected by the UV-light. All manipulations were carried out under nitrogen atmosphere.

All synthesized compounds were characterized by $^1\text{H-NMR}$ spectroscopy, mass spectrometry and elemental analysis.

2.2 Synthesis

2.2.1 Preparation of 3,9-Diisothiocyanatoacridine (2).



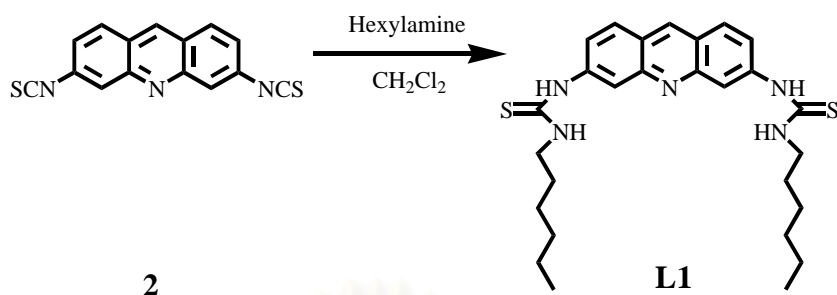
To a solution of 3,9-diaminoacridine hemisulfate **1** (0.5625 g, 1.02 mmol) in dichloromethane (50 mL) was added K_2CO_3 (2.79 g, 20 mmol) in water (50 mL) and stirred for 30 minutes. Thiophosgene (0.2 mL, 2.5 mmol) was added into the mixture and refluxed for 2 hours in a nitrogen atmosphere. The mixture was cooled to room temperature and organic layer was separated, washed with water and dried over anhydrous Na_2SO_4 . The solvent was removed in vacuo. The residue was purified by column chromatography (SiO_2) with 20% hexane/ CH_2Cl_2 as eluent to yield 0.5286 g (90%) of **2** as a yellow solid.

Characterization data for (2).

$^1\text{H NMR}$ (400 MHz, CDCl_3 , ppm) 7.35-7.38 (d, 2H, *ArH*, $J=8.8$ Hz) 7.95-7.97 (d, 2H, *ArH*, $J = 7.6$ Hz) 8.69 (s, 1H, *ArH*).

สถาบันวิทยบริการ
จุฬาลงกรณ์มหาวิทยาลัย

2.2.2 Preparation of 3,9-Di(hexylthioureido)acridine (L1).



In a 50 mL two-necked round bottom flask equipped with a magnetic bar, 3,9-diisothiocyanatoacridine **2** (0.5793 g, 1.97 mmol) was dissolved in dichloromethane (20 mL) and *n*-hexylamine (0.44 mL, 4.99 mmol) was then added. The mixture was stirred overnight at room temperature under nitrogen atmosphere. After the reaction was completed, the resulting solid was filtered off to obtain a yellow-orange solid **L1** (0.4590 g, 94% yield). The product was dried in *vacuo* and kept in a desiccator.

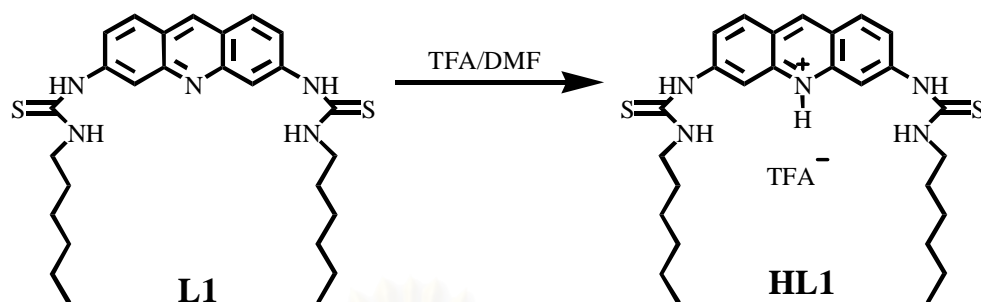
Characterization data for (L1).

¹H-NMR spectrum (400 MHz, DMSO-d₆, ppm) δ 0.90-0.92 (bm, 6H, CH₂CH₃, *J* = 6.1 Hz), 1.34 (bs, 12H, CH₂CH₂CH₂CH₂CH₃), 1.58-1.63 (m, 4H, CH₂CH₂CH₂, *J* = 20.0 Hz) 3.53-3.55 (bd, 4H, NHCH₂CH₂, *J* = 4.8 Hz) 7.58-7.60 (d, 2H, ArH, *J* = 8.7 Hz) 8.03-8.05 (d, 2H, ArH, *J* = 8.8 Hz) 8.22 (s, 2H, CSNHCH₂) 8.30 (s, 2H, ArH) 8.88 (s, 1H, ArH) 9.93 (s, 2H, ArNHCS)

Elemental analysis: Anal. Calcd for C₂₇H₃₇N₅S₂: C, 65.41; H, 7.52; N, 14.13; Found: C, 65.27; H, 7.63; N, 14.15.

EI Mass (m/z): 530.0 (100) [M+Cl]⁺, calcd : 530.2.

2.2.3 Preparation of 3,9-Di(hexylthioureido)acridinium Triflate (HL1).



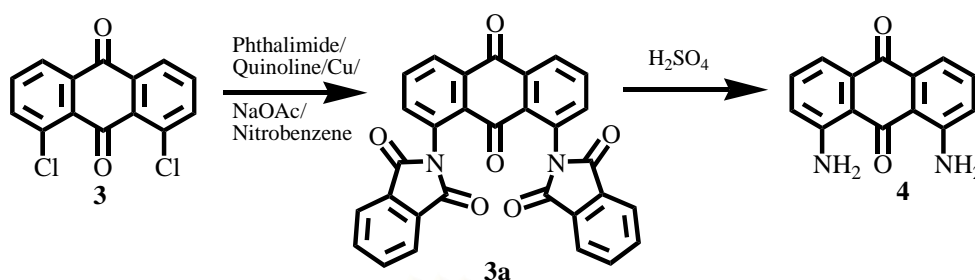
In a 50 mL two-necked round bottom flask equipped with a magnetic bar, 3,9-di(hexylthioureido)acridine **L1** (0.2530 g, 0.51 mmol) was dissolved in dimethylformamide (10 mL) and trifluoromethanesulfonic acid (0.12 mL, 1.70 mmol) was then added. The mixture was stirred for 2 hours at room temperature under nitrogen atmosphere. The solvent was removed in vacuo. The resulting solid was recrystallized in CH_2Cl_2 /hexane to give an orange solid of **HL1** (0.3234 g, 98% yield).

Characterization data for (L1).

$^1\text{H-NMR}$ spectrum (400 MHz, DMSO-d_6 , ppm) δ 0.85-0.89 (m, 6H, CH_2CH_3 , $J = 13.2$ Hz), 1.30 (bs, 12H, $\text{CH}_2\text{CH}_2\text{CH}_2\text{CH}_2\text{CH}_3$), 1.55-1.61 (m, 4H, $\text{CH}_2\text{CH}_2\text{CH}_2$, $J = 20.8$ Hz) 3.51-3.53 (bd, 4H, NHCH_2CH_2 , $J = 5.6$ Hz) 7.58-7.60 (d, 2H, ArH, $J = 8.8$ Hz) 8.25-8.27 (d, 2H, ArH, $J = 9.2$ Hz) 8.58 (s, 2H, ArH) 9.09 (s, 2H, CSNHCH_2) 9.46 (s, 1H, ArH) 10.49 (s, 2H, ArNHCS) 15.29 (s, 1H, ArNH)

สถาบันวิทยบริการ
จุฬาลงกรณ์มหาวิทยาลัย

2.2.4 Preparation of 1,8-Diaminoanthracene-9,10-dione, (4).



A stirred mixture of 1,8-dichloroanthracene-9,10-dione, **3** (41.6 g, 0.15 mol), phthalimide (52.7 g, 0.385 mol), anhydrous sodium acetate (29.6 g, 0.361 mol), and nitrobenzene (77 mL) was heated to 180 °C. Quinoline (25 mL) and copper powder (300 mesh, 0.72 g) were added, and the mixture was heated at 200 °C for 1 hour. The reaction mixture was allowed to cool and left to stand overnight. The mixture was filtered, washed with nitrobenzene (3 x 100 mL), ethanol (3 x 100 mL), hot water (3 x 200 mL), ethanol (2 x 100 mL), and ether (2 x 100 mL), and dried to give the intermediate diphthalimide, **3a**, as a yellow solid. The crude solid of **3a** was added to concentrated H₂SO₄ (400 mL) with stirring and the mixture heated at 95 °C for 45 minutes. The reaction mixture was cooled to 5 °C, and crushed ice (150 g) was slowly added. The mixture was poured into ice/water (1.5 L) while stirring, and the resulting precipitate was collected by filtration, washed with water and dried in vacuo. Recrystallization from ethanol afforded red/purple needles of **4** (27.0 g, 75% yield).

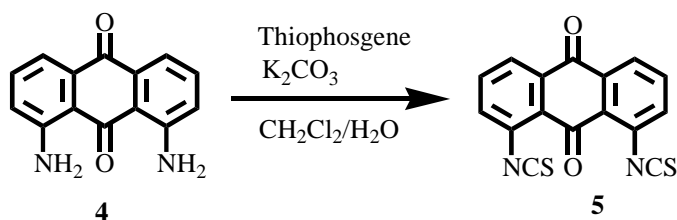
Characterization data for (4).

¹H NMR (DMSO d₆) 7.15 (2H, dd, *J* = 8.5 and 1.4 Hz, H-2,7), 7.34 (2H, dd, *J* = 7.4 and 1.4 Hz, H-4,5), 7.45 (2H, dd, *J* = 8.5 and 7.4 Hz, H-3,9), 7.86 (4H, br s, NH₂).

EI Mass (m/z): 238.0 (100), calcd ([M + H]⁺) 239.1.

mp: 270-271 °C.

2.2.5 Preparation of 1,8-Diisothiocyanatoanthracene-9,10-dione (5).

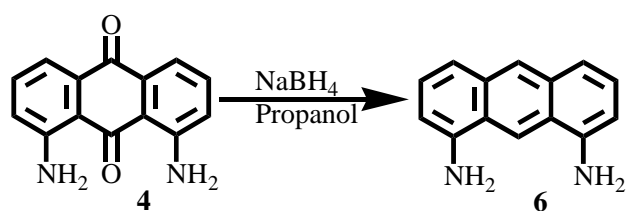


To a solution of 1,8-diaminoanthracene-9,10-dione **4** (0.2427 g, 1.02 mmol) and catalytic amount of 18-crown-6 in dichloromethane (50 mL) was added K₂CO₃ (2.79 g, 20 mmol) and stirred for 30 minutes. Thiophosgene (0.2 mL, 2.5 mmol) was then added into the mixture and refluxed for 2 hours in a nitrogen atmosphere. The mixture was cooled to room temperature, water (50 mL) was added and organic layer was separated, washed with water and dried (anhydrous Na₂SO₄). The solvent was removed in vacuo. The resulting solid was purified by column chromatography (SiO₂) with 20% hexane/CH₂Cl₂ as eluent to yield a pale yellow solid of **5**. (0.2660 g, 81% yield)

Characterization data for (5).

¹H NMR (400 MHz, CDCl₃, ppm) 7.57-7.59 (d, 2H, ArH, *J* = 7.6 Hz) 7.66-7.70 (t, 2H, ArH, *J* = 16.6 Hz) 8.12-8.14 (d, 2H, ArH, *J* = 8.0 Hz).

2.2.6 Preparation of 1,8-Diaminoanthracene (6).



1,8-diaminoanthracene-9,10-dione **4** (2.6634 g, 0.0112 mol) and NaBH₄ (7.054 g, 0.186 mol) were added to a 2-necked round bottom flask equipped with a magnetic bar and attached to a condenser under nitrogen atmosphere. Isopropanol (100 mL) was added via syringe into the mixture, which was then allowed to stir and reflux for 65 hours. After the reaction was completed, the reaction mixture was cooled to 5 °C and poured into ice/water (400 mL). The mixture was filtered, washed with water (4 x 100 mL) and dried under vacuum. The dark red precipitate was re-dissolved in CH₂Cl₂ and purified by column chromatography with 1-5% CH₂Cl₂/MeOH as eluent. A deep green (but also fluorescent yellow) fraction was eluted off and the solvent was removed in vacuo. Recrystallization from CH₂Cl₂ and n-Hexane afforded green crystals of **6** (1.239 g, 53% yield).

Characterization data for (6).

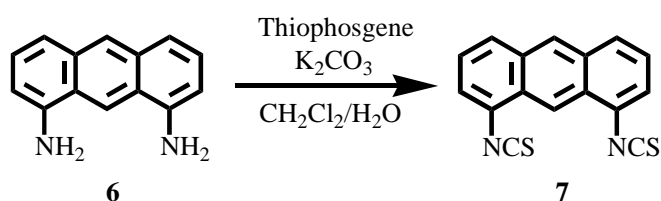
¹H NMR (300 MHz, CD₃OD): δ = 6.72 (d, 2H), 7.25 (t, 2H), 7.46 (d, 2H), 8.30 (s, 1H), 8.55 (s, 1H)

¹³C NMR (75.5 MHz, CD₃OD): δ = 107.53, 113.45, 118.78, 122.89, 125.84, 126.52, 132.34, 142.17.

HRMS CI Mass : *m/r* 208.1000 (*M'*), calcd: 208.1000

mp 154-156°C

2.2.7 Preparation of 1,8-Diisothiocyanatoanthracene (7).

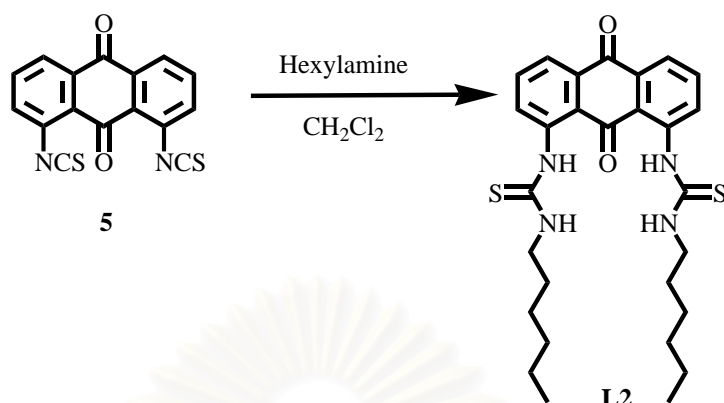


To a solution of 1,8-diaminoanthracene **6** (0.2159 g, 1.04 mmol) in dichloromethane (50 mL) was added K₂CO₃ (2.79 g, 20 mmol) in water (50 mL) and stirred for 30 minutes. Thiophosgene (0.2 mL, 2.5 mmol) was added into the mixture and the mixture was refluxed overnight in a nitrogen atmosphere. The mixture was cooled to room temperature and water was added (50 mL). The organic layer was separated, washed with water and dried over anhydrous Na₂SO₄. The solvent was removed in vacuo. The resulting solid was purified by column chromatography (SiO₂) with 20% hexane/CH₂Cl₂ as eluent to yield a yellow solid of **7** (0.2788 g, 92%).

Characterization data for (7).

¹H NMR (400 MHz, CDCl₃, ppm) 7.61-7.42 (t, 2H, ArH, *J*=65.2 Hz) 7.84-7.89 (d, 4H, ArH, *J*=8.4 Hz) 8.28 (s, 1H, ArH) 8.32 (s, 1H, ArH)

2.2.8 Preparation of 1,8-Di(hexylthioureido)anthracene-9,10-dione (**L2**).



In a 50 mL two-necked round bottom flask equipped with a magnetic bar, 1,8-diisothiocyanatoanthracene-9,10-dione **5** (0.6536 g, 2.03 mmol) was dissolved in dichloromethane (20 mL) and *n*-hexylamine (0.44 mL, 4.99 mmol) was then added. The mixture was stirred overnight at room temperature under nitrogen atmosphere. After the reaction was completed, the solvent was removed in vacuo, the precipitate was collected and purified by column chromatography with 10% EtOAc/CH₂Cl₂ as eluent and crystallization from CH₂Cl₂/hexane to obtain a yellow solid of **L2** (0.9267 g, 87%). The product was dried in *vacuo* and kept in a desiccator.

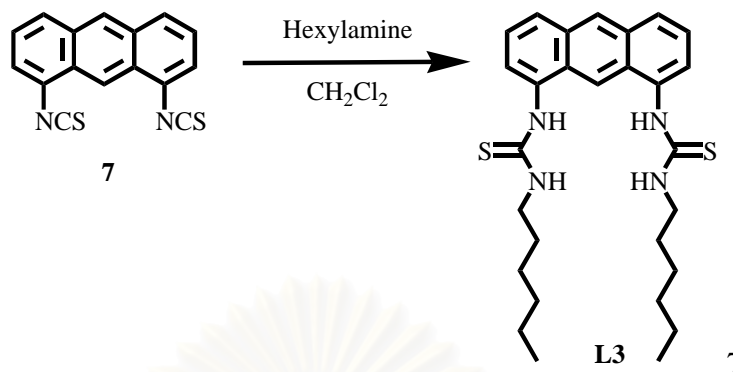
Characterization data for (**L2**).

¹H NMR (400 MHz, DMSO-d₆, ppm) δ 0.81-0.84 (t, 6H, CH₂CH₃, *J* = 12.4 Hz), 1.25 (bs, 12H, CH₂CH₂CH₂CH₂CH₃), 1.53 (bs, 4H, CH₂CH₂CH₂), 3.43-3.44 (bd, 4H, NHCH₂CH₂, *J* = 10.0 Hz) 7.69-7.73 (t, 2H, ArH, *J* = 15.6 Hz) 7.81-7.83 (d, 2H, ArH, *J* = 7.2 Hz) 8.52-8.54 (d, 2H, ArH, *J* = 8.0 Hz) 9.16 (s, 2H, CSNHCH₂) 10.96 (s, 2H, ArNHCS)

Elemental analysis: Anal. Calcd for C₂₈H₃₆N₄O₂S₂: C, 64.09; H, 6.91; N, 10.68; Found: C, 63.98; H, 7.00; N, 10.67.

EI Mass *m/z* (%) = 559.1 (100) [M+Cl]⁺. calcd: 559.2

2.2.9 Preparation of 1,8-Di(hexylthioureido)anthracene (L3).



In a 50 mL two-necked round bottom flask equipped with a magnetic bar, 1,8-diisothiocyanatoanthracene **7** (0.5673 g, 1.97 mmol) was dissolved in dichloromethane (20 mL) and *n*-hexylamine (0.44 mL, 4.99 mmol) was then added. The mixture was stirred overnight at room temperature under nitrogen atmosphere. After the reaction was completed, the solvent was removed in vacuo, the precipitate was collected and purified by column chromatography with 0-1% MeOH/CH₂Cl₂ as eluent. Crystallization in a CH₂Cl₂/hexane solution gave a yellow solid of **7** (0.7679 g, 80%). The product was dried in *vacuo* and kept in a desiccator.

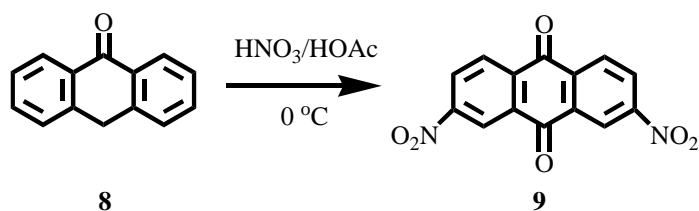
Characterization data for (L3).

¹H NMR (400 MHz, DMSO-d₆, ppm) δ 0.89 (bs, 6H, CH₂CH₃), 1.30 (bs, 12H, CH₂CH₂CH₂CH₂CH₃), 1.56 (bs, 4H, CH₂CH₂CH₂) 3.48-3.50 (d, 4H, NHCH₂CH₂, *J* = 6.0 Hz) 7.72-7.56 (t, 2H, ArH, *J* = 65.2 Hz) 7.87 (s, 2H, CSNHCH₂) 7.99-8.02 (d, 4H, ArH, *J* = 8.4 Hz) 8.67 (s, 1H, ArH) 8.71 (s, 1H, ArH) 9.70 (s, 2H, ArNHCS)

Elemental analysis: Anal. Calcd for C₂₈H₃₈N₄S₂: C, 67.97; H, 7.74; N, 11.32; Found: C, 67.77; H, 7.74; N, 11.33.

EI Mass *m/z* (%) =529.2 (100) [M+Cl]⁺, calcd: 529.2.

2.2.10 Preparation of 2,7-Dinitroanthracene-9,10-dione (9).



Anthrone (21.25 g, 0.109 mol) **8** was added with stirring to a cooled solution of fuming nitric acid (142 mL) at such a rate as to maintain a reaction temperature of 5 °C. After completion of the addition (ca. 1.5 hours), the reaction mixture was allowed to reach ambient temperature. The reaction mixture was added to glacial acetic acid (430 mL) with cooling, lightly stoppered, and allowed to stand at room temperature for 1 week. The precipitate was collected by filtration, washed with glacial acetic acid (3 x 25 mL) and hexane (3 x 25 mL), and dried. The crude solid was suspended in glacial acetic acid (4 L) and heated at reflux until the evolution of nitrous fumes had ceased (ca. 2h). The mixture was allowed to cool to room temperature and left to stand for 48 hours. The resulting precipitate was collected by filtration, washed with glacial acetic acid (3 x 30 mL) and hexane (3 x 30 mL). Recrystallization from nitrobenzene/glacial acetic acid (1:1 v/v) and dring in vacuo yielded a pale-yellow solid of **9**(10.34 g, 32%).

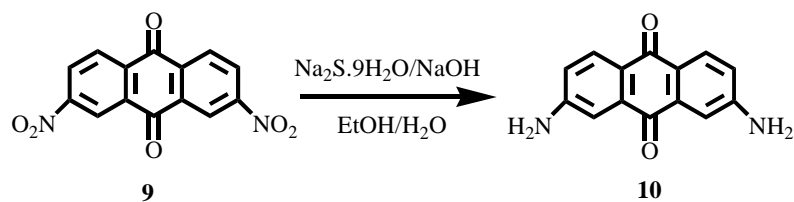
Characterization data for (9).

$^1\text{H NMR}$ (DMSO d_6 , ppm) δ : 8.48 (2H, dd, $J = 8.4$ and 1.4 Hz, H-4,5), 8.71 (2H, dt, $J = 8.4$ and 1.9 Hz, H-3,9), 8.83 (2H, t, $J = 1.9$ Hz, H-1,8).

EI Mass (rel intensity) m/z 298.0 (100), calcd (M^+) 298.0.

mp. 290-291 °C.

2.2.11 Preparation of 2,7-Diaminutesoanthracene-9,10-dione (10).



To a stirred suspension of 2,7-dinitroanthracene-9,10-dione **9** (9.4 g, 31.5 mmol) in ethanol (340 mL) was added a solution of sodium sulfide nonahydrate (34.1 g, 142 mmol) and sodium hydroxide (13.5 g, 338 mmol) in water (590 mL). The mixture was heated at reflux for 6 hours and left to stand overnight. The ethanol was removed in vacuo and the residue was cooled to 0-5 °C. The precipitate was collected by filtration, repeatedly washed with water, and dried. Recrystallization from ethanol/water afforded the product as a reddish orange solid (7.35 g, 98%).

Characterization data for (10).

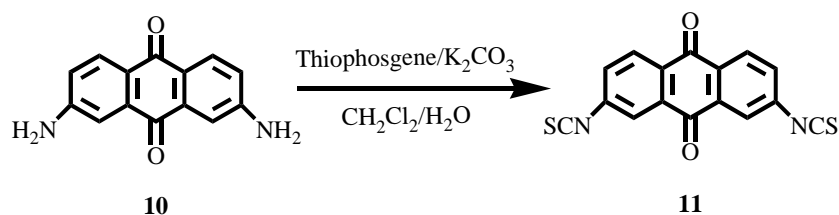
¹H NMR (DMSO d₆, ppm) δ: 6.42 (4H, br s, NH₂) 6.89 (2H, dd, *J* = 8.5 and 1.5 Hz, H-3,9), 7.23 (2H, d, *J* = 1.5 Hz, H-1,8), 7.84 (2H, d, *J* = 8.5 Hz, H-4,5).

EI Mass (rel intensity) *m/z* 239.0 (35); calcd ([M + 1]⁺) 239.1.

mp. 337-338 °C.

สถาบันวิทยบริการ
จุฬาลงกรณ์มหาวิทยาลัย

2.2.12 Preparation of 2,7-Diisothiocyanatoanthracene-9,10-dione (**11**).

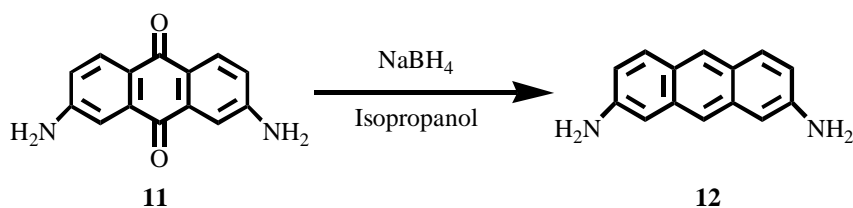


To a solution of 2,7-diaminoanthracene-9,10-dione **10** (0.2335 g, 0.98 mmol) in dichloromethane (50 mL) was added K₂CO₃ (2.79 g, 20 mmol) in water (50 mL) and stirred for 30 minutes. Thiophosgene (0.2 ml, 2.5 mmol) was added into the mixture and refluxed for 2 hours in a nitrogen atmosphere. The mixture was cooled to room temperature and organic layer was separated, washed with water and dried (anhydrous Na₂SO₄). The solvent was removed in vacuo. The residue was purified by column chromatography (SiO₂) with 20% hexane/CH₂Cl₂ as eluent to yield a pale yellow solid of **11**. (0.2844 g, 90%)

Characterization data for (**11**).

¹H NMR (400 MHz, CDCl₃, ppm) 7.57-7.59 (d, 2H, ArH, *J* = 7.6 Hz) 7.64-7.66 (d, 2H, ArH, *J* = 8.0 Hz) 8.07 (s, 2H, ArH)

2.2.13 Preparation of 2,7-Diaminutesoanthracene (12).



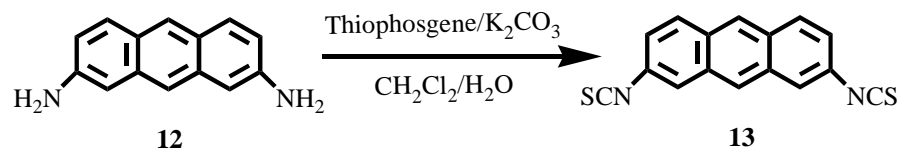
2,7-diaminoanthracene-9,10-dione **11** (2.7397 g, 0.0115 mol) and NaBH₄ (7.054 g, 0.186 mol) were added to a 2-necked round bottom flask equipped with a magnetic bar and attached to a condenser under nitrogen atmosphere. Isopropanol (100 mL) was added into the mixture, which was then allowed to stir and reflux for 65 hours. After the reaction was completed, the reaction mixture was cooled to 5 °C and poured into ice/water (400 mL). The mixture was filtered, washed with water (4 x 100 mL) and dried under vacuum. The dark red precipitate was re-dissolved in CH₂Cl₂ and purified by column chromatography (SiO₂) with 1-3% CH₂Cl₂/MeOH as eluent. A yellow fraction was eluted and the solvent was removed in vacuo. Recrystallization from CH₂Cl₂ and n-Hexane afforded green crystals of **L2** (1.5088 g, 68% yield).

Characterization data for (12).

¹H NMR (400 MHz, CDCl₃, ppm) 6.55 (bs, 1H, NH₂) 7.36-7.38 (t, 2H, ArH, *J* = 8.4 Hz) 7.63-7.65 (d, 4H, ArH, *J* = 8.0 Hz) 7.95 (s, 1H, ArH) 8.06 (s, 1H, ArH)

สถาบันวิทยบริการ
จุฬาลงกรณ์มหาวิทยาลัย

2.2.14 Preparation of 2,7-Diisothiocyanatoanthracene (13).

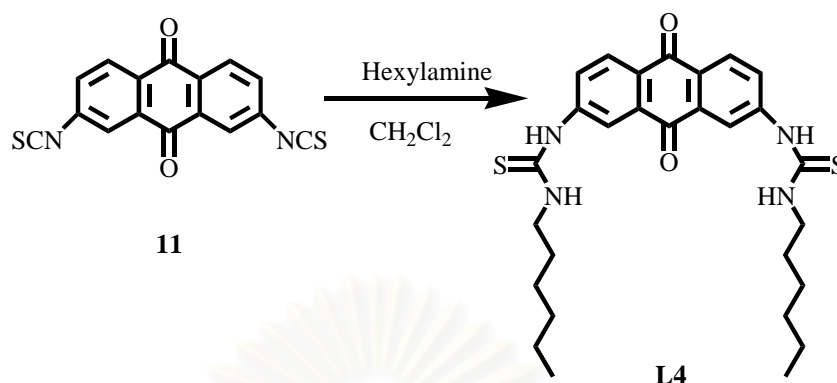


To a solution of 2,7-diaminoanthracene **12** (0.2157 g, 1.04 mmol) and a catalytic amount of 18-crown-6 in dichloromethane (50 mL) was added K_2CO_3 (2.79 g, 20 mmol) and stirred for 30 minutes. Thiophosgene (0.2 mL, 2.5 mmol) was added into the mixture and refluxed overnight in a nitrogen atmosphere. The mixture was cooled to room temperature, water was added (50 mL) and organic layer was separated, washed with water and dried over anhydrous Na_2SO_4 . The solvent was removed in vacuo. The residue was collected by filtration and purified by column chromatography (SiO_2) with 20% hexane/ CH_2Cl_2 as eluent to yield a yellow solid of **L3** (0.2453 g, 81%).

Characterization data for (13).

$^1\text{H NMR}$ (400 MHz, CDCl_3 , ppm) 7.37-7.39 (t, 2H, ArH, $J = 8.0$ Hz) 7.64-7.76 (d, 4H, ArH, $J = 7.6$ Hz) 8.30 (s, 1H, ArH) 8.38 (s, 1H, ArH)

2.2.15 Preparation of 1,8-Di(hexylthioureido)anthracene-9,10-dione (L4).



In a 50 mL two-necked round bottom flask equipped with a magnetic bar, 2,7-diisothiocyanatoanthracene-9,10-dione (0.6576 g, 2.04 mmol) was dissolved in dichloromethane (20 mL) and *n*-hexylamine (0.44 mL, 4.99 mmol) was then added. The mixture was stirred overnight at room temperature under nitrogen atmosphere. After the reaction was completed, the precipitate was collected by filtration to yield a yellow solid of **L4** (0.7739 g, 77%). The product was dried in *vacuo* and kept in a desiccator.

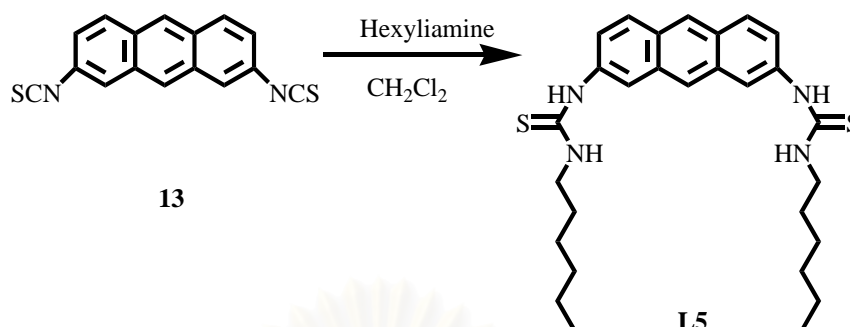
Characterization data for (L4).

$^1\text{H NMR}$ (400 MHz, DMSO- d_6 , ppm) δ 0.89-0.92 (t, 6H, CH_2CH_3 , $J = 13.6$ Hz), 1.33-1.38 (m, 12H, $\text{CH}_2\text{CH}_2\text{CH}_2\text{CH}_2\text{CH}_3$), 1.56-1.61 (m, 4H, $\text{CH}_2\text{CH}_2\text{C}2-3.53$ (bd, 4H, NHCH_2CH_2 , $J = 5.2$ Hz) 8.04-8.06 (d, 2H, ArH , $J = 8.0$ Hz) 8.13-8.15 (d, 2H, ArH , $J = 8.4$ Hz) 8.28 (s, 2H, CSNHCH_2) 8.46 (s, 2H, ArH) 10.16 (s, 2H, ArNHCS)

Elemental analysis: Anal. Calcd for $\text{C}_{28}\text{H}_{36}\text{N}_4\text{O}_2\text{S}_2$: C, 64.09; H, 6.91; N, 10.68; Found: C, 63.98; H, 7.00; N, 10.67.

EI MS m/z (%) = 559.0 (100) $[\text{M}+\text{Cl}]^+$, calcd: 559.2.

2.2.16 Preparation of 1,8-Di(hexylthioureido)anthracene (L5).



In a 50 mL two-necked round bottom flask equipped with a magnetic bar, 2,7-diisothiocyanatoanthracene **13** (0.5818 g, 1.99 mmol) was dissolved in dichloromethane (20 mL) and *n*-hexylamine (0.44 mL, 4.99 mmol) was then added. The mixture was stirred overnight at room temperature under nitrogen atmosphere. After the reaction was completed, the precipitate was collected by filtration to yield a yellow solid of **L5** (0.8171 g, 83%). The product was dried in *vacuo* and kept in a desiccator.

Characterization data for (L5).

¹H NMR (400 MHz, DMSO-d₆, ppm) δ 0.91 (bs, 6H, CH₂CH₃), 1.33 (bs, 12H, CH₂CH₂CH₂CH₂CH₃), 1.59 (bs, 4H, CH₂CH₂CH₂) 3.51 (bs, 4H, NHCH₂CH₂) 7.49-7.51 (d, 2H, ArH, *J* = 8.0 Hz) 8.00-8.02 (d, 4H, ArH, *J* = 8.4 Hz) 8.10 (s, 2H, CSNHCH₂) 8.34 (s, 1H, ArH) 8.46 (s, 1H, ArH) 9.77 (s, 2H, ArNHCS)

Elemental analysis: Anal. Calcd for C₂₈H₃₈N₄S₂: C, 67.97; H, 7.74; N, 11.32; Found: C, 67.97; H, 7.57; N, 11.37.

EI MS *m/z* (%) = 529.0 (100) [M+Cl]⁻, calcd: 529.2

2.3 Preparation of Tetrabutylammonium Salts

In a 50 mL two-necked round bottom flask equipped with a magnetic bar, 0.8 M solution of tetrabutylammonium hydroxide in methanol (5.0 mL, 4.00 mmol) was added to a stirred solution of a dicarboxylic acid (2.00 mmol) in methanol (15 mL) and stirring was continued overnight at room temperature under nitrogen atmosphere. The solvent was evaporated and the solid was dried for several days under high vacuum over P₂O₅. The resulting tetrabutylammonium salts was stored under anhydrous condition before use.

2.4 Complexation Studies

2.4.1 ¹H-NMR Titration Studies for Complexes of Compounds L1-L5 with Anion Guests

Typically, a 0.01 M solution of a ligand (5.0×10^{-6} mol) in DMSO-d₆ (0.5 mL) was prepared in a 5-mm NMR tube. An initial ¹H-NMR spectrum of the solution of the ligand was recorded. A 0.1 M stock solution of guest molecules (3.0×10^{-5} mol) in DMSO-d₆ (0.3 mL) was prepared in a vial (shown in Table 2.1). The solution of a guest molecule was added *via* microsyringe (10 μL portions) to the NMR tube. ¹H-NMR spectra were recorded after each addition.

2.4.2 UV-vis Titration Studies for Complexes of Compounds L1-L5 with Anion Guests

A solution of 2.0×10^{-5} M of all ligands in 0.01 M tetrabutyl ammonium hexafluorophosphate were prepared by adding 1 mL of a stock solution of ligand (1×10^{-4} M) in a 5 mL volumetric flask. Stock solutions of 1.0×10^{-3} M and 5.0×10^{-3} M of a tetrabutylammonium anion in 5.0 mL of 0.01 M tetrabutyl ammonium hexafluorophosphate were prepared in volumetric flask (table 2.1). The stock solution of ligand (2 mL) was added to a 1 cm quartz cuvette. Absorption spectra of ligand were recorded from 270 nm to 600 nm at ambient temperature. The solution of a

anion guest was added directly to the cuvette by a microburette and stirred for 40 seconds. Absorption spectra were measured after each addition. Table 2.2 shows guest : host ratios used in titration experiments.

Table 2.1 Amounts of tetrabutylammonium salts that used in anion complexation studies by UV-Vis titrations.

Tetra <i>n</i> -butylammonium anions	Weight (g) for 0.01 M anions	Weight (g) for 0.05 M anions
hydrogensulphate	0.01698	-
dihydrogenphosphate	0.01697	0.08470
Benzoate	0.01817	-
Oxalate ($^-\text{OOC}\text{COO}^-$)	0.02864	0.14240
Malonate ($^-\text{OOC}\text{CH}_2\text{COO}^-$)	0.02934	0.14675
Succinate ($^-\text{OOC}(\text{CH}_2)_2\text{COO}^-$)	0.03005	0.15025
Glutarate ($^-\text{OOC}(\text{CH}_2)_3\text{COO}^-$)	0.03075	0.15375
Adipate ($^-\text{OOC}(\text{CH}_2)_4\text{COO}^-$)	0.03145	0.15727
Pimilate ($^-\text{OOC}(\text{CH}_2)_5\text{COO}^-$)	0.03215	0.16075

2.4.3 Anion Complexation Studies of Compounds L1, L3 and L5 by Fluorescence Titrations

A solution of 2.0×10^{-5} M of a ligand **L1** in a 0.01 M tetrabutyl ammonium hexafluorophosphate were prepared by adding 1 mL of a stock solution of ligand (1×10^{-4} M) in a 5 mL volumetric flask. Solutions of 2.0×10^{-6} M of a ligand **L3** and **L5** in a 0.01 M tetrabutyl ammonium hexafluorophosphate were prepared by adding 1 mL of a stock solution of ligand (1×10^{-4} M) in a 50 mL volumetric flask. Stock solutions of 1.0×10^{-3} M of a tetrabutylammonium anion in dried dimethylsulfoxide were prepared in a 50 mL volumetric flask. Solutions of 1.0×10^{-4} M of a tetrabutylammonium anion were prepared by adding 1 mL of a stock solution of anion (1×10^{-3} M) in a 10 mL volumetric flask.

Fluorescence spectra of all ligands and anion complexes were recorded at ambient temperature. The solution of a guest was added directly to 2.00 mL of 2×10^{-6} M ligand in a cuvette by microburette and stirred for 40 seconds. Fluorescence spectra were measured after each addition. Table 2.2 shows guest : host ratios used in titration experiments.

Table 2.2 The concentration of anions that used in anion complexation studies by UV-Vis titrations.

No.	Anion added volume (μ l)	Total anion volume (μ l)	Total volume (ml)	mole ratio	[Anion] $\times 10^{-6}$ M	[Ligand] $\times 10^{-6}$ M
1	0	0	2.00	0.0	0	22.800
2	20	20	2.02	0.4	9.901	22.574
3	20	40	2.04	0.9	19.608	22.353
4	20	60	2.06	1.3	29.126	22.136
5	20	80	2.08	1.8	38.462	21.923
6	20	100	2.10	2.2	47.619	21.714
7	20	120	2.12	2.6	56.604	21.509
8	20	140	2.14	3.1	65.421	21.308
9	20	160	2.16	3.5	74.074	21.111
10	20	180	2.18	3.9	82.569	20.917
11	20	200	2.20	4.4	90.909	20.727
12	40	240	2.24	5.3	107.14	20.357
13	40	280	2.28	6.1	122.81	20.000
14	40	320	2.32	7.0	137.93	19.655
15	40	360	2.36	7.9	152.54	19.322
16	40	400	2.40	8.8	166.67	19.000
17	100	500	2.50	11.0	200.00	18.240
18	100	600	2.60	13.2	230.77	17.538
19	100	700	2.70	15.4	259.26	16.889
20	100	800	2.80	17.5	285.71	16.286
21	200	1000	3.00	21.9	333.33	15.200
22	200	1200	3.20	26.3	375.00	14.250

2.5 Electrochemical Studies

2.5.1 Apparatus

Cyclic voltammetry and square wave voltammetry were performed using an AUTOLAB PGSTAT 100 (Ecochemie, Netherland) thermostat with a three electrode consisting of a glassy carbon with a conducting area of 3 mm diameter, a platinum

wire counter electrode and a Ag/AgNO₃ reference electrode. All scans were carried out at room temperature and scan rates were varied.

Table 2.3 The concentration of anions that used in anion complexation studies with ligand **L3** and **L5** for fluorescence titrations.

No.	Anion added volume (μl)	Total anion volume (μl)	Total volume (μl)	mole ratio	[Anion] x 10 ⁻⁶ M	[Ligand] x 10 ⁻⁶ M
1	0	0	2.00	0.0	0	1.9808
2	20	20	2.02	0.5	0.8987	1.9611
3	20	40	2.04	0.9	1.7798	1.9419
4	20	60	2.06	1.4	2.6438	1.9231
5	20	80	2.08	1.8	3.4912	1.9046
6	20	100	2.10	2.3	4.3224	1.8864
7	20	120	2.12	2.7	5.1380	1.8686
8	20	140	2.14	3.2	5.9383	1.8512
9	20	160	2.16	3.7	6.7238	1.8340
10	20	180	2.18	4.1	7.4948	1.8172
11	20	200	2.20	4.6	8.2519	1.8007
12	40	240	2.24	5.5	9.7254	1.7685
13	40	280	2.28	6.4	11.147	1.7375
14	40	320	2.32	7.3	12.520	1.7076
15	40	360	2.36	8.2	13.846	1.6786
16	40	400	2.40	9.2	15.128	1.6506
17	100	500	2.50	11.5	18.154	1.5846
18	100	600	2.60	13.7	20.947	1.5237
19	100	700	2.70	16.0	23.533	1.4672
20	100	800	2.80	18.3	25.935	1.4148
21	200	1000	3.00	22.9	30.257	1.3205
22	200	1200	3.20	27.5	34.039	1.2380

2.5.2 Cleaning Procedure for Electrode

Cleaning of the glassy carbon electrode was done using a BAS polishing kit with stepwise finer abrasives down to 0.03 and 0.1 μM alumina powder slurry. The electrode was then sonicated in 0.005 M H₂SO₄ for 5 minutes and then soaked with dimethylformamide. This cleaning procedure was repeated after each measurement. The platinum wire counter electrode was cleaned by immersed in 3 M HNO₃ for 30 minutes, rinsed with distilled water and wiped to dryness before use. The reference electrode was cleaned by immersing in 3 M HNO₃ for 30 minutes and rinsing with distilled water.

2.5.3 Preparation of The Main Solution

Unless otherwise indicated, all experiments were carried out in an electrolyte solution of 0.1 M tetrabutylammonium hexafluorophosphate (TBAPF₆) in dimethylformamide. The reference electrode contained 0.01 M AgNO₃ in 0.1 M TBAPF₆ in dimethylformamide. The background solution contained only 0.1 M TBAPF₆ (1.9372 g) in dimethylformamide.

2.5.4 CV Measurements

All CV measurements were carried out in a cell compartment enclosed with a build-in Teflon cap to avoid the interference from gas oxygen. All solutions were bubbled with nitrogen at least 5 minutes before each measurement.

Cyclic voltammetry were recorded over ranges of scan rates from 0.02 to 1.0 V/s. The values of E_p and I_p were determined graphically from the CV by plotting a tangent to the leading baseline of the peak to correct for the background current. At a scan rate of 0.020 V/s the half-wave potential $E_{1/2}$ was determined as $(E_{pa}+E_{pc})/2$. Square wave voltammograms were recorded at 60 Hz and amplitude 0.030 V.

2.6 Computations

Full geometry optimizations of all investigated molecules and complexes were computed using two different methods, density functional theory (DFT) and two-layered ONIOM (DFT:AM1). DFT calculations and have been performed with the Becke's three parameters hybrid density functional using the Lee, Yang and Parr correlation functional (B3LYP). All geometry optimizations have been carried out using the hybrid density functional B3LYP with the 6-31G(d) basis set and two-layered ONIOM(B3LYP/6-31G(d):AM1). The single point calculations at the B3LYP/6-31G(d)//ONIOM(B3LYP/6-31G(d):AM1), MP2(fc)B3LYP/6-31G(d)//ONIOM(B3LYP/6-31G(d):AM1), B3LYP/6-31G(d) and MP2(fc)B3LYP/6-31G(d)//B3LYP/6-31G(d) levels of theory were carried out.

All calculations were performed with the GAUSSIAN 03 program. The MOLDEN 4.2 program was utilized to display molecular structures and observed the geometry convergence via the Gaussian output files. The molecular graphics of all species were generated with the MOLEKEL 4.3 program.

The Mulliken electronegativity (χ), chemical hardness (η) and electronic chemical potential (μ) for all isomers of the 3,9-bis-*N*-(*n*-hexylthioureido)acridine conformers were computed using orbital energies of the highest occupied molecular orbital (HOMO) and the lowest unoccupied molecular orbital (LUMO) at the B3LYP/6-31G(d) level of theory. The chemical hardness, electronic chemical potential and Mulliken electronegativity were derived from the first ionization potential (I) and electron affinity (A) of the N -electron molecular system with a total energy (E) and external potential ($v(\vec{r})$) using the relations:

$$\chi = -\left(\frac{\partial E}{\partial N}\right)_{v(\vec{r})} = -\mu \approx \frac{1}{2}(I + A) \quad \text{and} \quad \eta = -\left(\frac{\partial^2 E}{\partial N^2}\right)_{v(\vec{r})} \approx \frac{1}{2}(I - A),$$

and the first ionization potential and electron affinity are $I = E(N-1) - E(N)$ and $A = E(N) - E(N+1)$.⁽⁶⁵⁾ According to the Koopmans theorem,⁽⁶⁶⁾ I and A were computed from the HOMO and LUMO energies using the relations: $I = -E_{\text{HOMO}}$ and $A = -E_{\text{LUMO}}$. Therefore, $\eta = \Delta E_{\text{HOMO-LUMO}}/2$, $\mu = (E_{\text{HOMO}} + E_{\text{LUMO}})/2$ and $\chi = -(E_{\text{HOMO}} + E_{\text{LUMO}})/2$ were employed as the previous works.⁽⁶⁷⁻⁶⁹⁾

The ^1H NMR chemical shifts were calculated with the IEFPCM/B3LYP/6-31G(d) computations using the gauge-invariant atomic orbitals (GIAO) method.⁽⁷⁰⁻⁷²⁾ The ^1H NMR chemical shifts referenced to tetramethylsilane (TMS) of which the calculated absolute shift $\sigma(\text{H})$ is 31.1731 ppm were obtained from the single-point GIAO IEFPCM/B3LYP/6-31G(d) NMR calculations as in dimethyl sulphoxide (DMSO) solvent.

CHAPTER III

RESULTS AND DISCUSSIONS

3.1 Synthesis of Anion Receptor and Sensor Containing Dihexylthiourea Anthracene.

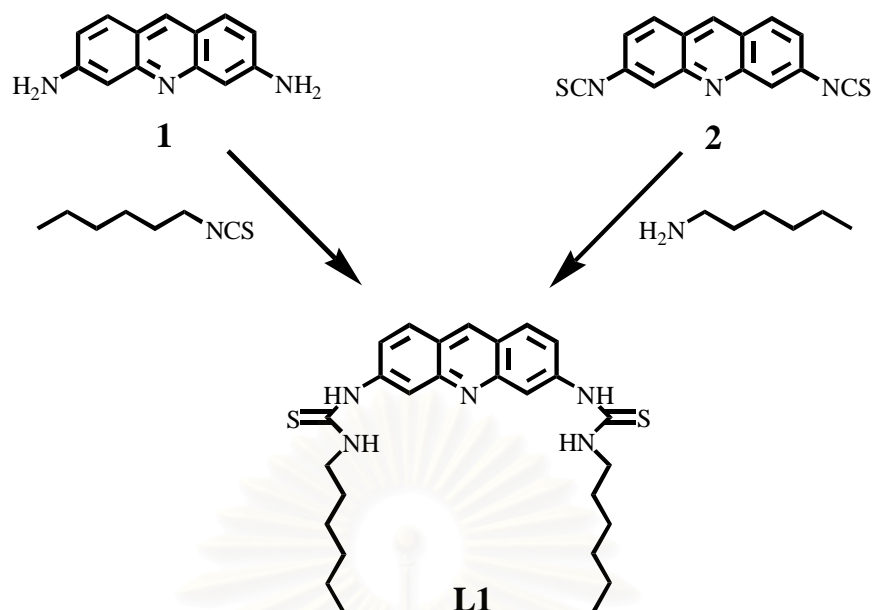
It is our interest to synthesize anion sensors by combining receptor units with signaling units. The most common modes of signal transduction typically involve electrochemical or optical changes in the sensor incurred by association of anions with the receptors. Of particular interest in this regard are “colorimetric anion sensors” species that would allow the so-called “naked-eye” detection of anions without resort to any instrument.

This research is aimed at the synthesis of anion sensors containing organic dyes giving optical and/or electrochemical signal. Thiourea moieties are used for anion receptors because they can interact with anionic species effectively by hydrogen bonding especially Y-shape anions such as carboxylate and dihydrogenphosphate anion. Different sensing units are directly linked to the receptor units that were designed to have various distances for different anions.

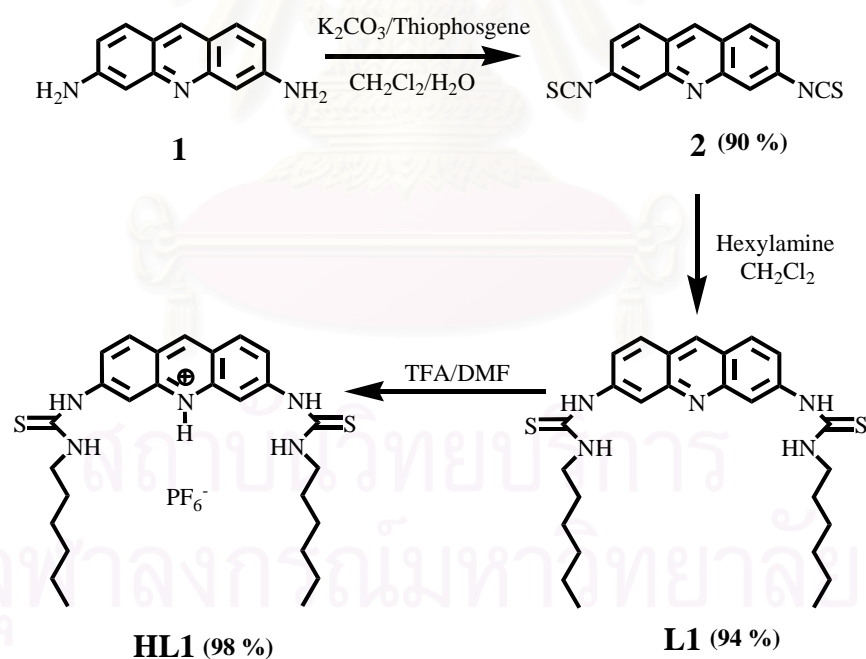
3.1.1 Synthesis and Characterization of Sensor L1 and HL1

The synthesis of 3,9-di(hexylthiouredo)acridine (**L1**) can possibly be carried out in two pathways as shown in Scheme 3.1. We first plan to synthesize compound **L1** by a coupling reaction between 3,9-diaminoacridine (**1**) and hexylthioisocyanate. The reaction seems to be straight forward, but compound **L1** cannot be synthesized by this pathway. Moreover, many solvents and catalysts have been tried, but no reaction occurs. This reaction requires lone pair electron of the amine nitrogen to attack the positive thioisocyanate carbon atom. For 3,9-diaminoacridine (**1**), two amine groups are directly link to the aromatic ring; therefore, the lone pair electron of the amino nitrogen can delocalize into the aromatic ring. This delocalization decreases the nucleophilicity of the N-atom.

Therefore, the starting material was changed from 3,9-diaminoacridine (**1**) to 3,9-diisothiocyanatoacridine (**2**), and then compound **2** reacted with hexylamine to yield **L1**. The successful pathway to synthesize compound **L1** is shown in Scheme 3.2.



Scheme 3.1 Possible synthetic pathways of 3,9-di(hexylthiouredo)acridine (**L1**)



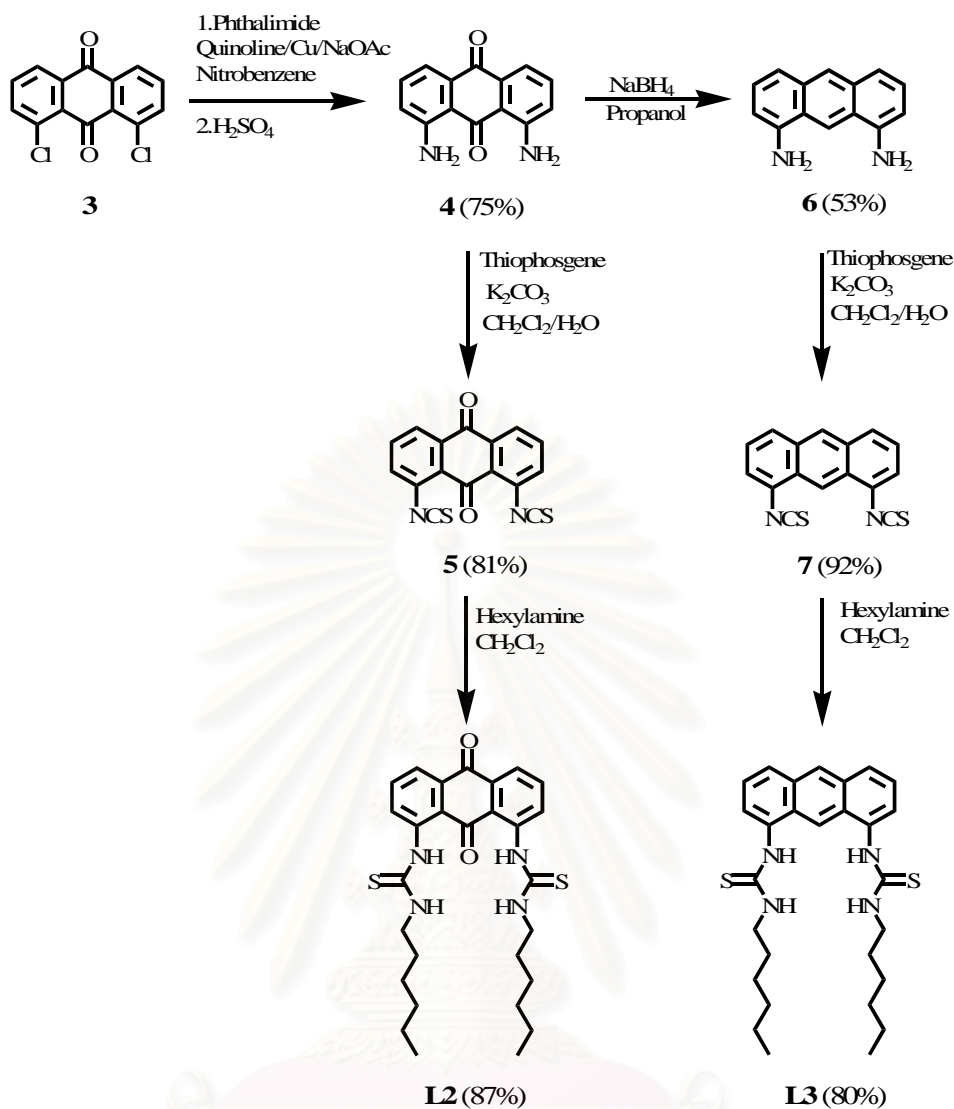
Scheme 3.2 Synthetic pathways of 3,9-di(hexylthiouredo)acridine (**L1**) and protonate form **HL1**

Compound 3,9-diisothiocyanatoacridine (**2**) was obtained by heterogeneous reaction of 3,9-diaminoacridine (**1**) with thiophosgene in the presence of K_2CO_3 and refluxed CH_2Cl_2/H_2O . After purification by column chromatography with 20% hexane/ CH_2Cl_2 as eluent and crystallization from CH_2Cl_2 /hexane, compound **2** was obtained in 90% yield as a yellow solid. Reacting compound **2** with n-hexylamine in CH_2Cl_2 gave compound **L1** as a yellowish orange solid in 94% yield. From 1H -NMR spectrum, the NH thiourea proton appears at 9.93 ppm (ArNHCS) for the one adjacent to aromatic ring and 8.22 ppm (CSNHCH₂) for the other. The two doublets of aromatic protons showed up at 7.58-7.60 ppm and 8.03-8.05 ppm. The singlet of two aromatic protons appeared at 8.30 ppm. The singlet aromatic proton showed up at 8.88 ppm. ESI mass spectra also supported the structure of this compound showing an intense line at m/z 530.0 due to the $[M + Cl]^-$ species. Elemental analysis was in good agreement with the proposed structure.

The protonated form of compound **L1** was synthesized by the reaction of **L1** with trifluoromethanesulfonic acid in dimethylformamide. The mixture was stirred for 2 hours at room temperature under nitrogen atmosphere. The solvent was removed in vacuo. The precipitate was recrystallized in CH_2Cl_2 /hexane and the resulting solid was filtered to obtain an orange residue of 3,9-diaminoacridinium triflate (**HL1**), in 98% yield. The 1H -NMR spectrum of compound **HL1** showed the protonated imine NH peak at 15.29 ppm (ArNH). The NH thiourea proton shifted downfield from 9.93 ppm of the neutral form to 10.49 ppm (ArNHCS) for the one adjacent to aromatic ring and from 8.22 ppm to 9.09 ppm (CSNHCH₂) for the other.

3.1.2 Synthesis and Characterization of Compounds **L2** and **L3**

1,8-Di(hexylthioureido)anthracene-9,10-dione (**L2**) and 1,8-di(hexylthioureido)anthracene (**L3**) were designed to have receptors, thiourea groups, in the same position, but different signaling units. The signaling unit of compound **L2** is anthraquinone group designed for transducing optical and electrochemical signal. For compound **L3**, the anthracene skeleton was designed for just only optical response that caused absorbance or fluorescence emission change when complexing with anions. The synthesis of compound **L2** and **L3** began with the commercialized precursor 1,8-dichloroanthracene-9,10-dione (**3**). The synthetic procedure is shown in Scheme 3.3.



Scheme 3.3 Synthetic pathways of compounds **L2** and **L3**

1,8-Diaminoanthracene-9,10-dione (**4**) was prepared using Gabriel synthesis. The reaction was started with 1,8-dichloroanthracene-9,10-dione and phthalimide in the present of anhydrous sodium acetate, nitrobenzene, quinoline and copper powder. After heating to 200 °C, the reaction mixture was allowed to cool and left to stand overnight. The mixture was filtered, washed and dried to give the intermediate diphthalimide as a pale-yellow/ orange. The crude diphthalimide solid was reduced to diamino by heated in concentrated H₂SO₄. Crystallization from ethanol then yielded the product as red/purple needles in 75% yield.

Compound 1,8-dithiocyanatoanthracene-9,10-dione (**5**) was obtained by reaction of **4** with thiophosgene and K₂CO₃ containing 18-crown-6 as catalyst in CH₂Cl₂. After

purification by column chromatography and crystallization, compound **5** was obtained in 81 % yield as a yellow solid. Treating compound **5** with *n*-hexylamine in CH₂Cl₂ gave compound **L2**. After purification by column chromatography and crystallization a yellow residue was obtained in 87 % yield. From ¹H-NMR spectrum, the NH thiourea proton appear at 10.96 ppm (ArNHCS) for the adjacent to aromatic ring and 9.16 ppm (CSNHCH₂) for the adjacent to hexyl group. The triplet of two aromatic proton appeared at 7.69-7.73 ppm. The two doublets of aromatic protons showed up at 7.81-7.83 ppm and 8.52-8.54 ppm. ESI mass spectra also supported the structure of this compound showing an intense line at *m/z* 559.1 due to the [M + Cl]⁻ species. Elemental analysis was in good agreement with the proposed structure.

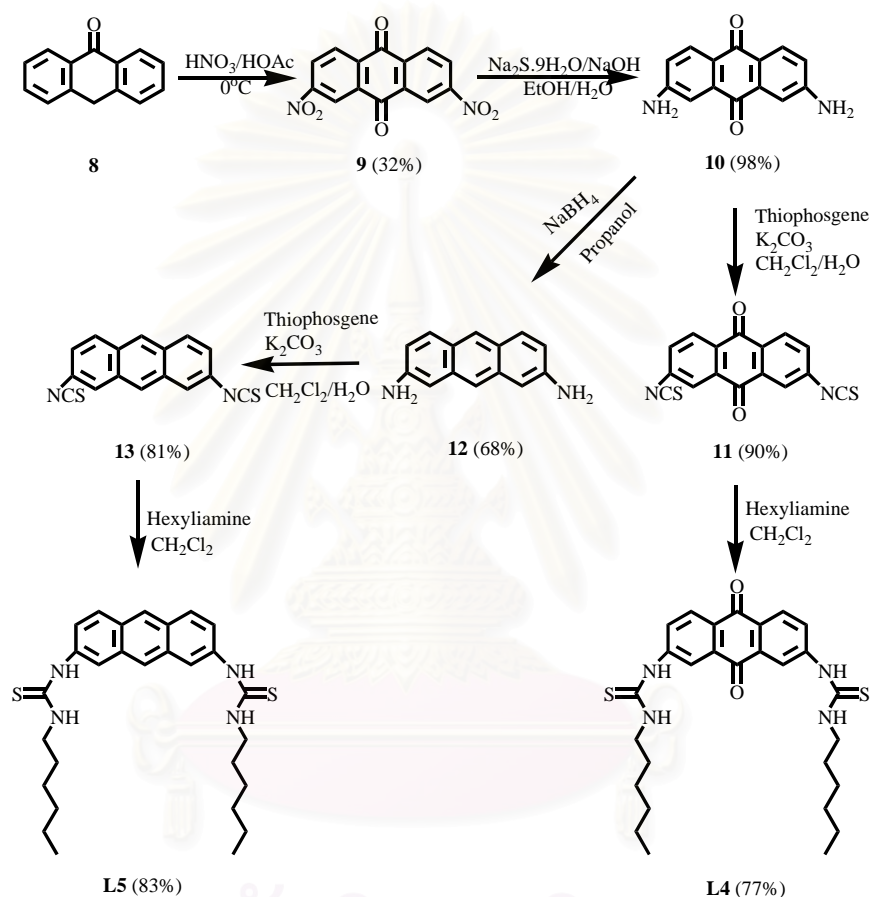
To synthesize 1,8-diaminoanthracene (**6**), 1,8-diaminoanthracene-9,10-dione (**4**) was reduced by sodiumborohydride (NaBH₄) in refluxed isopropanol. The dark red precipitate was purified by column chromatography over silica gel. A deep green (but also fluorescent yellow) fraction was eluted off, the solvent was removed and recrystallized to afford a green crystal **6** in 53% yield.

1,8-Dithioisocyanateanthracene (**7**) was prepared by heterogeneous reaction of 1,8-diaminoanthracene with thiophosgene and potassium carbonate in refluxed dichloromethane and water. After the reaction completed, the mixture was cooled to room temperature, organic layer was separated, washed with water and dried over anhydrous Na₂SO₄. After the solvent was removed, the resulting solid was purified by column chromatography to yield a yellow solid **7** in 92% yield.

Compound 1,8-di(hexylthioureido)anthracene (**L3**) was synthesized by a similar procedure as compound **L2**, coupling 1,8-diisothiocyanate-anthracene with *n*-hexylamine in dichloromethane. After purification by column chromatography and crystallization from CH₂Cl₂/hexane, compound **L3** was obtained as a yellow solid in 80% yield. From ¹H-NMR spectrum, the NH thiourea proton appeared at 9.70 ppm (ArNHCS) for the proton adjacent to aromatic ring and 7.87 ppm (CSNHCH₂) for the proton adjacent to hexyl group. The two singlets of aromatic protons showed up at 8.71 ppm and 8.67 ppm. The doublet of four aromatic proton appeared at 7.99-8.02 ppm. The triplet aromatic proton showed up at 7.72-7.56 ppm. ESI mass spectra also supported the structure of this compound showing an intense line at *m/z* 529.2 due to the [M + Cl]⁻ species. Elemental analysis was in good agreement with the proposed structure.

3.1.3 Synthesis and Characterization of Compounds L4 and L5

Compounds **L4** and **L5** can be synthesized from anthrone (**8**) by a procedure shown in Scheme 3.4. 2,7-Dinitroanthracene-9,10-dione (**9**) was prepared by nitration of anthrone (**8**) using fuming nitric acid and glacial acetic acid. Recrystallization from nitrobenzene/glacial acetic acid afforded a pure sample of compound **9** in 32% yield.



Scheme 3.4 Synthetic pathways of compounds **L4** and **L5**

The reduction of compound **9** by sodium sulfide nonahydrate and sodium hydroxide in refluxed ethanol/water afforded a redish orange solid 2,7-diaminoanthracene-9,10-dione (**10**) in 98% yields. 2,7-Dithioisocyanateanthracene-9,10-dione (**11**) was synthesized by the similar procedure as compound **2** and afforded a pale yellow solid in 90% yield. Coupling dithioisocyanate **11** with hexylamine afforded 1,8-di(hexylthioureido)anthracene-9,10-dione (**L4**) in 77% yield. From the $^1\text{H-NMR}$ spectrum, the NH thiourea proton appeared at 10.16 ppm (ArNHCS) for the one adjacent to aromatic ring and 8.28 ppm (CSNHCH_2) for the one adjacent to hexyl group. The two

doublets of aromatic protons showed up at 8.04-8.06 ppm and 8.13-8.15 ppm and the singlet of two aromatic protons appeared at 8.46 ppm. ESI mass spectra also supported the structure of this compound showing an intense line at m/z 559.0 due to the $[M + Cl]^-$ species. Elemental analysis was in good agreement with the proposed structure.

The synthesis of 2,7-di(hexylthiouredo)anthracene (**L5**) was started with a similar precursor as compound **L4**. From diamino **10**, reduction employing the same procedure as 1,8-diamino **5** resulted in 2,7-diamino **12** in 68% yield. 2,7-Dithioisocyanatoanthracene (**13**) was synthesized by the similar procedure as compound **2** and a pale yellow solid of **13** was obtained in 81% yield. Treating dithioisocyanate **14** with hexylamine afforded 1,8-di(hexyl thioureido)anthracene (**L5**) in 83% yield. From the 1H -NMR spectrum, the NH thiourea proton appear at 9.77 ppm (ArNHCS) for the one adjacent to aromatic ring and 8.10 ppm (CSNHCH₂) for the one adjacent to hexyl group. The doublet of aromatic protons showed up at 7.49-7.51 ppm. The doublet of four aromatic protons appeared at 8.00-8.02 ppm. The two singlets of one aromatic proton appeared at 8.34 and 8.46 ppm. ESI mass spectra also supported the structure of this compound showing an intense line at m/z 529.0 due to the $[M + Cl]^-$ species. Elemental analysis was in good agreement with the proposed structure.

3.2 Theoretical Studies of Synthetic Compounds

3.2.1 Conformational, Stability and Protonation of Compounds **L1** and **HL1**.

The structures of all conformers of compound **L1** and their protonated forms **HL1** optimized at the B3LYP/6-31G(d) and two-layered ONIOM(B3LYP/6-31G(d):AM1) levels were obtained. The B3LYP/6-31G(d) optimized structures of compound **L1** conformers and their corresponding protonated structures are shown in Figure 3.1. The **L1a**, **L1b**, **L1c** are conformers of compound **L1** in the gas phase and **HL1c**⁺, **HL1b**⁺, **HL1a**⁺ are conformers of protonated **HL1** form in the gas phase.

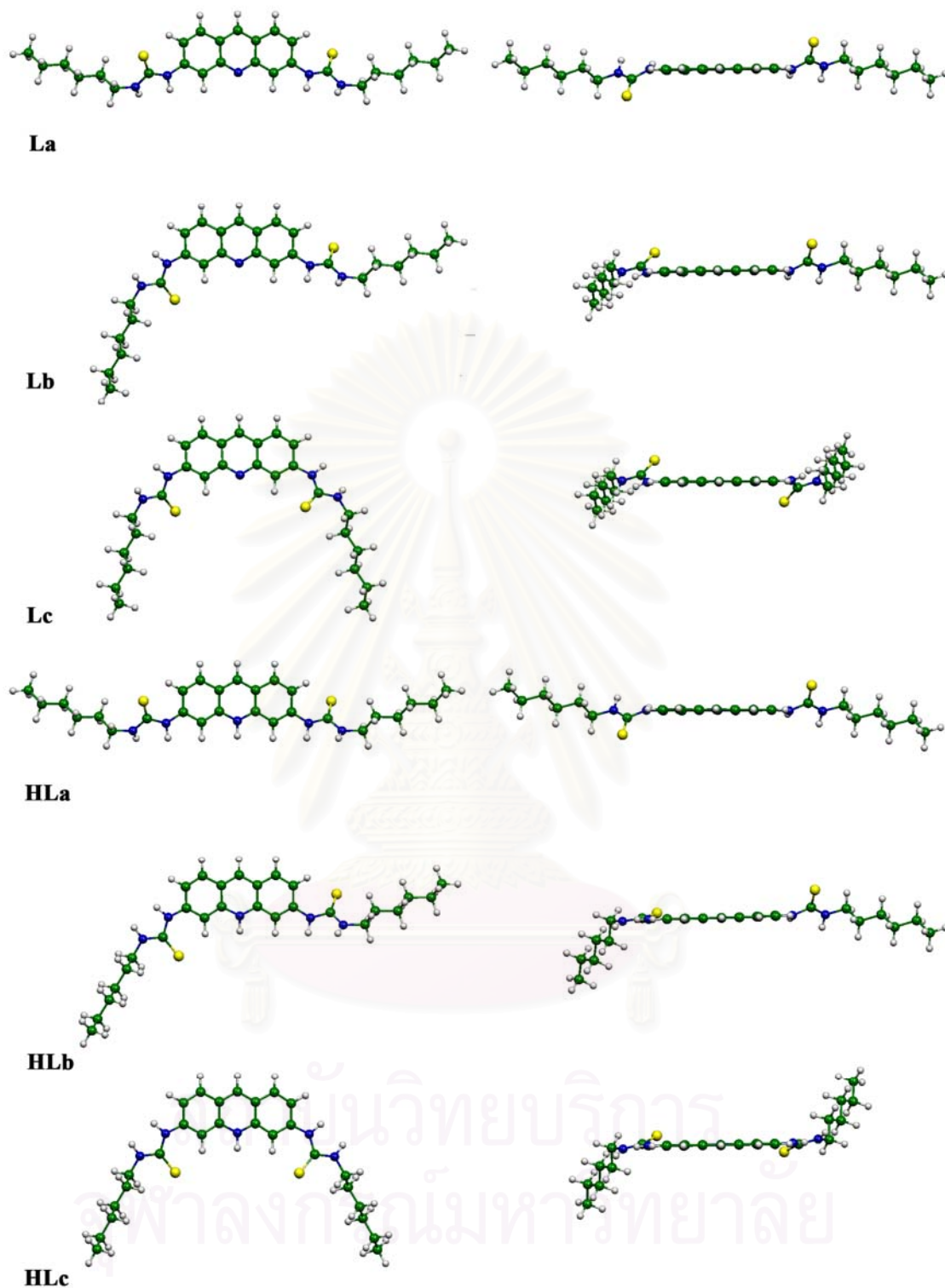


Figure 3.1. B3LYP/6-31G(d)-optimized structures of 3,9-di(hexylthioureido)acridine conformers (a) **L1a**, (b) **L1b** and (c) **L1c**, and their protonated forms (d) **HL1a**⁺, (e) **HL1b**⁺ and (f) **HL1c**⁺ left and right figures are front and top views of their molecular structures, respectively.

Total energies of the compound **L1** conformers and their protonated conformers were computed at ONIOM(B3LYP/6-31G(d):AM1), B3LYP/6-31G(d), B3LYP/6-31G(d)//ONIOM(B3LYP/6-31G(d):AM1), MP2(fc)/6-31G(d)//ONIOM(B3LYP/6-31G(d):AM1) and MP2(fc)/6-31G(d)//B3LYP/6-31G(d) levels and their relative energies are tabulated in Table 3.1. Relative stabilities of the compound **L1** conformers and their protonated species are in decreasing orders: **L1a** > **L1b** > **L1c** and **HL1c**⁺ > **HL1b**⁺ > **HL1a**⁺, respectively.

Table 3.1 Relative energies of 3,9-di(hexylthioureido)acridine conformers and their protonated conformers computed at various levels of theory

Conformer/ system	ΔE (kcal/mol)				
	ONIOM ^a	B3LYP/6- 31G(d)	B3LYP/6- 31G(d)// ONIOM ^a	MP2(fc)/6 -31G(d)// ONIOM ^a	MP2(fc)/6 -31G(d)// B3LYP/6- 31G(d)
<i>Neutral form</i>					
L1a	0.00	0.00	0.00	0.00	0.00
L1b	1.17	1.38	1.17	1.93	1.83
L1c	3.27	3.01	3.27	3.31	3.58
<i>Protonated form</i>					
HL1a	4.18	4.15	4.18	3.53	3.78
HL1b	1.59	1.81	1.59	1.69	1.76
HL1c	0.00	0.00	0.00	0.00	0.00

^a The two-layered ONIOM(B3LYP/6-31G(d):AM1).

Based on the MP2(fc)/6-31G(d)//B3LYP/6-31G(d) calculations, the maximum ranges of relative energies for the neutral and protonated species of compound **L1** conformers are 3.58 kcal/mol and 3.78 kcal/mol, respectively. The protonation of compound **L1** conformers, their reaction energies, enthalpies and Gibbs free energies derived from vibration frequencies calculations at the ONIOM(B3LYP/6-31G(d):AM1) and B3LYP/6-31G(d) levels are shown in Table 3.2. Protonation reactions of the compound **L1** conformers derived from any levels of theory are always exothermic and spontaneous processes. Based on the B3LYP/6-31G(d) method, the protonation enthalpies for conformers **L1a**, **L1b** and **L1c** are -248.07, -251.91 and -255.31 kcal/mol, respectively. The **L1a** conformer is the most stable species of the neutral form and more

stable than that of **L1b** and **L1c** by 1.33 and 3.58 kcal/mol, respectively. On the other hand, the **HL1c**⁺ conformer is the most stable species of the protonated form and more stable than that of **HL1b**⁺ and **HL1a**⁺ by 1.76 and 3.78 kcal/mol, respectively. It should be noted that the molecular energies of either neutral form or protonated forms were hardly different in the gas phase.

Table 3.2 Reaction energies and thermodynamic properties of the protonation of compound **L1** conformers computed at two different levels of theory

Protonation	ONIOM (B3LYP/6-31G(d):AM1)			B3LYP/6-31G(d)		
	ΔE^a	ΔH^a	ΔG^a	ΔE^a	ΔH^a	ΔG^a
L1a + H ⁺ → HL1a ⁺	-246.538	-246.401	-246.684	-248.248	-248.207	-248.082
L1b + H ⁺ → HL1b ⁺	-250.262	-250.116	-251.135	-251.963	-251.907	-252.312
L1c + H ⁺ → HL1c ⁺	-253.665	-253.489	-255.093	-255.408	-255.308	-257.066

^a In kcal/mol

3.2.2 Conformational and Stability of Compounds **L2** and **L3**.

The structures and total energies of compounds **L2** and **L3** optimized at the B3LYP/6-31G(d) levels were obtained. In contrast to compound **L1**, compounds **L2** and **L3** were shown just only one minimized structure because of more bulky structure. The intramolecular hydrogen bonds between quinone oxygen and thiourea NH protons of compound **L2** were observed and shown in Figure 3.2. The anthracene signaling unit of compound **L3** was slightly distorted. The dihedral angles between two aromatic rings are 2.233 Å and 8.799 Å for compounds **L2** and **L3**, respectively. The distortion of compound **L3** should be resulted from the repulsion between four partial positive thiourea NH hydrogens and/or between thiourea NH hydrogens and the anthracene aromatic proton located in the center of the cavity.

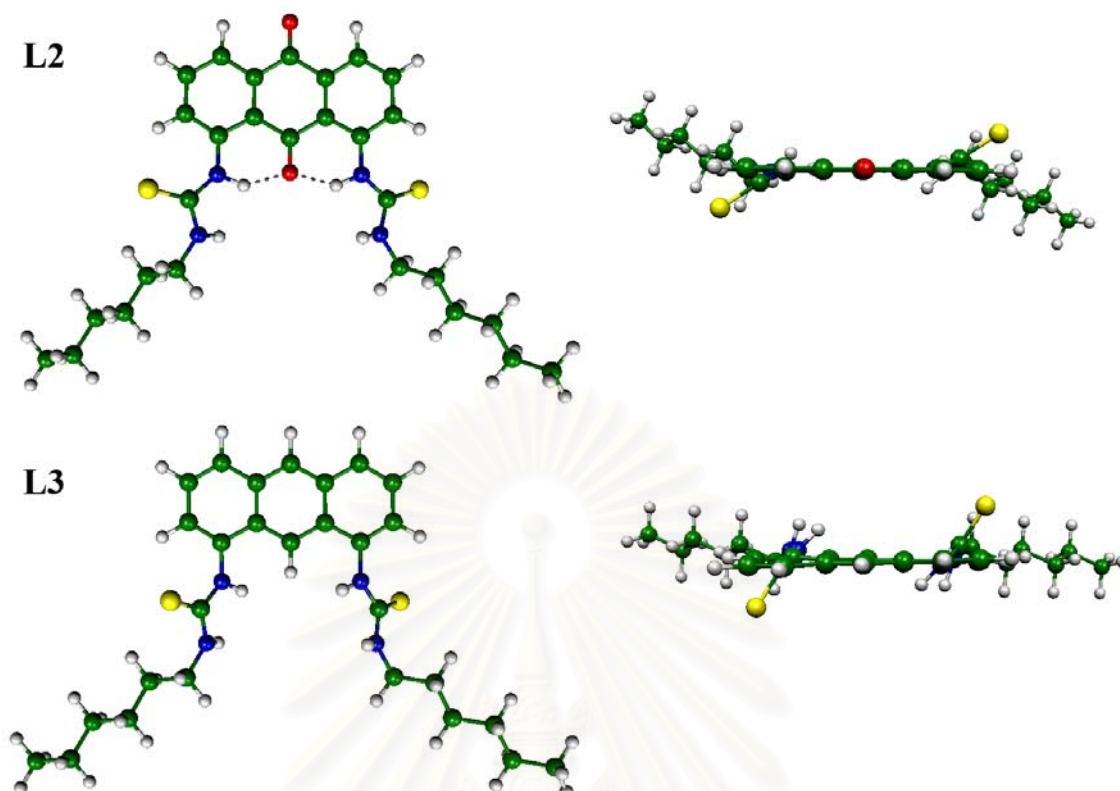


Figure 3.2. B3LYP/6-31G(d)-optimized structures of **L2** and **L3** conformer (a) **L2** and (b) **L3**. Left and right figures are front and top views of their molecular structures, respectively.

3.2.3 Conformational and Stability of Compounds **L4** and **L5**.

The structures of all conformers of compounds **L4** and **L5** optimized at the B3LYP/6-31G(d) and two-layered ONIOM(B3LYP/6-31G(d):AM1) levels were obtained. The geometrical parameters for the B3LYP/6-31G(d)-optimized structures of compounds **L4** and **L5** conformers structures are listed in Figure 3.3.

Total energies of the compounds **L4** and **L5** conformers were computed at the ONIOM(B3LYP/6-31G(d):AM1) and B3LYP/6-31G(d) levels and their relative energies are tabulated in Table 3.3. Relative stabilities of conformers of compounds **L4** and **L5** are decreasing in the following orders: **L4a** > **L4b** > **L4c** and **L5a** > **L5b** > **L5c**, respectively.

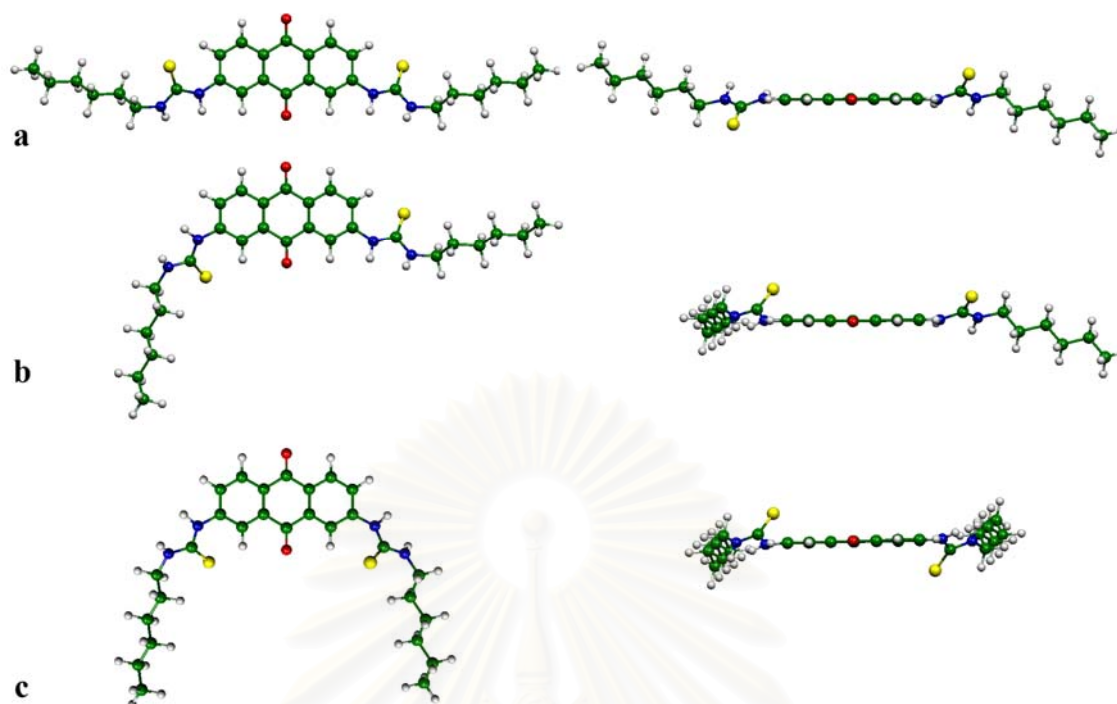


Figure 3.3. B3LYP/6-31G(d)-optimized structures of 2,7-di(hexylthioureido)anthracene-9,10-dione (**L4**) conformers (a) **L4a**, (b) **L4b** and (c) **L4c**. Left and right figures are front and top views of their molecular structures, respectively.

Table 3.3 Reaction energies of conformers of compounds **L4** and **L5** computed at two different levels of theory

Ligand	ONIOM		B3LYP/6-31G(d)	
	E(au)	ΔE_{rel} (kcal/mol)	E(au)	ΔE_{rel} (kcal/mol)
L4a	-1782.296409	0.00	-2253.96125	0.00
L4b	-1782.294726	1.06	-2253.95957	1.05
L4c	-1782.292911	2.20	-2253.95789	2.11
L5a	-1633.032265	0.00	-2104.69662	0.00
L5b	-1633.031918	0.22	-2104.69614	0.30
L5c	-1633.031204	0.67	-2104.69526	0.85

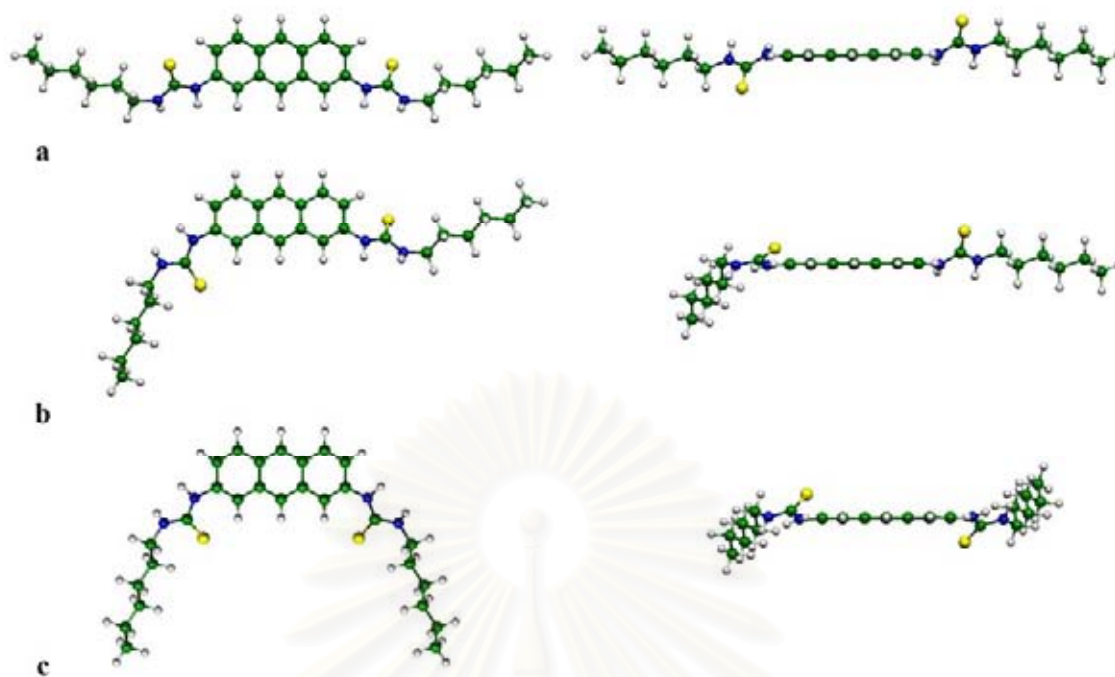


Figure 3.4 B3LYP/6-31G(d)-optimized structures of 2,7-di(hexylthioureido) anthracene conformers (a) **L5a**, (b) **L5b** and (c) **L5c** left and right figures are front and top views of their molecular structures, respectively.

3.2.4 Electronic Structure of Compounds **L1** and **HL1**

Energies of the highest occupied molecular orbital (HOMO), E_{HOMO} , the lowest unoccupied molecular orbital (LUMO), E_{LUMO} and the frontier molecular orbital energy gap, $\Delta E_{\text{HOMO-LUMO}}$ are shown in Table 3.4. Relative reactivities of the neutral and protonated species of compound **L1** conformers are in orders: **L1c** > **L1b** > **L1a** and **HL1a**⁺ > **HL1b**⁺ > **HL1c**⁺, respectively. As the **L1c** conformer is the most active structure of the neutral species, its protonation is therefore the most favorable reaction and the most stable structure of the protonated species such as an **HL1c**⁺ is then formed. The **HL1c**⁺ conformer is therefore the least active species of the protonated species. The chemical hardnesses of all species are in order: **L1a** > **L1b** > **L1c** > **HL1c**⁺ > **HL1b**⁺ > **HL1a**⁺. Mulliken electronegativities of the neutral and protonated species of **L1** derived from their chemical potentials are within 3.547 to 3.662 and 6.981 to 7.010, respectively. The B3LYP/6-31G(d)-computed HOMOs and LUMOs for all species of compound **L1** are shown in Figure 3.6. LUMOs of the neutral structures **L1a**, **L1b** and **L1c** shown in Figure 3.6 are very similar to their corresponding orbitals of the protonated structures **HL1a**⁺, **HL1b**⁺ and **HL1c**⁺, respectively. HOMOs of the neutral structures of compound

L1 are obviously situated on apex carbon and nitrogen atoms of the acridine ring but never situated on any atoms of the acridine ring of the protonated structures. This phenomenon shows that a valence electron in molecular orbitals of the neutral form transfer to amino-proton atom (H5) which is located at the middle of the acridine ring to enhance the protonated structure.

Table 3.4 The E_{HOMO} , E_{LUMO} and frontier molecular orbital energy gap, $\Delta E_{\text{HOMO-LUMO}}$ of the 3,9-di(hexylthioureido)acridine conformers and their corresponding protonated forms computed at the B3LYP/6-31G(d) level of theory

species	E_{HOMO}^a	E_{LUMO}^a	$\Delta E_{\text{HOMO-LUMO}}^a$	$\eta^{a,b}$	$\mu^{a,c}$	$\chi^{a,d}$
L1a	-5.391	-1.933	3.458	1.729	-3.662	3.662
L1b	-5.303	-1.899	3.404	1.702	-3.601	3.601
L1c	-5.223	-1.872	3.351	1.675	-3.547	3.547
HL1a	-8.192	-5.803	2.389	1.195	-6.997	6.997
HL1b	-8.179	-5.783	2.396	1.198	-6.981	6.981
HL1c	-8.264	-5.755	2.509	1.255	-7.010	7.010

^a In eV. ^b Chemical hardness, $\eta = \Delta E_{\text{HOMO-LUMO}}/2$.

^c Electronic chemical potential, $\mu = (E_{\text{HOMO}} + E_{\text{LUMO}})/2$.

^d The Mulliken electronegativity, $\chi = -(E_{\text{HOMO}} + E_{\text{LUMO}})/2$.

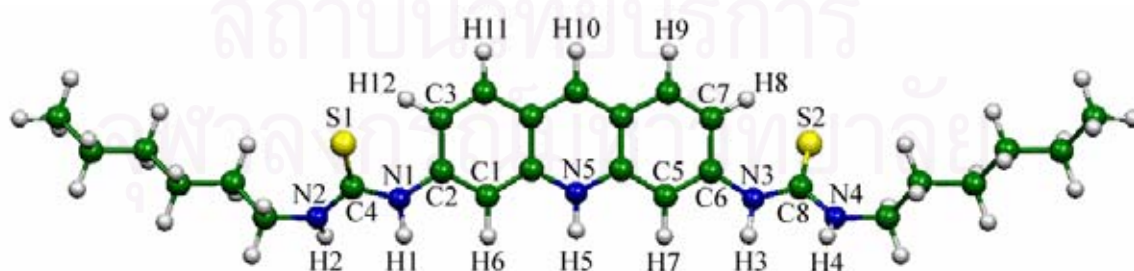


Figure 3.5 Atomic labeling of the 3,9-di(hexylthioureido)acridine.

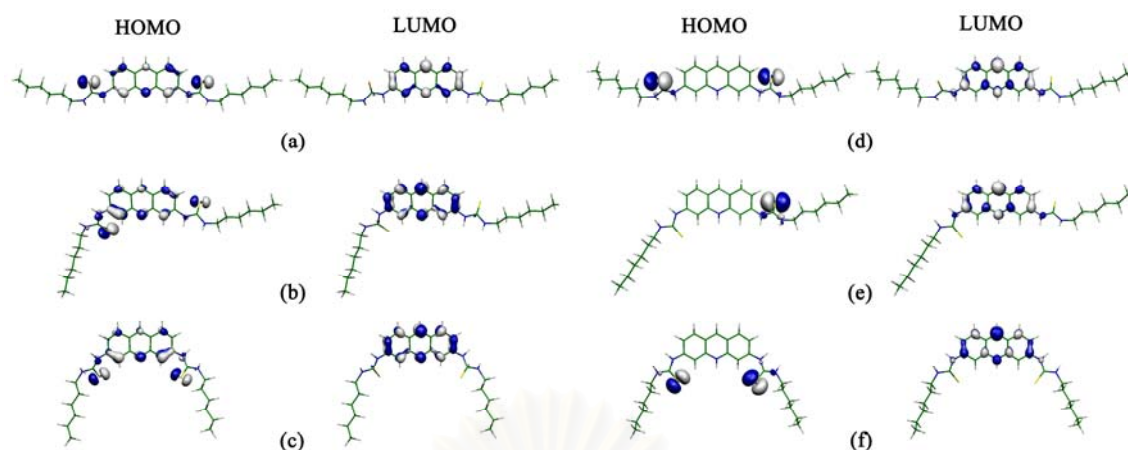


Figure 3.6 The B3LYP/6-31G(d)-computed molecular orbitals contoured at an iso-surface value of 0.05 a.u. for LUMO and HOMO of conformers (a) **L1a**, (b) **L1b**, (c) **L1c**, (d) **HL1a**⁺, (e) **HL1b**⁺ and (f) **HL1c**⁺.

Electrostatic potential surfaces of the neutral and protonated structures of compound **L1** conformers were generated from the Gaussian output files of their B3LYP/6-31G(d) computation with GFPRINT and POP=FULL keywords using the Molekel 4.3 software.⁽⁷³⁾ Electrostatic potential surfaces (in a.u.) presented over electronic isodensity $\rho = 0.05 \text{ eA}^{-3}$ for **L1a**, $V_s = 31.5436$, **L1b**, $V_s = 87.5226$, **L1c**, $V_s = 63.9896$, **HL1a**⁺, $V_s = 18.3433$, **HL1b**⁺, $V_s = 45.3886$ and **HL1c**⁺, $V_s = 101.865$ are shown in Figure 3.7. The color maps of electronic isodensity surfaces in Figure 3.7 show strong negative charge on the imino-nitrogen atom (N5 as shown in Figure 3.5) for the neutral structures but show weak negative charge on the amino-nitrogen atoms (N1, N2, N3 and N4) for the protonated structures. Nevertheless, amino-hydrogen atoms of thiourea groups of either the neutral or protonated conformers show strong positive charges.

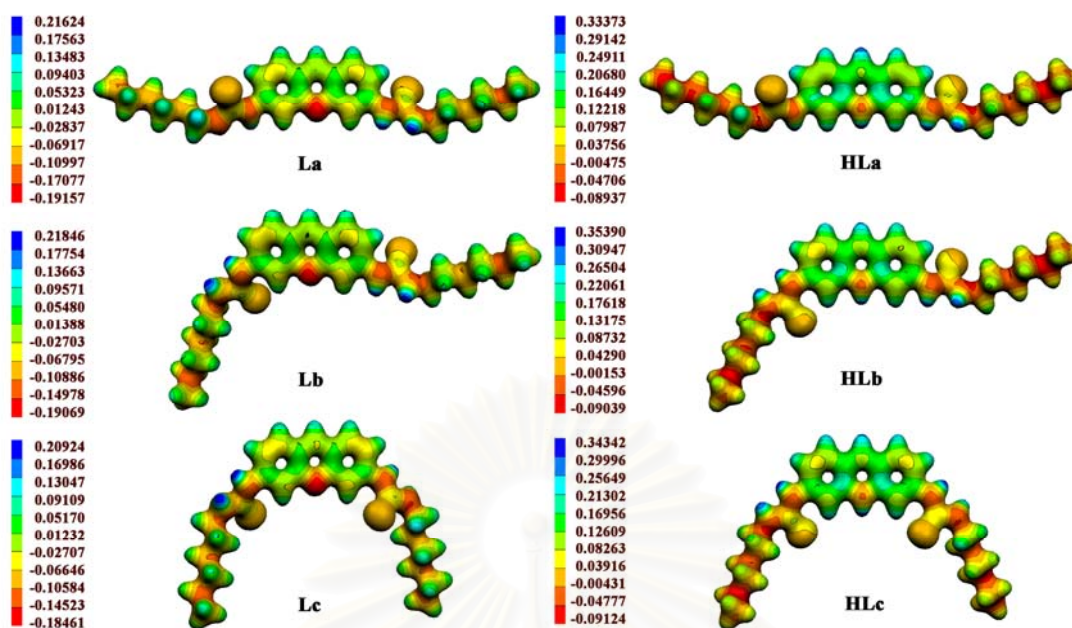


Figure 3.7 Electronic potential surface (in a.u.) presented over electronic isodensity $\rho=0.05 \text{ eA}^{-3}$ for (a) **L1a**, $V_s=31.5436$, (b) **L1b**, $V_s=87.5226$, (c) **L1c**, $V_s=63.9896$, (d) **HL1a**⁺, $V_s=18.3433$, (e) **HL1b**⁺, $V_s=45.3886$ and (f) **HL1c**⁺, $V_s=101.865$.

3.2.5 ¹H NMR Chemical Shifts of Compounds L1 and HL1 Species

The B3LYP/6-31G(d)-computed proton chemical shifts for conformers of the neutral and protonated species of compound **L1** are shown in Table 5. The ¹H NMR spectra of compound **L1** conformers and their corresponding protonated forms in DMSO referenced to TMS were obtained at 298.15 K. Based on the principle of weighted-average chemical shift,⁽⁷⁴⁾ a single peak of the observed ¹H NMR chemical shift is an average value of the corresponding protons of all present conformers. The single peak of H5 chemical shift ($\delta_{\text{observed}}^{\text{H5}}$) of the protonated species can be evaluated by the following weighted-average equation.

$$\delta_{\text{observed}}^{\text{H5}} = \delta_{\text{HL1a}^+}^{\text{H5}} \cdot f_{\text{HL1a}^+} + \delta_{\text{HL1b}^+}^{\text{H5}} \cdot f_{\text{HL1b}^+} + \delta_{\text{HL1c}^+}^{\text{H5}} \cdot f_{\text{HL1c}^+},$$

where $\delta_{\text{HL1a}^+}^{\text{H5}}$, $\delta_{\text{HL1b}^+}^{\text{H5}}$ and $\delta_{\text{HL1c}^+}^{\text{H5}}$ are H5 chemical shifts of conformers **HL1a**⁺, **HL1b**⁺ and **HL1c**⁺ and f_{HL1a^+} , f_{HL1b^+} and f_{HL1c^+} are their mole fractions, respectively. As the **HL1c**⁺ is the most stable conformer, the mole fraction of **HL1c**⁺ therefore approaches unity and

others approach zero and $\delta_{\text{observed}}^{\text{H5}} = \delta_{\text{HL1c}^+}^{\text{H5}}$ was possibly assumed. As the **HL1c⁺** is the most stable conformer of compound **L1** and its C_{2v} symmetry, the proton chemical shifts of its equivalent protons in which H1 and H3, H2 and H4, H6 and H7, H8 and H12, and H9 and H11 are equivalent, are therefore expected to correspond to the measured ^1H NMR spectrum, (Figure 3.8 and Table 3.5). For the neutral system of the 3,9-di(hexylthioureido)acridine, chemical shifts of H1 ($\delta_{\text{observed}}^{\text{H1}}$) which is equivalent to H3, was expected to approach the H1 chemical shift of the La ($\delta_{\text{La}}^{\text{H1}}$) which is the most stable conformer. As the **L1a** is the most stable conformer of compound **L1** and its C_{2v} symmetry, the proton chemical shifts of its equivalent protons are therefore expected to correspond to the measured ^1H NMR spectrum, (Figure 3.8 and Table 3.5).

Table 3.5 ^1H NMR chemical shifts for the 3,9-di(hexylthioureido)acridine conformers and their corresponding protonated forms

Species	^1H NMR ^a							
	computed ^b			measured ^c	computed ^b			measured ^d
	L1a	L1b	L1c		HL1a ⁺	HL1b ⁺	HL1c ⁺	
H1	7.94	7.74	7.80	9.93	8.07	8.08	8.02	10.49
H2	6.58	6.51	6.56	8.22	7.13	6.99	7.08	9.08
H3	7.94	7.88	7.80	9.93	8.07	8.08	8.02	10.49
H4	6.58	6.58	6.56	8.22	7.13	7.17	7.08	9.08
H5	-	-	-	-	9.47	10.24	10.34	15.29
H6	7.84	9.17	9.16	8.30	7.43	10.13	9.95	8.58
H7	7.84	7.79	9.16	8.30	7.43	7.45	9.95	8.58
H8	8.78	8.87	7.62	7.58-7.60	8.89	8.93	7.69	7.58-7.60
H9	8.58	8.56	8.56	8.036-8.05	8.74	8.72	8.77	8.25-8.27
H10	9.18	9.19	9.07	8.88	10.14	9.45	9.40	9.46
H11	8.58	8.68	8.56	8.036-8.05	8.74	8.78	8.77	8.25-8.27
H12	8.78	7.61	7.62	7.58-7.60	8.89	7.71	7.69	7.58-7.60

^a In ppm based on the tetramethylsilane (TMS, 32.1687 ppm) reference, computed at the B3LYP/6-31G(d) level with IEFPCM model in DMSO.

^b In DMSO using the IEFPCM model ($\epsilon = 46.7$) at the B3LYP/6-31G(d) level.

^c The values are expected to correspond the L1a conformer.

^d The values are expected to correspond the HL1c⁺ conformer.

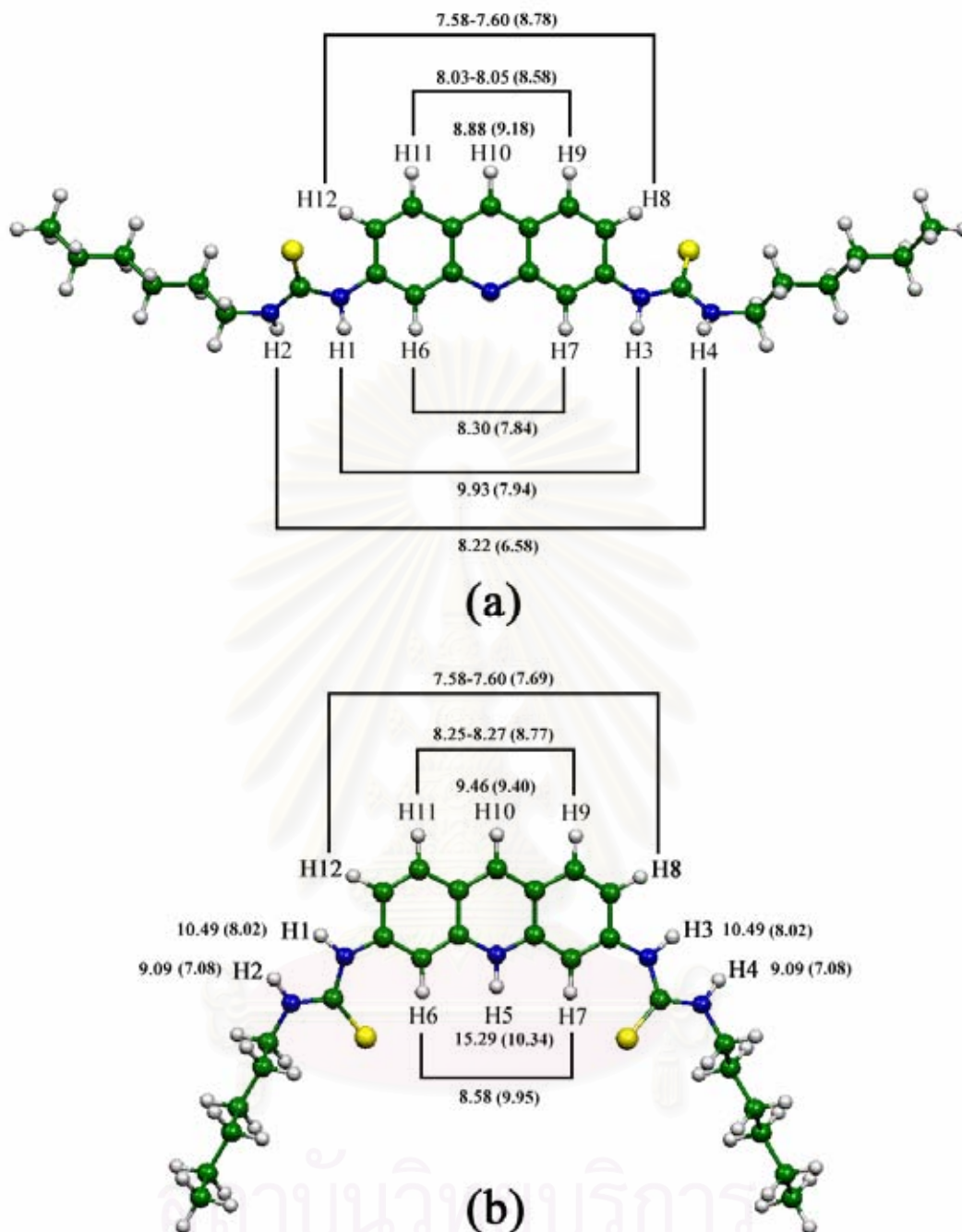


Figure 3.8 Proton chemical shifts of the measured and B3LYP/6-31G(d)-computed ^1H -NMR (in parenthesis) of the most stable structure of (a) the neutral and (b) protonated forms of 3,9-di(hexylthioureido) acridine conformers. The chemical shifts are in ppm referenced to the TMS standard.

3.2.6 FT-IR Spectra of Compound L1 and HL1 Species

Vibration frequencies of the neutral and protonated species of compound **L1** were computed at the B3LYP/6-31G(d) level and obtained from the measurement in potassium bromide method using Nicolet Impact 410 FT-IR spectrometer at room temperature. The measured and computed IR spectra are shown in Figure 3.9 and their selected vibration modes are listed in Table 3.6. The computed spectra in Figure 3.9 are derived from the B3LYP/6-31G(d) vibration frequencies of which wave numbers were corrected using empirical scaling factor of 0.9641 determined by Scott and Radom.⁽⁷⁵⁾ This figure shows equivalences of N-H and C-H protons chemical shifts for the neutral species **L1a** and protonated **HL1c⁺** according to their C₂-molecular symmetries. Table 3.6 shows the NH stretching of N-H5 (mode 17) of **HL1c⁺** species at 3426.5 cm⁻¹ which is combined with NH stretching of H2 and H4 at 3432.1 cm⁻¹ appearing as one peak as shown in Figure 3.44 (b). Nevertheless, these vibration modes are not possible to be certainly assigned for the experimental IR spectra. Difference between IR spectral peaks of protonated (**HL1c⁺**) and neutral (**L1a**) structures appearing within 1430 to 1300 cm⁻¹ are able to be observed in Figure 3.9. This region contains at least three vibration modes of NH bending of H5 proton.

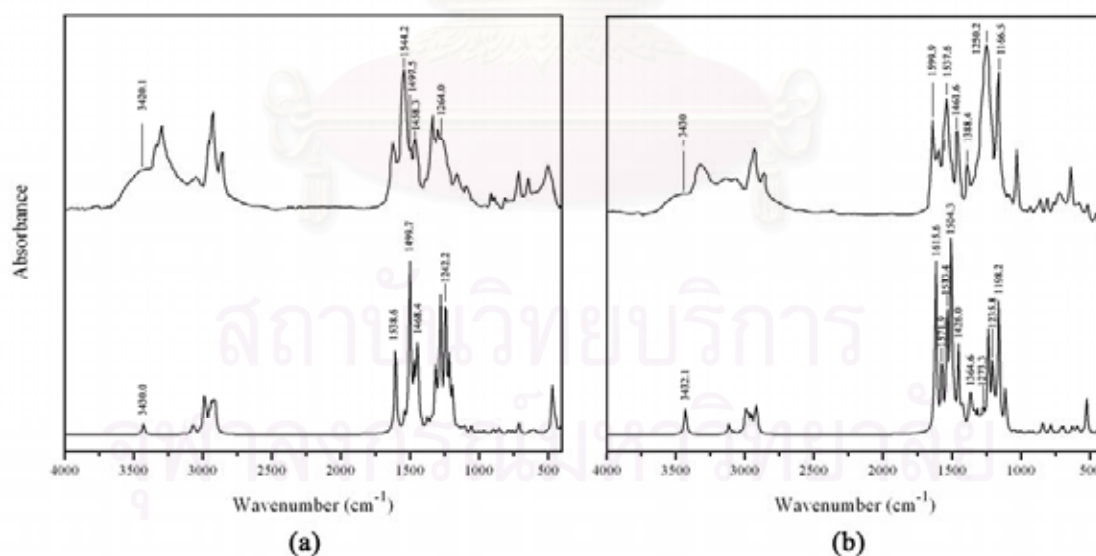


Figure 3.9 FT-IR spectra of the (a) neutral and (b) protonated forms of **L1** Top and bottom are the measured and computed infrared spectra, respectively. The computed IR spectra are of the most stable species, **L1a** and **HL1c⁺**.

Based on the computed vibration spectra, the N-H stretching absorption bands, ν_{NH} are at 3430.0 cm^{-1} for the neutral form and 3432.1 with 3426.5 cm^{-1} for the protonated form. The absorption peaks at 3441.7 and 3387.9 cm^{-1} of the protonated structure belong to the thiourea NH groups (N-H1, N-H2, N-H3 and N-H4) and imino NH, respectively. The N-H bending absorption bands, δ_{NH} are at 1513.6 cm^{-1} for the neutral form and 1576 cm^{-1} for the protonated species.

Table 3.6 Selected wave numbers (cm^{-1}) and their corresponding intensities of the B3LYP/6-31G(d)-computed and observed IR vibration modes for the neutral and protonated species of 3,9-di(hexylthioureido)acridine. The computed IR vibration frequencies were scaled by 0.9614

Mode/Species	Computed Frequency ^a	IR intensities ^b	Observed Frequency ^a	Assignment ^c
<i>Neutral form</i> ^d				
1	1242.2	731	1264.0	NH _(1,2,3,4) bending + CH bending
2	1468.4	253	1458.3	NH _(1,2,3,4) bending
3	1499.7	837	1497.5	NH _(2,4) bending + CH bending
4	1538.6	82	1544.2	NH _(1,3) bending
5	3430.0	28	3420.1	NH _(1,2,3,4) stretching
<i>Protonated form</i> ^e				
6	1198.2	149	1166.5	NH ₍₅₎ bending + CH bending
7	1235.8	688	1250.2	NH _(1,3) bending + CH bending
8	1273.3	144	- ^f	NH ₍₅₎ bending + CH bending
9	1364.6	192	1388.4	NH ₍₅₎ bending + CC bending
10	1426.0	143	1461.6	NH ₍₅₎ bending + CH bending
11	1504.3	1259	- ^f	NH _(2,4) bending
12	1533.4	761	1537.6	NH _(1,2,3,4) stretching
13	1571.9	360	1599.9	NH _(1,3) bending
14	1615.6	1086	1640.0	NH ₍₅₎ bending + CH bending
15	3418.9	23	- ^g	NH _(3,4) stretching
16	3419.1	17	- ^g	NH _(1,2) stretching
17	3426.5	31	- ^g	NH ₍₅₎ stretching
18	3432.1	129	~ 3430	NH _(2,4) stretching

^a In cm^{-1} . ^b In km/mol . ^c The numbers in parentheses refer to hydrogen atoms of which numbers are defined in Fig. 1. ^d Based on La structure. ^e Based on **HL1c**⁺ structure.

^f No assignment. ^g They are combined to broaden peak at $\sim 3500 \text{ cm}^{-1}$.

3.3 Investigation of Binding Ability

All Compounds contain thiourea units for binding anions. This research aimed to compare the binding ability of synthetic compounds towards anions. Because of their importance in environmental and biological systems, dicarboxylate anions such as oxalate, malonate, succinate, glutarate, adipate and pimilate were chosen for studies. Anion binding studies of all compounds were carried out by ^1H NMR titrations, UV-Vis titration, fluorescence titration and cyclic voltammetry. Compounds **L1**, **L4** and **L5** contain thiourea moieties in the same position so the distance between two thiourea groups must be equal. Compounds **L2** and **L3** have shorter length between the receptor unit than those of compounds **L1**, **L4** and **L5**. The difference between compounds **L1**, **L4** and **L5** or between compounds **L2** and **L3** is different signaling units. The anion recognition *via* multi hydrogen-bonding interactions can also be easily monitored by anion-complexation induced change in ^1H -NMR spectra, cyclic voltammograms, fluorescence emission spectra, UV-vis absorption spectra and the naked eye.

3.3.1 The Complexation Studies of Synthetic Compounds with Various Dicarboxylate Anions by Using ^1H -NMR Titrations

The stability of the host-guest adducts is strongly dependent on the polarity of the media. In fact, salts are present as ion pairs or more likely as aggregates of ion pairs in apolar media. Comparison to a CDCl_3 solution which show strongly ion-pair effect, the free species which release from the ion pairs are determined to be more in the other more polar deuterated solvents such as CD_3OD , CD_3CN or $\text{DMSO-}d_6$.

Methanol is a typical protic or a hydrogen bond donor (HBD) solvent. On the contrary, dimethylsulfoxide and acetonitrile are solvents that commonly referred to as aprotic solvents, but they are in fact not aprotic (solvent without proton donor groups). In reactions where strong bases are employed, their protic character can be recognized. Hence, the term aprotic solvents should be replaced by nonhydroxylic or better by non-HBD solvents.⁽⁴⁷⁾

The electron pair donor and acceptor are one of the main criteria for complexation in supramolecular chemistry. In principle, a donor is able to form a complex with a receptor. Hereby, an electron pair donor (EPD) and an electron pair acceptor (EPA)

solvent should form a complex. Some solvents act as donors (nucleophiles) while some solvents serve as acceptors (electrophiles).

In principle, all solvents are amphoteric in this respect. EPD solvents are particularly important for cation complexation. The high EPD-properties make the solvent to be excellent cation solvators which is known as coordinating solvents. An empirical semiquantitative measure of the nucleophilic properties of EPD solvents is provided by the donor number *DN* (or donicity) of Gutmann.

Table 3.7 Donor numbers determined calorimetrically in dilute 1,2-dichloroethane solution at room temperature

Solvents	DN/kcalmol ⁻¹
Acetone	14.1
Acetonitrile	17.0
Dimethyl sulfoxide	29.8

Table 3.7 exhibits the donor numbers of some solvents. The higher of the donor number reflect to the stronger of the interaction between the solvent and the acceptor. The donor number has proven very useful in coordination chemistry, since it can be correlated with other physical properties for such reactions, e.g. thermodynamic (ΔG or K), kinetic (rates), electrochemistry (polarographic half-wave and redox potentials), and spectroscopy (chemical shifts of NMR signals).

Reciprocally, EPA solvents play a particular important role for anion complexation. An analogous empirical quantity for characterizing the electrophilic properties has been named acceptor number *AN* (acceptivity). Some organic solvents in the order of increasing acceptor numbers are given in Table 3.8.

Table 3.8 Acceptor numbers which are determined ^{31}P -NMR spectroscopically at 25 °C

Solvents	AN
Acetone	12.5
Acetonitrile	18.9
Dimethyl sulfoxide	19.3
Dichloromethane	20.4
Chloroform	23.1
Methanol	41.5
Water	54.8

In our preliminary experiments, we found that all ligands were able to dissolve in DMSO- d_6 . Moreover, either tetrabutylammonium anions or cation hexafluorophosphate salt that used in this thesis hardly dissolved in DMSO- d_6 and CD $_3$ CN. Therefore, CD $_3$ CN and DMSO- d_6 were perfect solvents for the whole experiments. The competitive interaction between the anion and the solvent from using DMSO- d_6 and CD $_3$ CN were also found. However, this effect is less than that from water.

For ^1H -NMR spectroscopy, this technique allows access to the detail of the interaction between a host and a guest molecule and has been widely employed to investigate receptor-substrate interactions. Therefore the binding ability of the novel multidentate thiourea receptors based on anthracene derivatives building block in dimethylsulfoxide- d_6 was investigated by ^1H -NMR titration technique to determine the stoichiometry of the complexes, association constant and Gibbs free energy. The concentration of hosts in this experiment is ~0.01 mol/L while the stock solution of guests is 10 fold-higher in concentration. No effort was made to maintain a constant pH, but care was taken to avoid water absorption from the atmosphere. The calculated association constants for the different curves were within 10% of the error.

All synthetic compounds contain four thiourea NH groups as hydrogen bond donors for binding dicarboxylate anions ($^-\text{O}_2\text{C}(\text{CH}_2)_n\text{CO}_2^-$). Compounds **L1-L5** have different position of thiourea group in anthracene derivatives suitable for recognition studies with dicarboxylate anions having various chain lengths. Thus, complexation studies of all synthetic compounds with dicarboxylate anions such as

tetrabutylammonium (TBA) acetate, oxalate, malonate, succinate, glutarate, adipate and pimelate were carried out.

We designed all compounds to have long alkyl chains in order to make them soluble in aprotic solvents such as CD_3CN and CDCl_3 . Nevertheless, they can dissolve in only protic solvents such as CH_3OH and $\text{DMSO-}d_6$. Hydrogen bonding plays a particularly important role in interactions between anions and protic solvents. Hence, protic solvents were good anion solvators. Therefore, $\text{DMSO-}d_6$ was used in all NMR titration experiments.

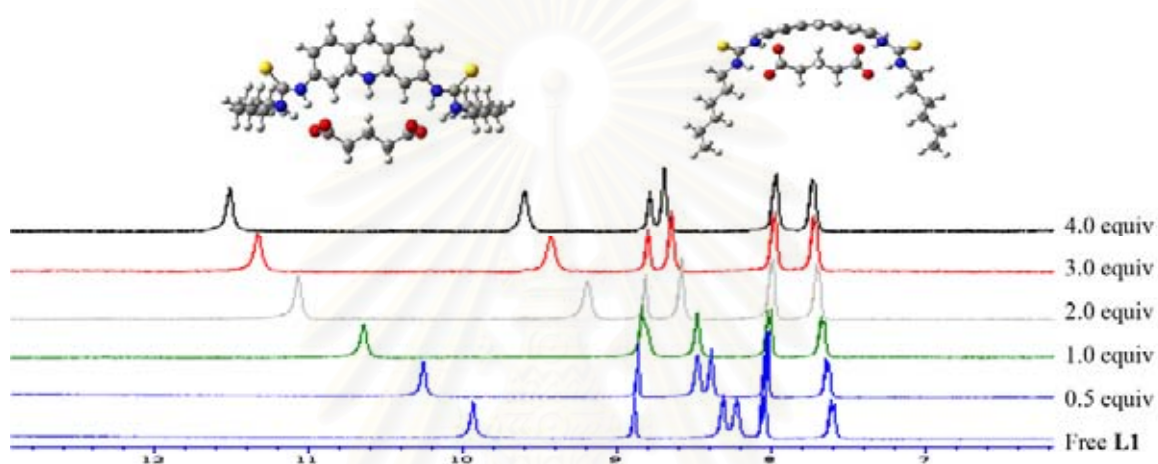


Figure 3.10 $^1\text{H-NMR}$ spectra of **L1** and glutarate in $\text{DMSO-}d_6$ with 400 MHz.

$^1\text{H-NMR}$ spectra of compounds **L1** with and without dicarboxylate anions in $\text{DMSO-}d_6$ at room temperature were recorded. The $^1\text{H-NMR}$ spectrum of compound **L1** showed a broad signal at 8.220 ppm due to the NH proton of one thiourea group and a signal at 9.934 ppm due to the NH proton that was adjacent to the aromatic ring. Upon addition of dicarboxylate anions, both signals of the NH protons shifted remarkably downfield as shown in Tables 3.9. The data in Tables 3.9 indicated that all carboxylate anions form complexes with compounds **L1** *via* hydrogen-bonding interactions between the thiourea and carboxylate groups. For example, all NH signals in $^1\text{H-NMR}$ spectra of titrations between **L1** with glutarate shifted downfield as shown in Figures 3.10.

Table 3.9 ¹H-NMR chemical shifts (ppm) for all compounds (in DMSO-*d*₆) in the absence and presence of 1 equiv. of dicarboxylate anions.

anion	L1		L2		L3		L4		L5	
	NH _A ^a	NH _B ^b	NH _A ^a	NH _B ^b	NH _A ^a	NH _B ^b	NH _A ^a	NH _B ^b	NH _A ^a	NH _B ^b
Free form	9.953	8.234	11.046	9.252	9.697	7.855	10.160	8.286	9.759	8.094
Oxalate	10.378	8.556	11.139	9.472	9.925	8.297	11.193	9.253	10.116	8.312
Malonate	10.171	8.444	11.161	9.468	9.814	-	10.362	8.482	9.952	8.230
Succinate	10.397	8.661	11.268	9.779	8.420	8.877	10.892	8.981	10.235	8.485
Glutarate	10.636	8.832	11.263	9.644	10.224	8.566	11.762	9.812	10.337	8.534
Adipate	10.445	8.584	11.184	9.477	10.007	8.388	10.773	8.724	10.180	8.349
Pimilate	10.394	8.514	11.133	9.374	9.977	8.379	11.718	9.739	10.110	8.277

^a thiourea NH that adjacent to aromatic anthraquinone

^b thiourea NH that adjacent to hexyl chain

Addition of more than 1.0 equiv. of dicarboxylate anions showed a slight downfield shift of the NH protons indicated that ligand formed complexes with dicarboxylate anions in a 1:1 stoichiometry (Figures 3.11 to 3.20). The association stoichiometry of **L1**-dicarboxylate anion complexes indicated by the titration curves were confirmed by the continuous variation method (Job's plots). The bell-shaped Job's plots which obtained from the modified data of ¹H-NMR titration of receptor **L1** with 0-100 μL of anionic solution added in DMSO-*d*₆ showed the symmetry curve with maxima for mole ratio $[G]_t / \{[G]_t + [H]_t\}$ about 0.5 or $[G]_t / [H]_t$ of 1 indicating a 1:1 complex (Figure 3.21). $\Delta\delta(1-X)$ is the supramolecular complex concentration as determined by the chemical shift changes ($\Delta\delta$) for the corresponding protons multiplied by their inverse mole fractions (1-X). These were supported by the titration curve for all signals which were fitted well to a 1:1 binding model.

The stoichiometry of **L1**-dicarboxylate anions complex was 1:1 as judged by monitoring the change in the peak positions of NH thiourea proton signal. When a 1:1 complex formation between receptor **L1** and each dicarboxylate anion takes place, the stability constant (β_1) for the equilibrium is expressed as.^[47]

$$\beta_1 = \frac{[HG]}{([H]_0 - [HG])([G]_0 - [HG])}$$

$$\beta_1 = \frac{n_{hg}/[H]_0}{(1 - n_{hg})(R - n_{hg})}$$

where $[H]_0$ represents initial concentration of the host

$[G]_0$ represents initial concentration of the guest

$[HG]$ represents concentration of the complex

$$[HG] = n_{hg}[H]_0$$

$$n_{hg} = \frac{I_{hg}}{I_{hg} + I_h}$$

where I_{hg} represents integration of the complex

I_h represents integration of the host

$$\text{and } R = [G]_0/[H]_0$$

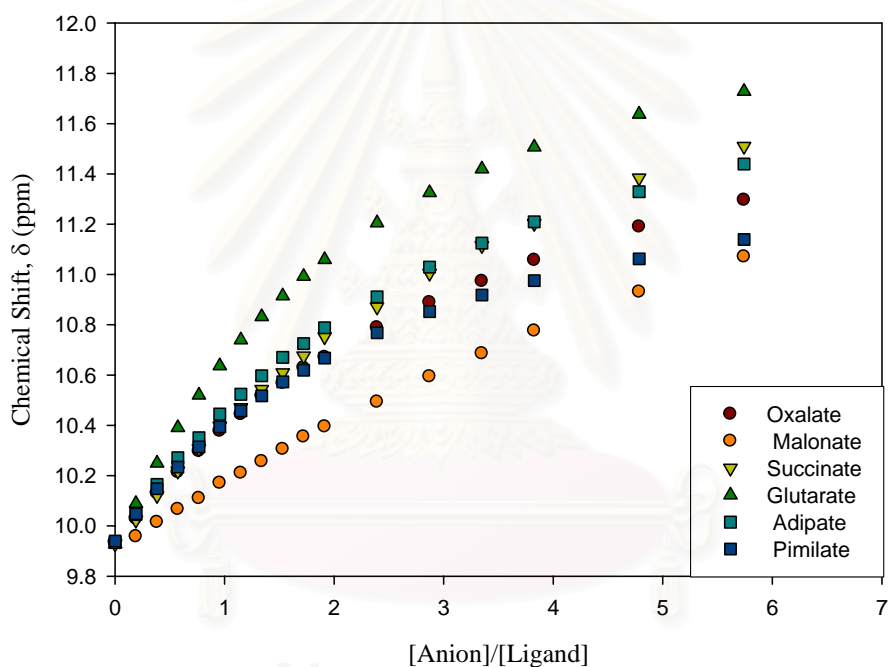


Figure 3.11 Titration curves between **L1** (NH_A) with various dicarboxylate anions in $DMSO-d_6$.

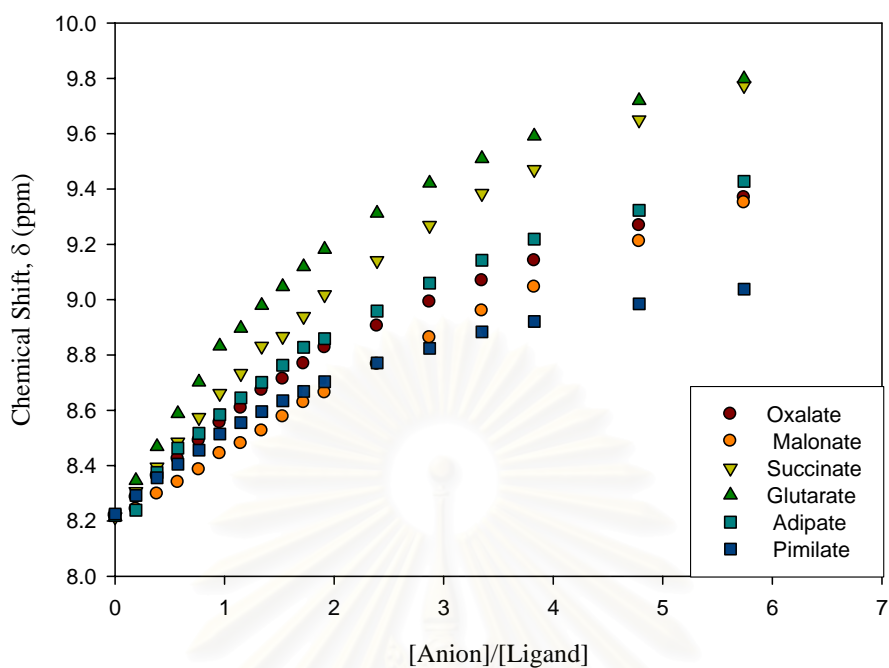


Figure 3.12 Titration curves between **L1** (NH_B) with various dicarboxylate anions in $DMSO-d_6$.

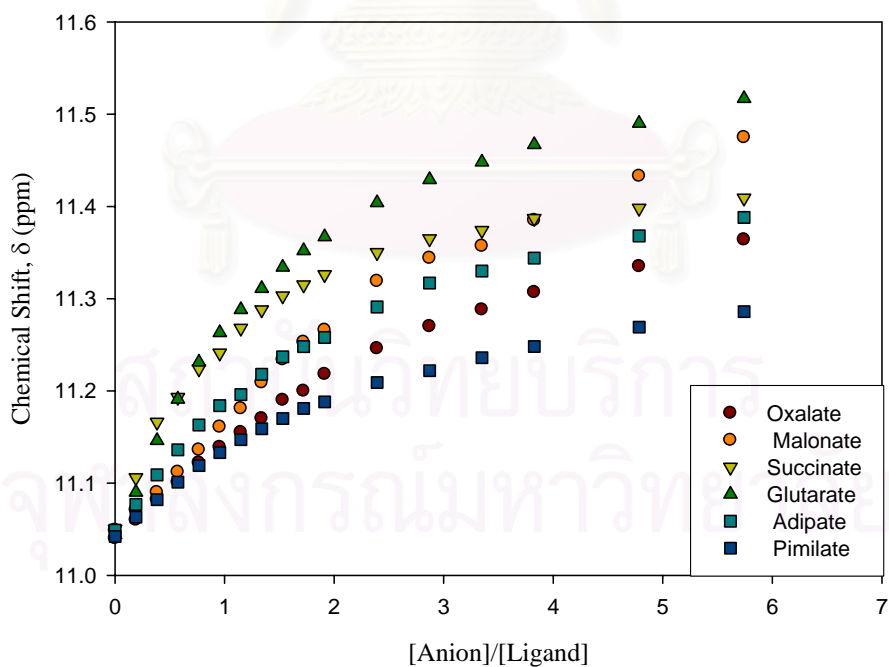


Figure 3.13 Titration curves between **L2** (NH_A) with various dicarboxylate anions in $DMSO-d_6$.

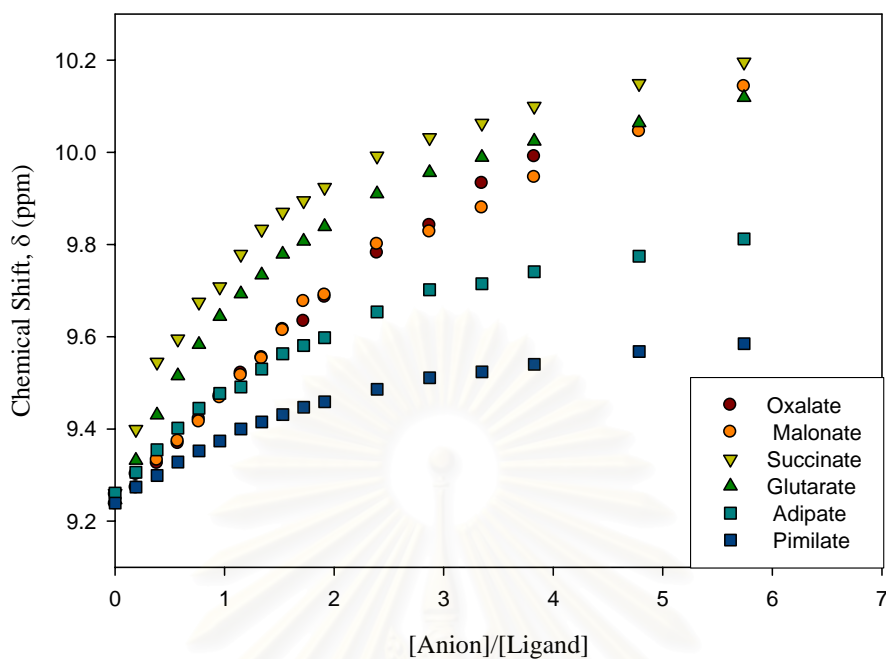


Figure 3.14 Titration curves between **L2** (NH_B) with various dicarboxylate anions in $DMSO-d_6$.

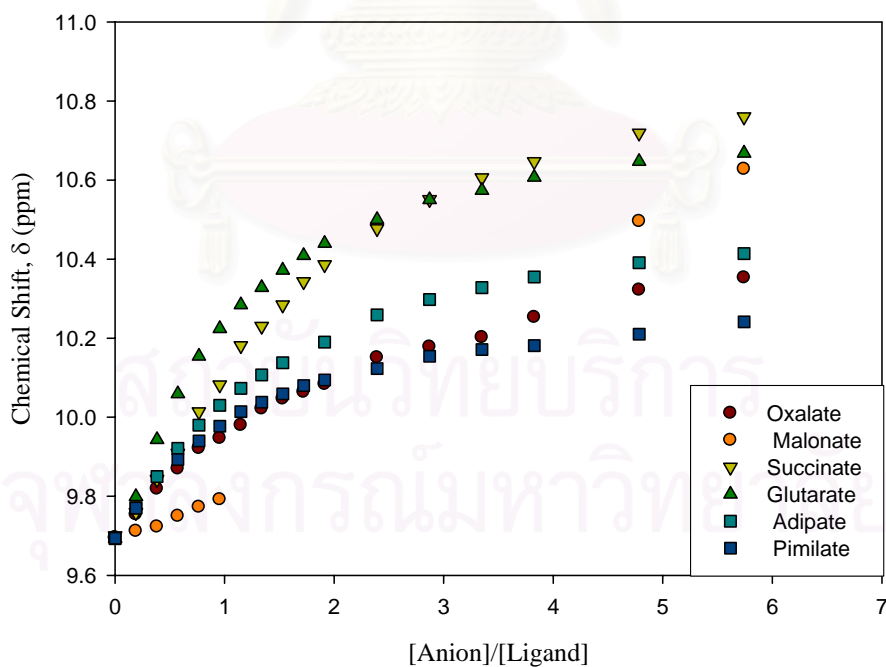


Figure 3.15 Titration curves between **L3** (NH_A) with various dicarboxylate anions in $DMSO-d_6$.

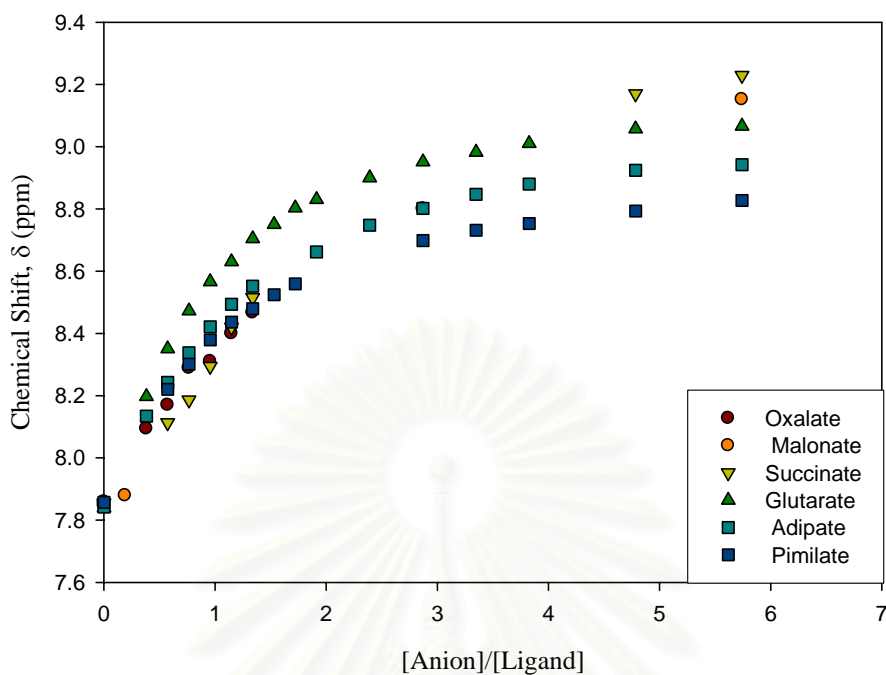


Figure 3.16 Titration curves between **L3** (NH_B) with various dicarboxylate anions in $DMSO-d_6$.

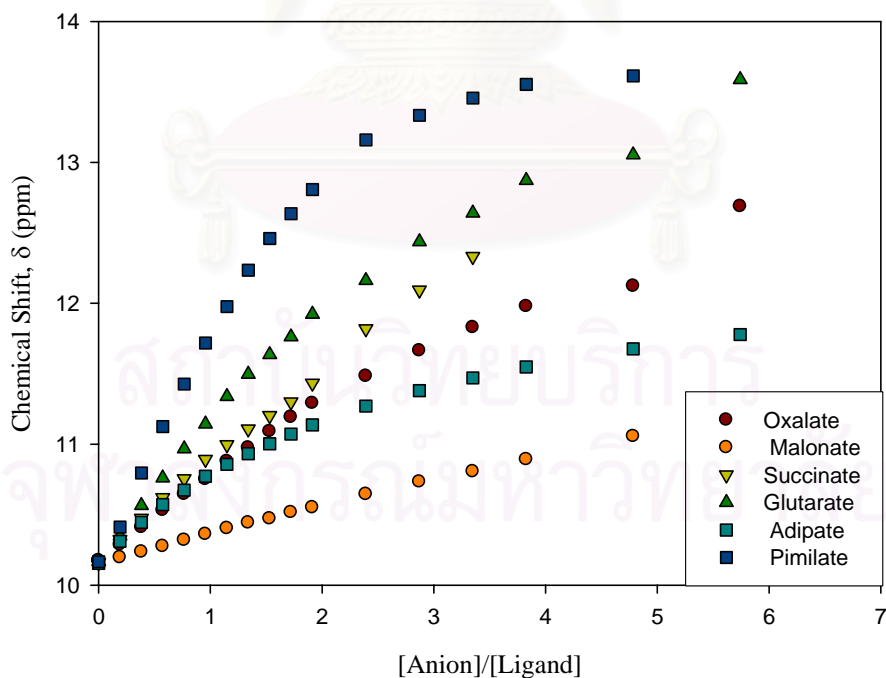


Figure 3.17 Titration curves between **L4** (NH_A) with various dicarboxylate anions in $DMSO-d_6$.

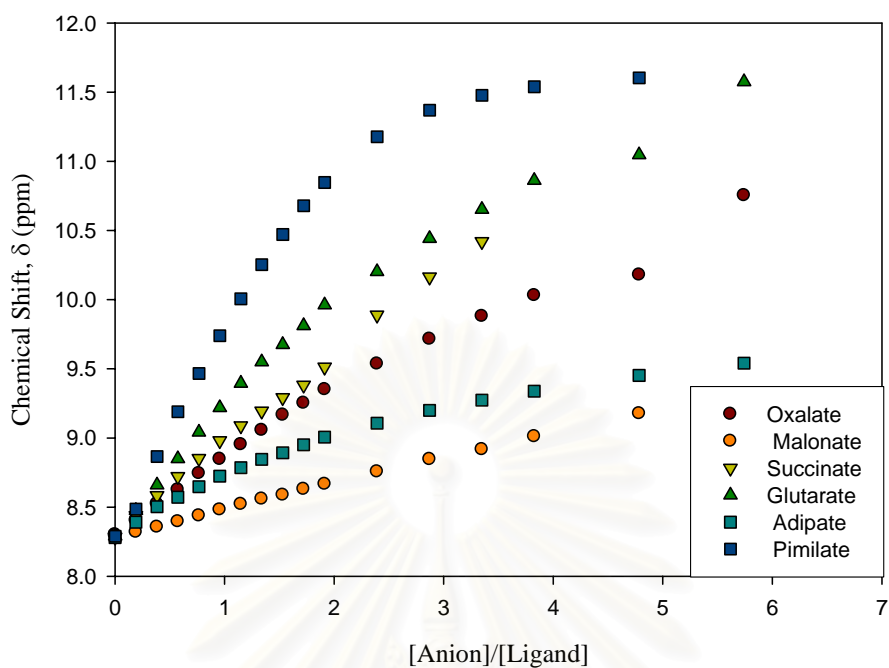


Figure 3.18 Titration curves between **L4** (NH_B) with various dicarboxylate anions in $DMSO-d_6$.

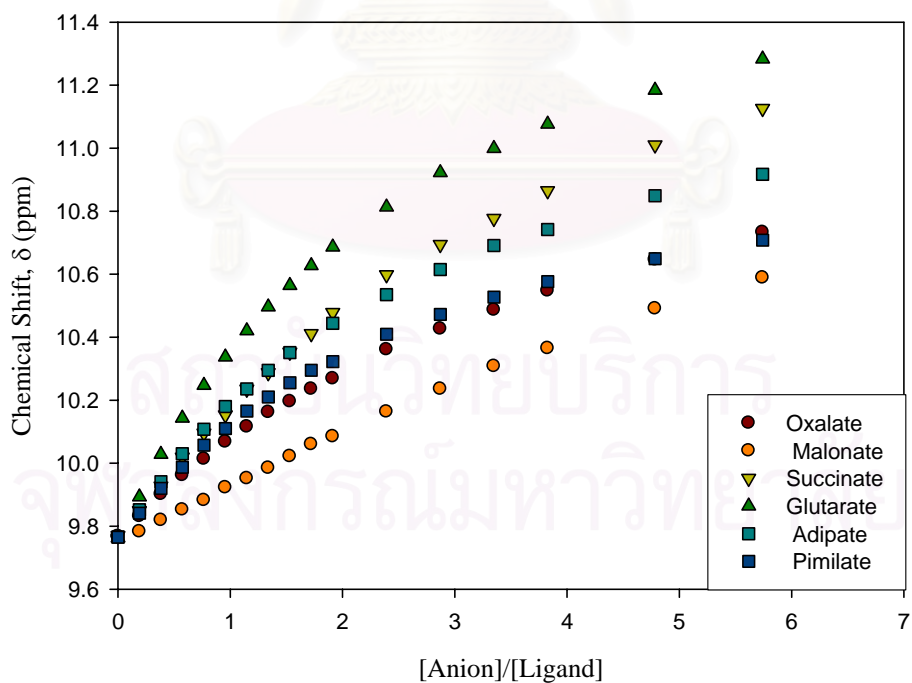


Figure 3.19 Titration curves between **L5** (NH_A) with various dicarboxylate anions in $DMSO-d_6$.

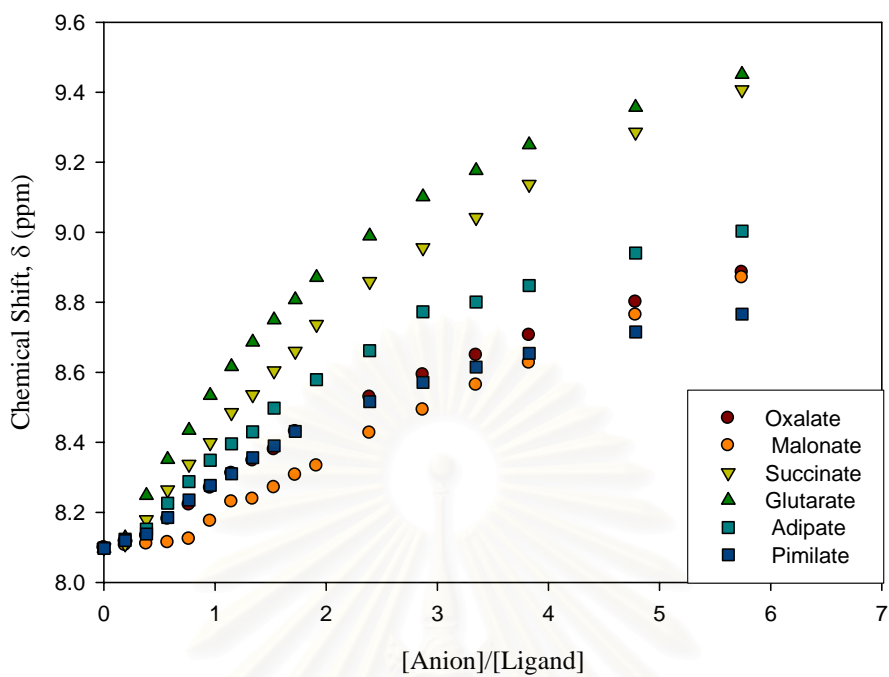


Figure 3.20 Titration curves between L5 (NH_B) with various dicarboxylate anions in DMSO-*d*₆.

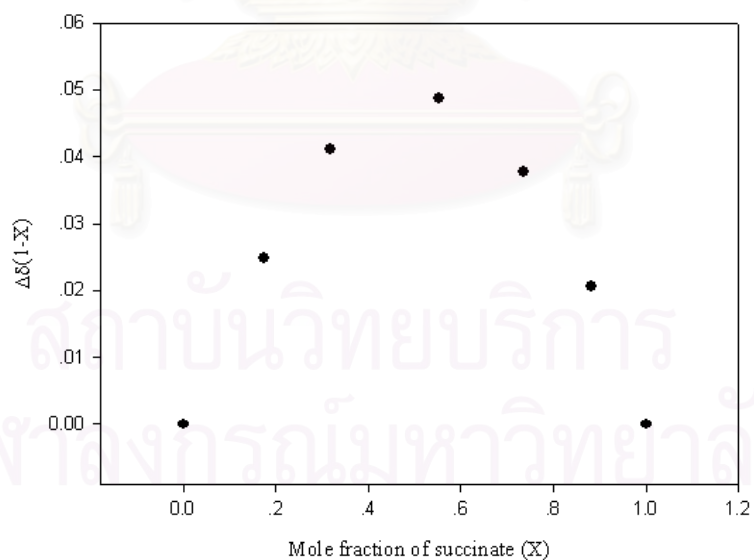


Figure 3.21 The Job's plot of compound L2 (NH_A) with succinate.

The binding constants (β_1) of dicarboxylate anions to the synthetic compounds were obtained by the complexation induced shift (CIS) of the thiourea NH protons. For the case of any 1:1 complexes which display the faster exchange rate than the NMR time scale, the association constant can be calculated using EQNMR program.⁴⁴ Binding constant values from both NH thiourea protons were presented in Table 3.10 and the average were shown in Table 3.11.

Table 3.10 Binding constants of compounds **L1-L5** [0.01 M] toward various dicarboxylate anions calculated from thiourea NH proton chemical shifts by WinEQNMR program.

anion ^a	L1		L2		L3		L4		L5	
	NH _A ^b	NH _B ^c	NH _A ^b	NH _B ^c	NH _A ^b	NH _B ^c	NH _A ^b	NH _B ^c	NH _A ^b	NH _B ^c
oxalate	19	13	19	*	31	*	23	27	14	8
malonate	*	*	18	14	*	*	*	*	3	*
succinate	13	12	169	104	69	*	16	13	14	12
glutarate	12	12	74	73	176	209	75	75	39	35
adipate	25	17	42	40	78	116	34	23	23	31
pimilate	37	29	42	52	131	128	107	108	35	22

^a all case counter cation is tetrabutylammonium

^b thiourea NH that adjacent to aromatic anthraquinone

^c thiourea NH that adjacent to hexyl chain

Table 3.11 Average binding constants of compounds **L1-L5** [0.01 M] toward various dicarboxylate anions.

Anion	L1	L2	L3	L4	L5
oxalate	16	19	31	25	11
malonate	*	16	*	*	3
succinate	13	137	69	15	13
glutarate	12	74	193	75	37
adipate	21	41	97	29	27
pimelate	33	47	130	108	29

Table 3.10 shows the binding constants of synthetic compounds toward dicarboxylate anions calculated from NH_A (thiourea NH that adjacent to aromatic anthraquinone) and NH_B (thiourea NH that adjacent to hexyl chain) by WinEQNMR program. Binding constants estimated from NH_A are slightly higher than estimated from NH_B . The average binding constants are summarized in Table 3.11

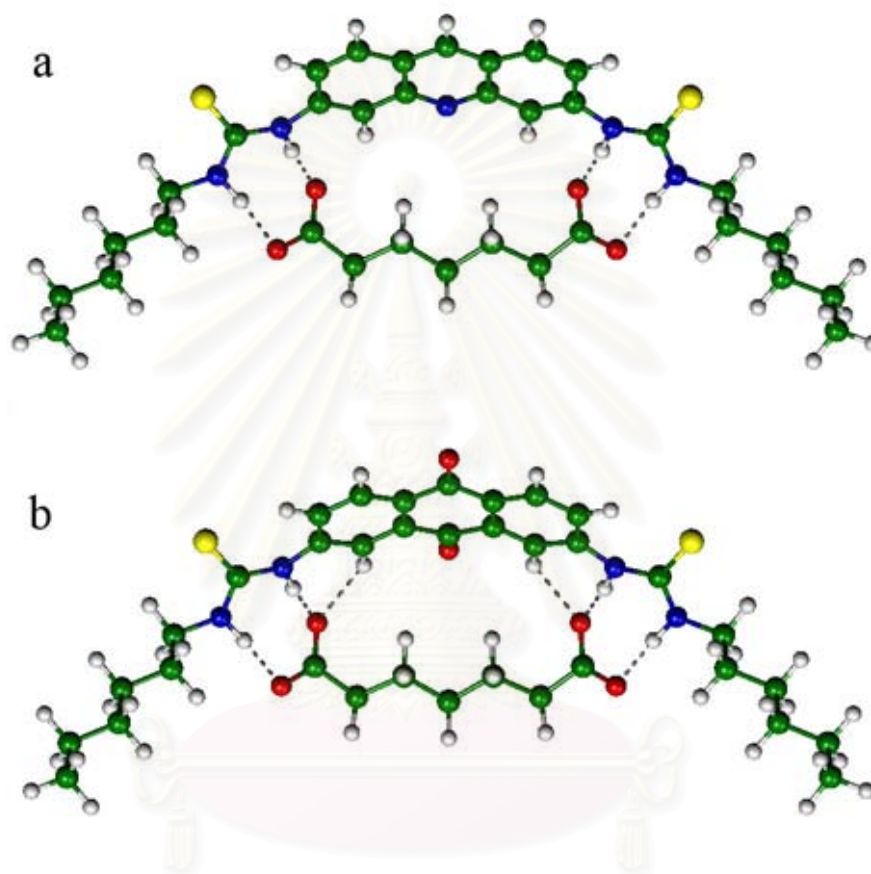


Figure 3.22 B3LYP/6-31G(d)-optimized structures for the complex between **L1** (a) and **L4** (b) with pimelate.

To explain the complexations behavior, we divided the synthetic compound in to two groups depend on the distant between NH moieties. First group consist of compound **L1**, **L4** and **L5**. These compound have longer distant between NH moieties than **L2** and **L3**. From binding constant values in Table 3.11, both compounds **L1** and **L4** form the most stable complexes with pimelate. Compound **L4** has about three time higher binding constant than compound **L1**. These results are supported by the optimized structure of compound **L4** and pimelate complexed and shown in Figure 3.22. As described above, the main interactions in these complexations are hydrogen bonding between thiourea NH

protons of host compound and carboxy oxygens of dicarboxylate anions. Both compounds **L1** and **L4** process four hydrogen bonding interactions with pimelate. However compound **L4** can form two more hydrogen bonds with oxygens of dicarboxylate anions using aromatic proton of the electron deficient anthraquinone.

Compound **L5** formed the most stable complexes with glutarate and the least stable complexes with malonate. The optimized structure of compound **L5** and glutarate or malonate complexed are shown in Figure 3.23. The similar results as compound **L4** are observed for compound **L5** and glutarate complexation, four hydrogen bonding between thiourea NH protons and carboxy oxygens and two hydrogen bonds between aromatic proton and carboxy oxygens. In contrast to the complexation with malonate, three hydrogen bonding between thiourea NH protons and carboxy oxygens and two hydrogen bonds between aromatic proton and carboxy oxygens are observed.

The shorter group consists of compounds **L2** and **L3**. Compound **L2** formed the most stable complexes with succinate and the least stable complexes with malonate. Compounds **L3** formed the most stable complexes with glutarate and the least stable complexes with malonate. These results indicated that the presence of quinone oxygen atom promoted hydrogen bonding between this atom and thiourea NH proton results the shorter distance between two thiourea NH protons. Thus, compound **L2** show stronger binding ability with the shorter dicarboxylate anion, succinate.



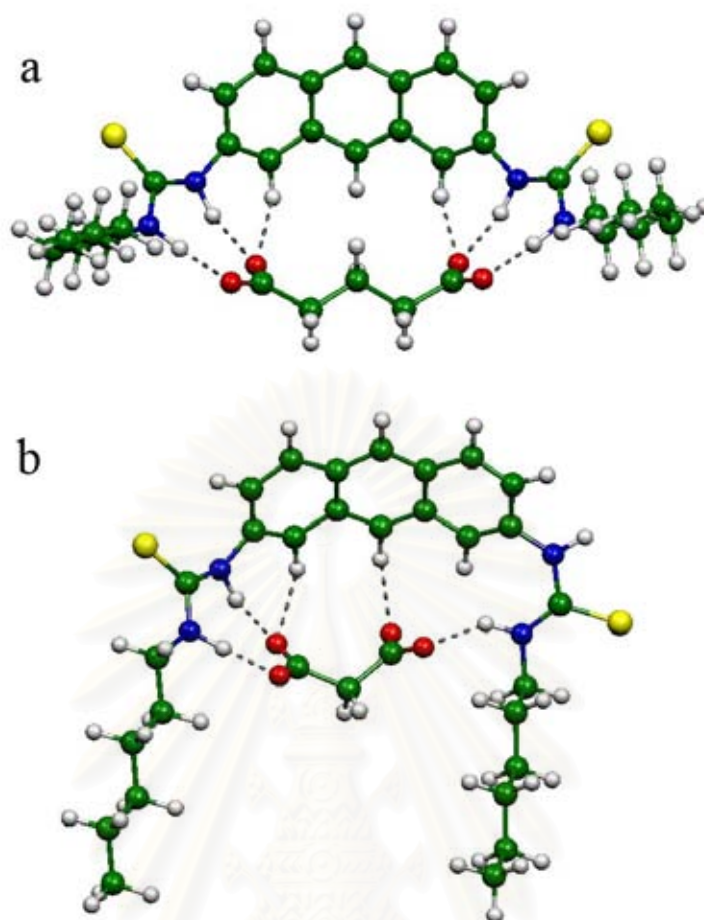


Figure 3.23 B3LYP/6-31G(d)-optimized structures for the complex between **L5** with adipate (a) and malonate (b).

3.3.2 The Complexation Studies of Synthetic Compounds with Various Dicarboxylate Anions by Using UV-Vis Titrations

The UV-vis spectra of compound **L1** in DMSO [2×10^{-5} M] was observed and shown in Figure 3.24. Free compound **L1** displayed a strong absorption band at 306 nm and 400 nm. Titration of **L1** as a function of dicarboxylate anions gave a decreasing intensity in both bands. Another new band at around 265 nm was developed but we cannot observe because of the limitation of the machine. It is suggested that the decreasing of the band at 306 nm and 400 nm is contributed to the complex formation. Three isobestic points were observed at 295 nm, 310 nm and 375 nm indicate that more than two species coexisted. The insert Figure 3.25 show the mole ratio plot that confirmed the 1: 2 ligand and anion ratio. Similarly results were observed when oxalate added to

compound **L2** in DMSO solution. In the absent of anion **L2** displayed a strong absorption band at 306 nm and 400 nm (Figure 3.25). Upon successive addition of oxalate both absorption bands were decreased.

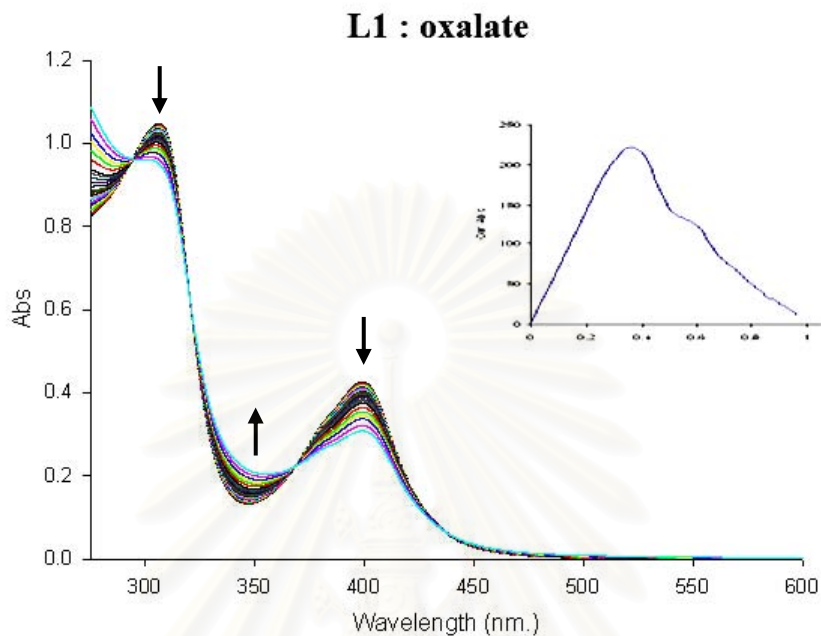


Figure 3.24 UV-vis titration spectra of compound **L1** with Oxalate in DMSO ($[L1] = 2.0 \times 10^{-5}$ M, $[oxalate] = 0-30$ equiv.). Insert show the mole ratio plot.

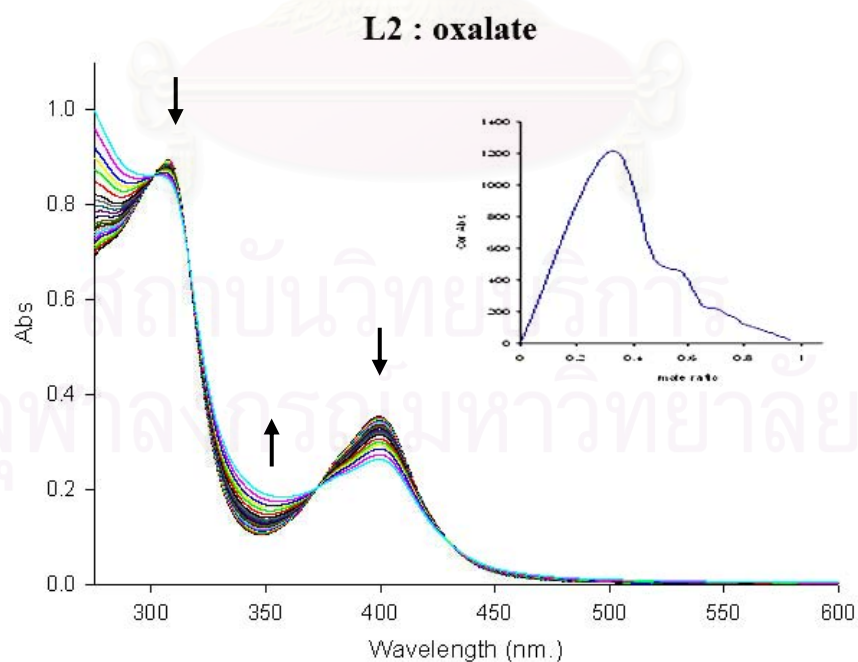


Figure 3.25 UV-vis titration spectra of compound **L2** with Oxalate in DMSO ($[L2] = 2.0 \times 10^{-5}$ M, $[oxalate] = 0-30$ equiv.). Insert show the mole ratio plot.

The UV-vis spectra of compound **L3** in DMSO [2×10^{-5} M] was observed and shown in Figure 3.27. Free ligand **L3** displayed a strong absorption band at 264 nm. Compound **L4** and **L5** showed absorption maxima band at 304 nm and 312 nm, respectively (Figure 3.27 and 3.28). Similarly phenomena with **L1** and **L2** were observed when successive additions of anion. Compounds **L3**, **L4** and **L5** showed the decreasing spectra upon addition of anions. The difference of **L3** from **L4** and **L5** was the mole ratio plot. The mole ratio plot of compound **L3** showed the 1:1 complexation while compound **L4** and **L5** showed the 1:2 complexation.

From the titration spectra, we have calculated the binding constant of synthetic compounds with various anion. The results are summarized in Table 3.8.

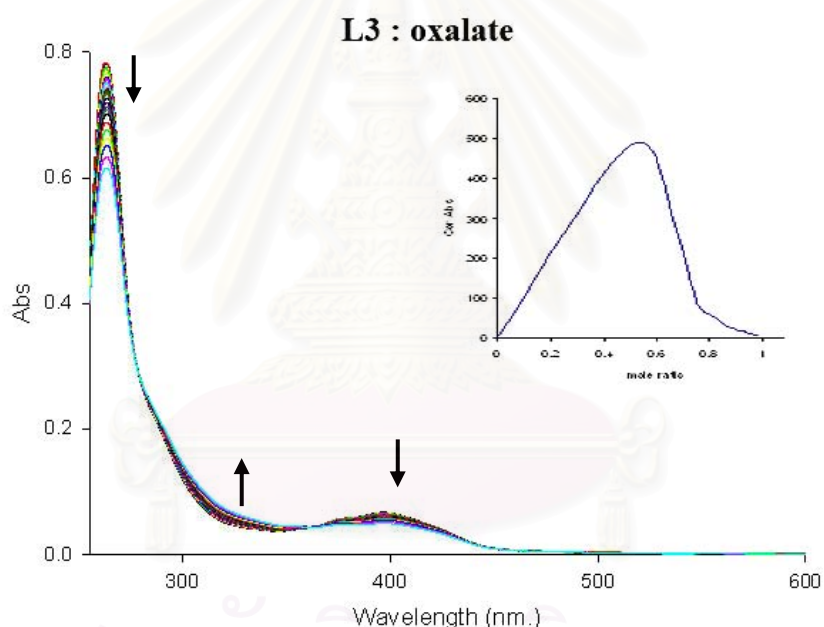


Figure 3.26 UV-vis titration spectra of compound **L3** with Oxalate in DMSO ($[L3] = 2.0 \times 10^{-5}$ M, $[oxalate] = 0-30$ equiv.).

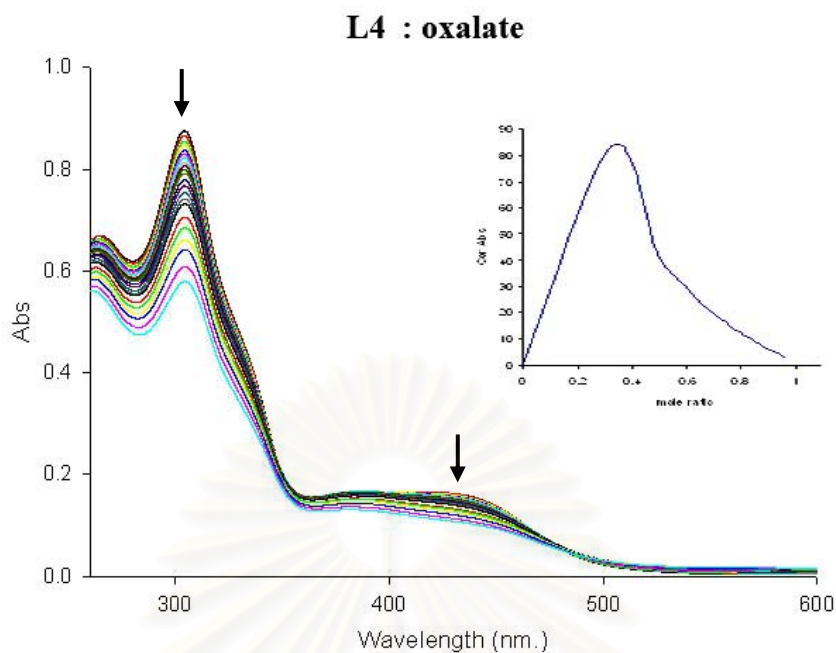


Figure 3.27 UV-vis titration spectra of compound **L4** with Oxalate in DMSO ($[L4] = 2.0 \times 10^{-5}$ M, $[oxalate] = 0-30$ equiv.).

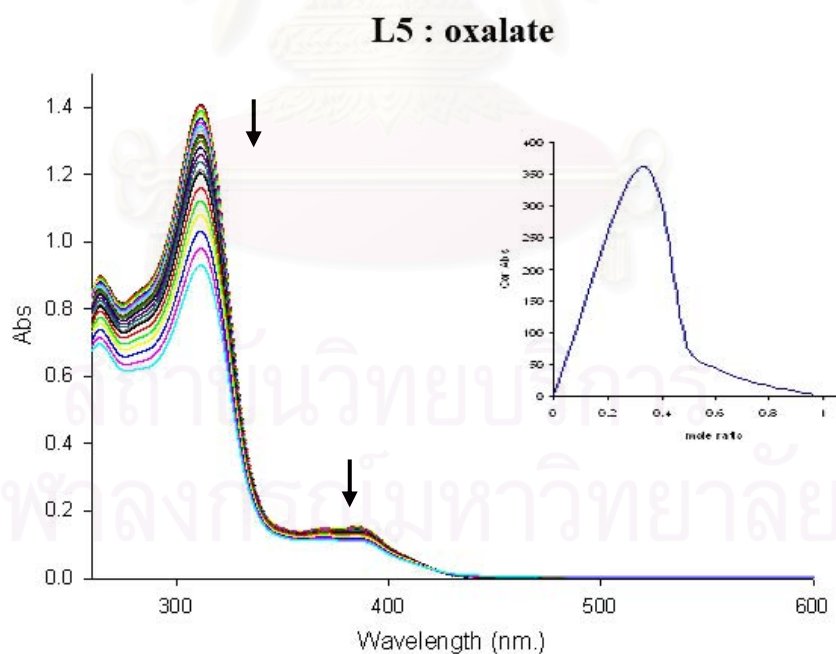


Figure 3.28 UV-vis titration spectra of compound **L5** with Oxalate in DMSO ($[L5] = 2.0 \times 10^{-5}$ M, $[oxalate] = 0-30$ equiv.).

Table 3.12 shows the binding constants from UV-vis titration of all compounds toward anions that obtained by specfit32 program. The $\log\beta_1$ results indicate that compound **L1**, **L3**, and **L4** form the highest selectivity and the most stable complexes with adipate, hydrogen sulfate and dihydrogen phosphate, respectively (Figure 3.29). Compound **L5** shows strongest binding abilities with oxalate as well as pimilate. Compound **L2** shows not significant difference in binding constants and lower selectivity than other synthetic compounds.

The synthetic compounds can be divided into two groups depend on the position of thiourea moieties. The shorter distance between thiourea moieties are compound **L2** and **L3**. Both of them contain thiourea moieties in the same position but difference signaling unit. The results can be summarized that binding constants of **L2** decreases in the order of dihydrogen phosphate > hydrogen sulfate > benzoate > malonate > succinate ~ glutarate > pimelate > adipate > oxalate. The binding constant order for **L3** is hydrogen sulfate > dihydrogen phosphate > benzoate > malonate > succinate ~ glutarate > pimelate > adipate > oxalate. From the binding constant series, we found that both compounds showed the strongest binding abilities with tetrahedral anion. This phenomenon because of four NH thiourea protons of both compounds preorganize and suitable for tetrahedral anion. The anthraquinone oxygen of compound **L2** was located in the center of thiourea cavity and formed intramolecular hydrogen bonding. In the present of dihydrogen phosphate, this oxygen can form intermolecular hydrogen bonding with the phosphate hydrogen. The absence of quinone oxygen caused **L3** to have bigger cavity than **L2**. Moreover, the aromatic hydrogen in the center of thiourea cavity can form intermolecular hydrogen bonding with oxyanion resulted in higher binding constant toward HSO_4^- than the isostructure dihydrogen phosphate.

The other groups are **L1**, **L4** and **L5**. This group has longer thiourea NH distance than the first one. The results can be summarized that binding constants of **L1** decreases in the order of adipate > succinate ~ hydrogen sulfate > glutarate > benzoate > dihydrogen phosphate > pimelate > malonate > oxalate. The binding constant order for **L4** is dihydrogen phosphate > glutarate > malonate > oxalate > pimelate > benzoate > succinate > hydrogen sulfate > adipate. The binding constant order for **L5** is oxalate > pimelate > benzoate > hydrogen sulfate > succinate ~ malonate > dihydrogen phosphate > glutarate > adipate.

Table 3.12 Binding constants of synthetic compounds toward various dicarboxylate anions calculated from UV-vis titration by SPECFIT32 program.

anion	Compound L1		Compound L2		Compound L3	Compound L4		Compound L5	
	log β 1	log β 2	log β 1	log β 2	log β 1	log β 1	log β 2	log β 1	log β 2
HSO₄⁻	4.37(0.29)	9.11(0.44)	5.49(0.37)	8.85(0.38)	6.43(0.45)	3.59(0.21)	8.60(0.38)	3.81(0.09)	7.15(0.26)
H₂PO₄⁻	3.73(0.10)	6.43(0.77)	5.72(0.30)	9.025(0.35)	3.57(0.13)	5.67(0.36)	8.26(0.98)	2.86(0.06)	4.51(0.81)
BzO⁻	4.02(0.08)	8.04(0.21)	4.99(0.29)	7.80(0.94)	4.13(0.31)	3.76(0.16)	*	4.18(0.24)	6.92(1.08)
Oxalate	2.49(0.23)	6.52(0.15)	2.35(0.21)	5.15(0.51)	3.83(0.28)	3.99(0.10)	6.40(1.07)	5.46(0.40)	7.90(0.97)
Malonate	3.06(0.08)	6.01(0.18)	4.08(0.37)	9.84(0.35)	4.08(0.27)	4.12(0.19)	8.01(0.33)	3.51(0.28)	*
Succinate	4.36(0.17)	9.75(0.31)	3.61(0.08)	6.36(0.29)	3.61(0.25)	3.68(0.09)	7.04(0.19)	3.58(0.28)	8.65(0.25)
Glutalate	4.26(0.07)	8.25(0.18)	3.66(0.12)	8.69(0.15)	3.13(0.16)	4.30(0.13)	8.75(0.28)	2.59(0.10)	5.77(0.18)
Adipate	6.37(0.54)	*	2.97(0.05)	*	3.76(0.21)	3.51(0.07)	6.99(0.09)	2.78(0.06)	5.54(0.25)
Pimelate	3.61(0.16)	7.77(0.25)	3.04(0.02)	*	4.04(0.11)	3.92(0.10)	8.04(0.16)	4.87(0.43)	*

* the binding constant cannot be calculated.

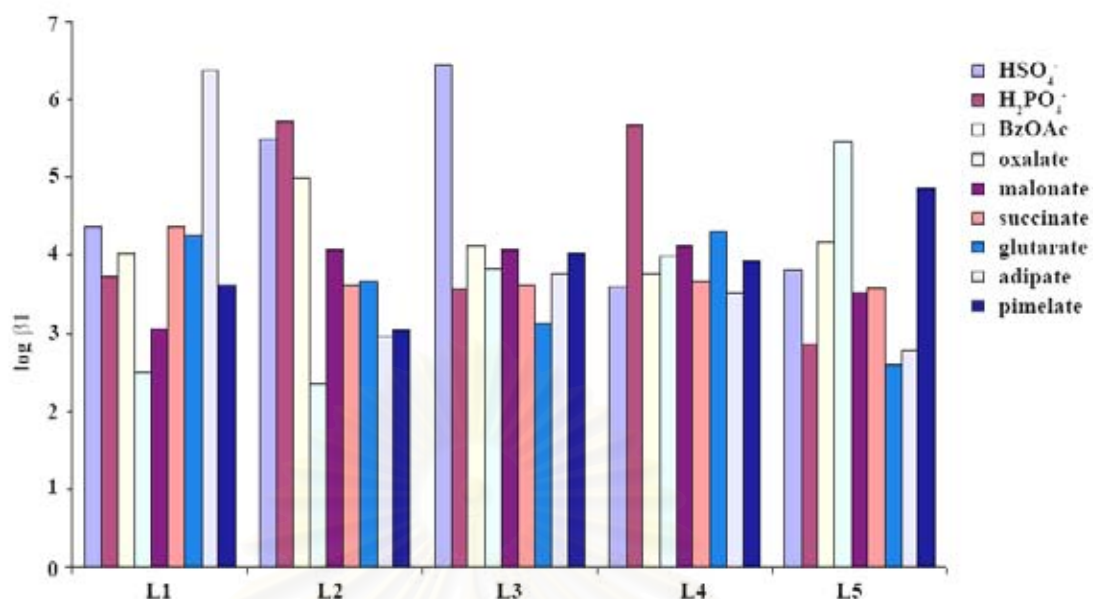


Figure 3.29 The selectivity of synthetic compounds toward anions

3.3.3 The Complexation Studies of Synthetic Compounds with Various Anions by Using Fluorometric Titrations

Fluorimetric titration method is one of the most popular methods for determining the binding constant of the complexation. When the complexation between host and guest was formed, the fluorescence emission intensity will be decreased or enhanced and used to determine binding properties. All synthetic compounds in this work can be shown fluorescence property but very weak emission intensity for **L2** and **L4**. Therefore compounds **L1**, **L3** and **L5** were chosen to study the complexation with various anions by fluorimetric titration.

Figure 3.30 shows the absorption and emission spectra of **L1** in dimethylsulfoxide. It was found that the two excitation wavelengths and the emission wavelength were 322 nm, 398 nm and 520 nm, respectively. The emission spectra ($\lambda_{\text{ex}} = 322 \text{ nm}$) of **L1** ($2.0 \times 10^{-5} \text{ M}$) in the presence of various equivalent of HSO_4^- are shown in Figure 3.31 from which it can be seen that the fluorescence intensity ($\lambda_{\text{em}} = 520 \text{ nm}$) of **L1** decreases continually upon addition of HSO_4^- with no significant change in the position of the emission maxima.

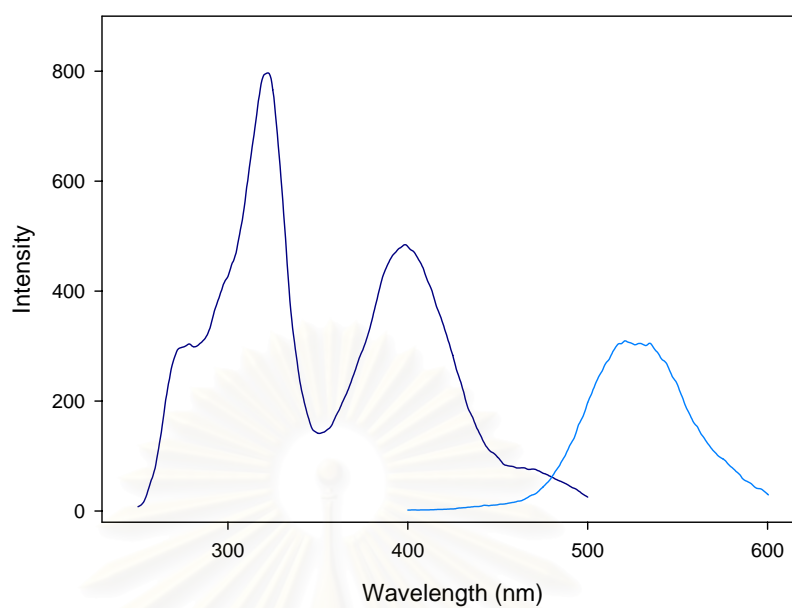


Figure 3.30 The absorption and the emission spectra of fluoroionophore **L1** in DMSO

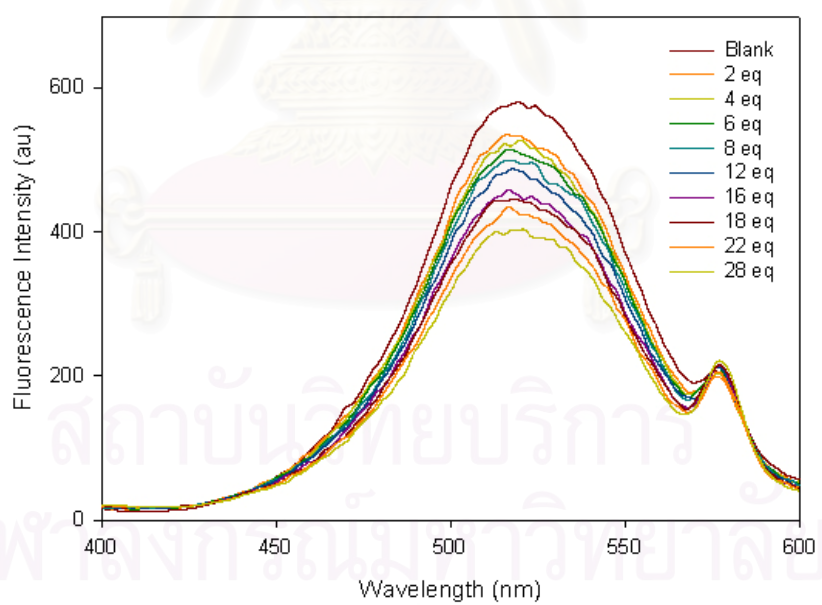


Figure 3.31 Emission spectra of **L1** ($2 \times 10^{-5} \text{M}$) was quenched by HSO_4^- ($\lambda_{\text{ex}} = 322 \text{ nm}$) in DMSO

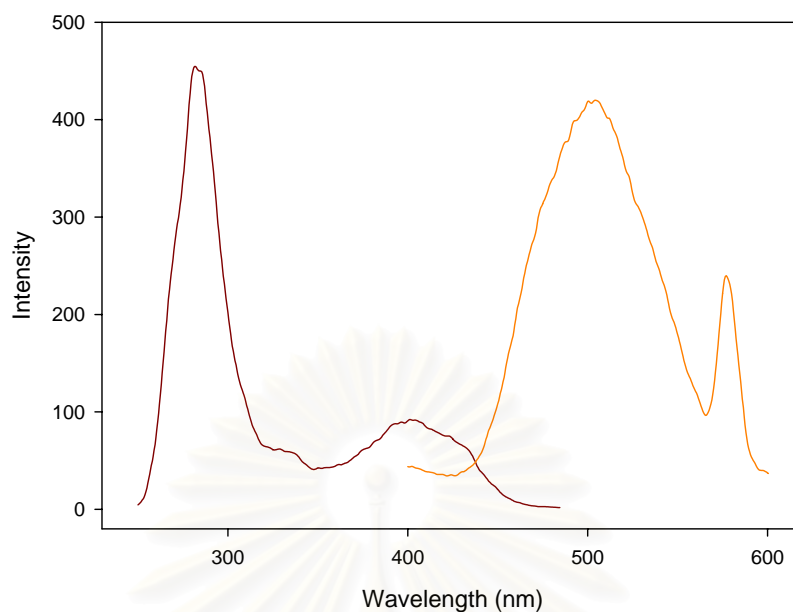


Figure 3.32 The absorption and the emission spectra of fluoroionophore **L3** in DMSO

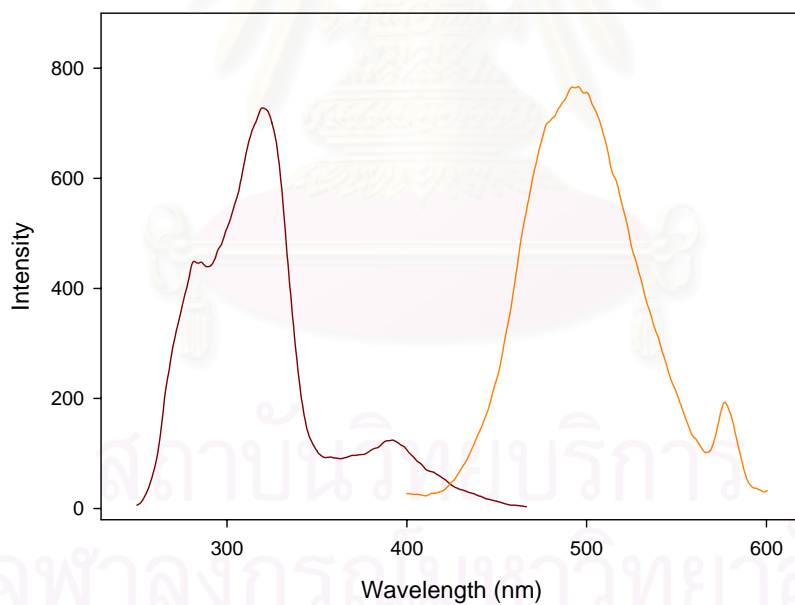


Figure 3.33 The absorption and the emission spectra of fluoroionophore **L5** in DMSO

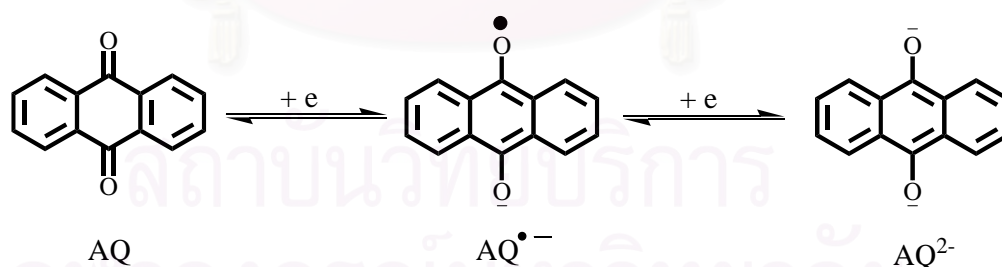
Figure 3.32 shows the absorption and emission spectra of **L3** in dimethylsulfoxide. It was found that the excitation wavelength and the emission wavelength were 282 nm and 500 nm, respectively. The emission spectra ($\lambda_{\text{ex}} = 282$ nm) of **L3** (2.0×10^{-6} M) in the presence of various equivalent of anions can be seen that the

fluorescence intensity ($\lambda_{em} = 500$ nm) of **L3** decreases continually upon addition of anions with no significant change in the position of the emission maxima.

Figure 3.33 shows the absorption and emission spectra of **L5** in dimethylsulfoxide. It was found that the excitation wavelength and the emission wavelength were 320 nm and 481 nm, respectively. The emission spectra ($\lambda_{ex} = 320$ nm) of **L5** (2.0×10^{-6} M) in the presence of various equivalent of anions can be seen that the fluorescence intensity ($\lambda_{em} = 481$ nm) of **L5** decreases continually upon addition of anions with no significant change in the position of the emission maxima

3.4 Electrochemical Studies

Electrochemical techniques have been widely used as transduction methods for the conversion of chemical phenomena such as ion binding into electrical signals. This process is usually referred as electrochemical recognition. The reduction of quinones is a reversible process, which can be induced both chemically (using reducing agents like NaBH_4) and electrochemically (using an applied potential). Anthraquinones are also commonly used in supramolecular systems as a reflection of its importance in natural electron transfer systems. In aqueous media the electrochemistry of most quinones is strongly pH dependent. In nonaqueous, aprotic solvents, quinone undergoes consecutive one-electron process according to the following Scheme 3.5.



Scheme 3.5 The reduction of anthraquinone processes.

Both compounds **L2** and **L4** processing anthraquinone moieties have been employed as electrochemical receptors and sensors. Herein, the aim of this section is to investigate the electroactivity of compounds **L2** and **L4** in non-aqueous solvent and complexation of compounds **L2** and **L4** with various anionic guests in connection with the possibility of electrochemical recognition. The cyclic voltammetric technique

was performed using solutions of **L2** and **L4** (1×10^{-3} M) in distilled anhydrous DMF with 0.1 M Bu_4NPF_6 as supporting electrolyte and using a glassy carbon working electrode, a Ag/Ag^+ reference electrode and a Pt wire as counter electrode. All solutions were purged with N_2 before measurements. The potential was scanned in the range of -2.0 to 0.0 V at 50 mV/s. The cyclic voltammograms of **L2** and **L4** are shown in Figure 3.34 and Figure 3.38, respectively. The values of the potential are shown in Table 3.3.9.

3.4.1 Cyclic Voltammograms of Compound **L2** in DMF

Figure 3.34 shows the cyclic voltammograms of compound **L2** in DMF. It is possible for the free ligand, NH_A species can form intramolecularly hydrogen bond to the oxygen atom of the anthraquinone species, while either NH_A or possibly NH_B can simultaneously act as intermolecular hydrogen bond donors. However, the strength of this intermolecular effect is difficult to assess for a number of reasons. First, the experiments are performed in the relatively polar aprotic solvent DMF. This solvent has been shown to reduce the ability of appropriate hydrogen bonding agents to coordinate to quinone species. Secondly, the concentration of **L2** species is relatively low (0.5 mM) which would not favour intermolecular interactions.

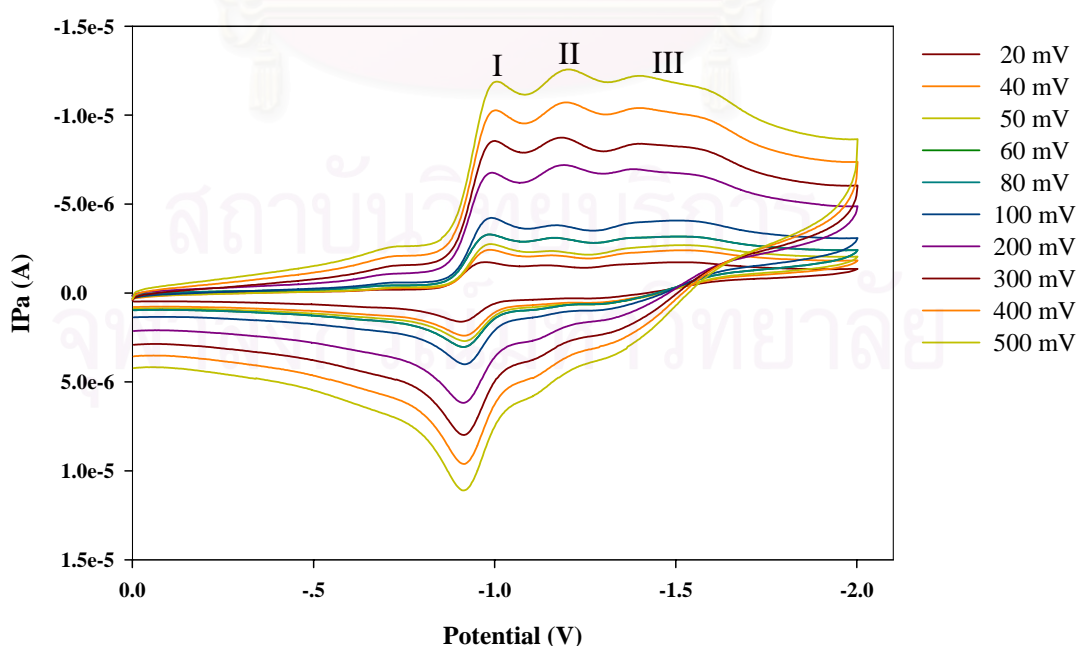


Figure 3.34 Cyclic voltammograms of compound **L2** with various scan rates

Cyclic voltammograms of compound **L2** in DMF with various scan rates are presented in Figure 3.34 and shown that the redox chemistry of **L2** is considerably different from other quinone compounds reported in the literatures.⁽⁷⁶⁻⁷⁹⁾ They exhibit reversible first waves around $E = -945$ mV represents the addition of one electron to the quinone moiety (AQ) to form a semiquinone anion radical (AQ \cdot^-). The second irreversible reduction wave ($E = -1172$ mV vs Ag/AgNO $_3$) should be corresponded to the present of intramolecular hydrogen bonding. The third irreversible reduction wave ($E = -1541$ mV vs Ag/AgNO $_3$) corresponds to the subsequent addition of a second electron to the semiquinone anion radical, producing a hydroquinone dianion (AQ $^{2-}$), as shown in Scheme 3.5.

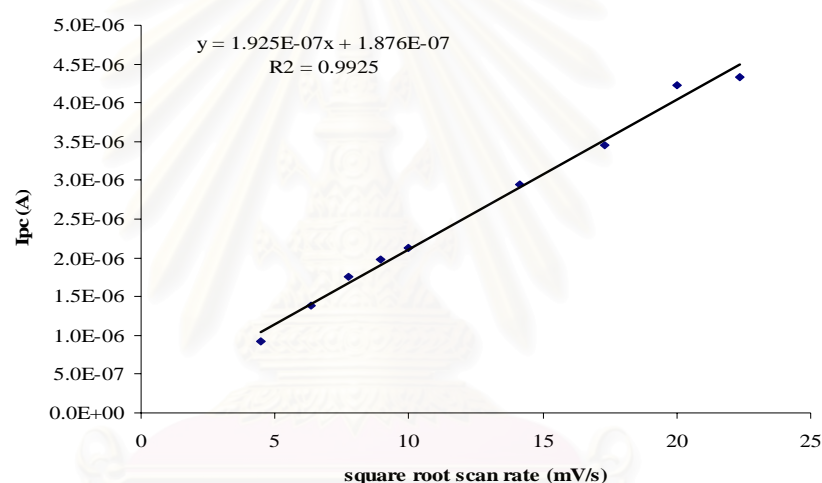


Figure 3.35 Plots of currents and square root of scan rates ($v^{1/2}$) for **L2**

All CVs measurements of the free compound **L2** were carried out by varied scan rates at 20, 40, 50, 60, 80, 100, 200, 300, 400 and 500 mV/s. Cyclic voltammograms of compound **L2** at various scan rates in DMF are depicted in Figure 3.34. The correlation between current (i) and square root of scan rates ($v^{1/2}$) was plotted and shown in Figure 3.35. The peak current of the first reduction of compound **L2** is linearly increasing by the square root of the scan rates in the range from 20 to 500 mV (Figure 3.44), indicating that compound **L2** follows the diffusion mechanism in the experimental conditions.

3.4.2 Electrochemical Studies of Compound L2 with Various Anions

Complexations between compound **L2** and various dicarboxylate anions were carried out in DMF using cyclic voltammetry using NBu_4PF_6 as supporting electrolyte. Interestingly, Figure 3.38 shows that the redox chemistry of **L2** in the absent of anion is considerably different from other quinone compounds reported in the literatures.⁷⁶⁻⁷⁹ Instead, we suggest that this unusual electrochemistry is caused by strong hydrogen bonding most likely from NH_A . In this case, the semireduced species ($\text{AQ}^{\cdot-}$) and the fully reduced species (AQ^{2-}) are stabilized by this effect. However, the electrochemical data suggests that the AQ^{2-} species enhance the intramolecular hydrogen bonding.

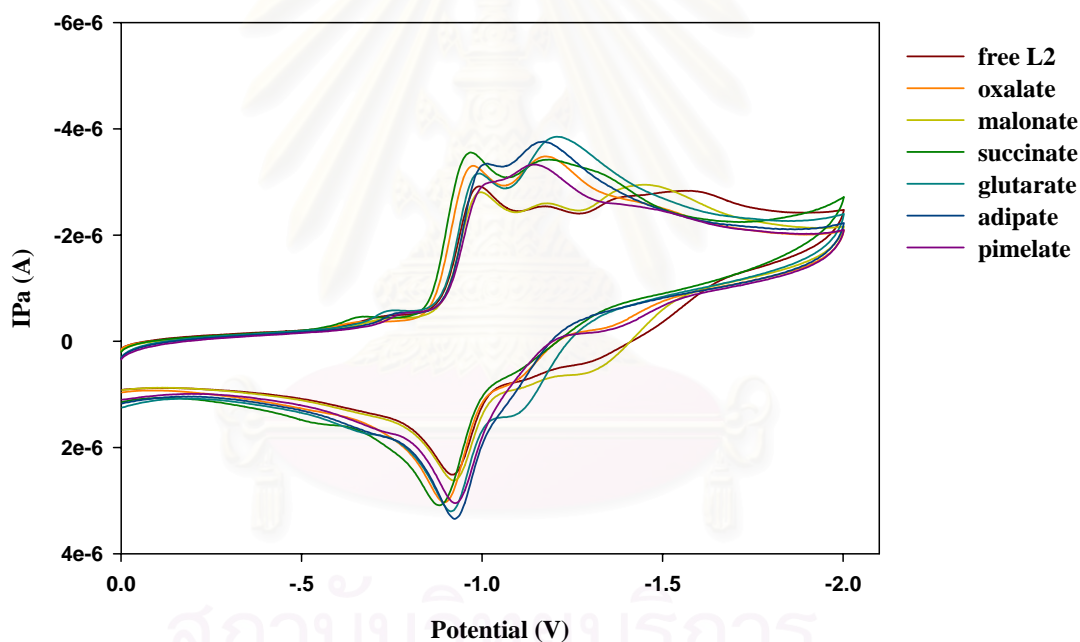


Figure 3.36 Cyclic voltammograms of compound **L2** upon addition 2 equiv. of dicarboxylate anions

where intramolecular hydrogen bonding stabilizes the AQ^{2-} species more than the $\text{AQ}^{\cdot-}$ species resulting the height of the second peak is less than that of the first in the voltammograms of all of the observed. However, the unique feature of compound **L2** is its ability to coordinate an appropriate anion. Here, some dicarboxylate anions are chosen as the guest and added to the electrochemical solution as the tetrabutylammonium salt. The effects of the addition of dicarboxylate anions on the

electrochemistry of compound **L2** have also been investigated. In our studies, anion addition was found to perturb the electrochemical character of **L2** (Figure 3.36). The data suggest that the electrochemical behaviour is linked to the hydrogen bond donor interactions. This clearly suggests that there is a strong influence of the anion binding site on the ability of the NH_A group to hydrogen bond to the quinone center was decreased in the strength. Hence, the hydrogen bond donor is unable to stabilize the reduced forms of the quinone center. However, the data presented here demonstrates that the electrochemistry of compound **L2** changes dramatically in the presence of succinate. Figure 3.37 shows the electrochemistry of **L2** in the presence and absence of various succinate concentrations. Upon successive addition of succinate, cyclic wave corresponded to AQ^{2-} species were decreased in peak height and disappeared when more than one equivalents of succinate were added. These results should be effected from compound **L2** and succinate complexation, and then resulting the more difficult to reduce semiquinone to dianion. Therefore the cyclic wave corresponding to the AQ^{2-} species may shift significantly to potential more than 2 Volt which is outside of the window allow by the solvent and electrode. On the other hand, the binding of anion to compound **L2** may inhibit the existence of species **L2**.

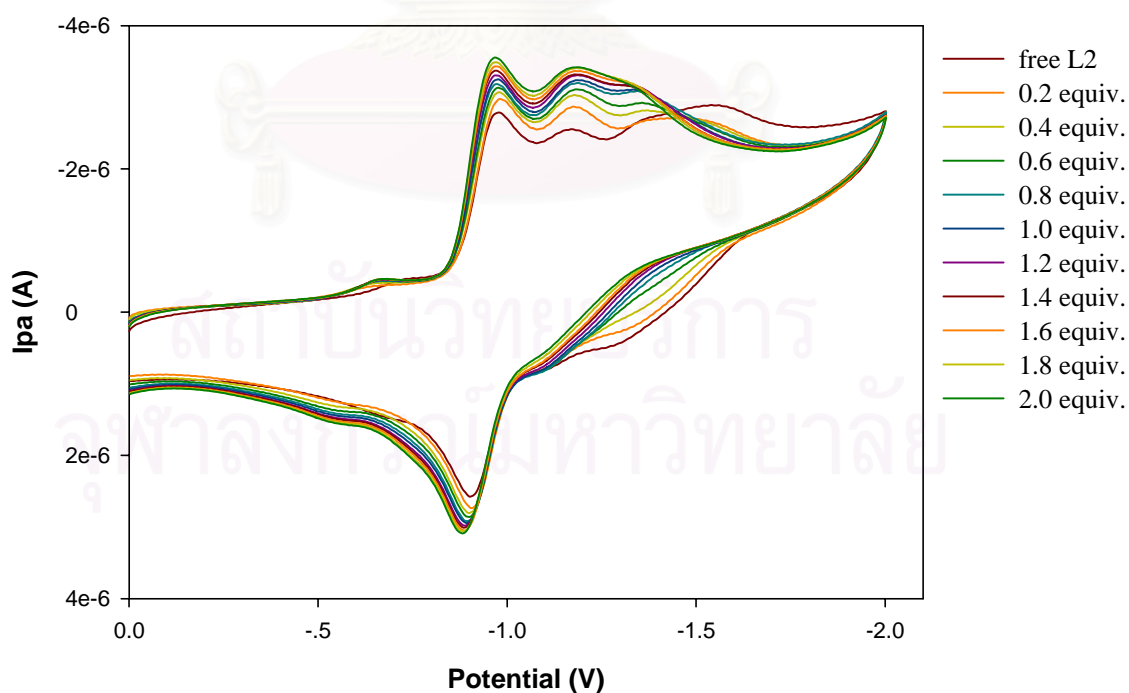


Figure 3.37 Cyclic voltammograms of compound **L2** upon addition of succinate

3.4.3 Cyclic Voltammograms of Compound L4 in DMF

Cyclic voltammetry measurements of compound **L4** were performed in DMF (Figure 3.38) and two quasi-reversible redox couples were observed. The first redox couple wave ($E_{1/2} = -1021$ mV vs Ag/AgNO₃) represents the addition of one electron to the quinone moiety (AQ) to form a semiquinone anion radical (AQ^{•-}). The second quasi-reversible reduction wave ($E_{1/2} = -1406$ mV vs Ag/AgNO₃) corresponds to the subsequent addition of a second electron to the semiquinone anion radical, producing a hydroquinone dianion (AQ²⁻).

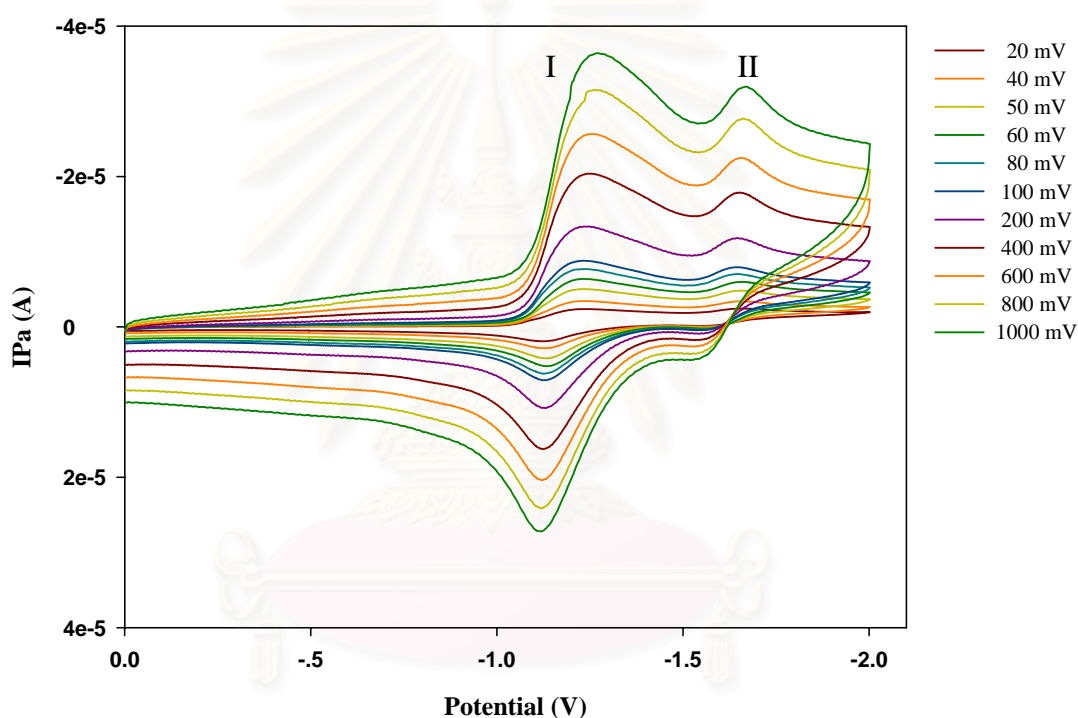


Figure 3.38 Cyclic voltammograms of compound **L4** with various scan rates

All CVs measurements of the free compound **L4** were carried out by varied scan rates at 20, 40, 50, 60, 80, 100, 200, 400, 600, 800 and 1,000 mV/s. Cyclic voltammograms of compound **L4** at various scan rates in DMF are depicted in Figure 3.38. The correlation between current (i) and square root of scan rates ($v^{1/2}$) was plotted and shown in Figure 3.39. The peak current of the first reduction of compound **L4** is linearly increasing by the square root of the scan rates in the range from 20 to

1,000 mV (Figure 3.39), indicating that the electron transfer of compound **L4** follows only the diffusion mechanism in the experimental condition.

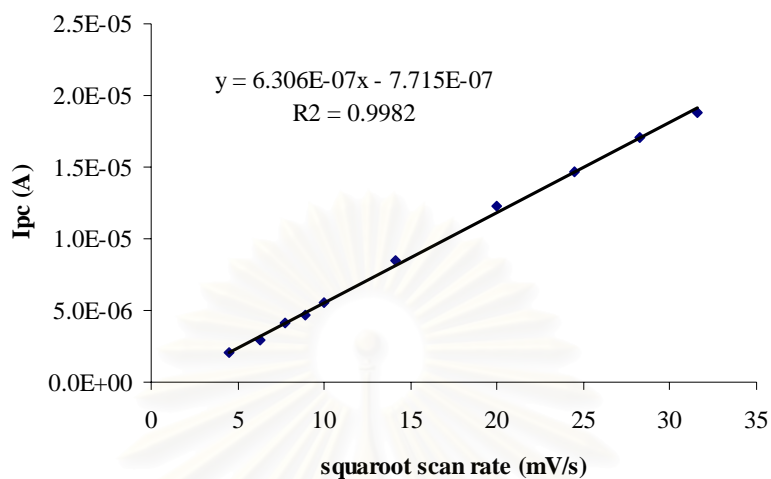


Figure 3.39 Plots of currents and square root of scan rates ($v^{1/2}$) for **L4**

Table 3.13 The characteristic values of compounds **L2** and **L4**

Ligands	L2			L4	
	I	II	III	I	II
E_{pa} (V)	-0.977	-1.175	-1.529	-1.208	-1.648
E_{pc} (V)	-0.919	*	-1.355	-1.132	-1.575
$E_{1/2}$	-0.948	*	-1.442	-1.170	-1.612
ΔE (V)	0.058	*	0.174	0.076	0.073
I_{pa}/I_{pc}	-1.084	*	-1.37	-1.099	-1.095

3.4.4 Electrochemical Studies of Compound **L4** with Various Anions

All quinones studied show two reduction peaks in nonaqueous aprotic media, corresponding to two single-electron reductions to give mono- and dianions. The values of $E_{1/2}$ vs Ag/AgNO₃, for the first and second reduction steps for all of the quinones, are given in Table 3.13 and are in good agreement with the literature.⁷⁷ The ratio of the cathodic peak current to the anodic peak current for the first redox process

is close to unity for all of the quinones, throughout the sweep rate range from 20 to 500 mV/s. Cathodic to anodic peak separations were typically 70-80 mV for the first reduction wave and about 100 mV for the second wave.

Complexations between compound **L4** and various dicarboxylate anions were carried out in DMF using cyclic voltammetry with NBu_4PF_6 as supporting electrolyte for employing the electrochemical properties of complex behaviors. Figure 3.40 shows that the redox chemistry of **L4** species is similarly to the literature reported regarding other quinone containing species.⁽⁷⁸⁾ The effects of the addition of dicarboxylate anions on the electrochemistry of compound **L4** have also been investigated. In our studies, anion addition was found to perturb the electrochemical character of **L4** (Figure 3.40). However, the data presented here demonstrates that the complexation between compound **L4** and adipate show the most change in the cyclic voltammograms of compound **L4**. Figure 3.41 shows the electrochemistry of **L4** upon successive addition of adipate. Cyclic waves corresponding to AQ^{2-} species decreased in peak height and disappeared. These phenomena are similar to compound **L2**.

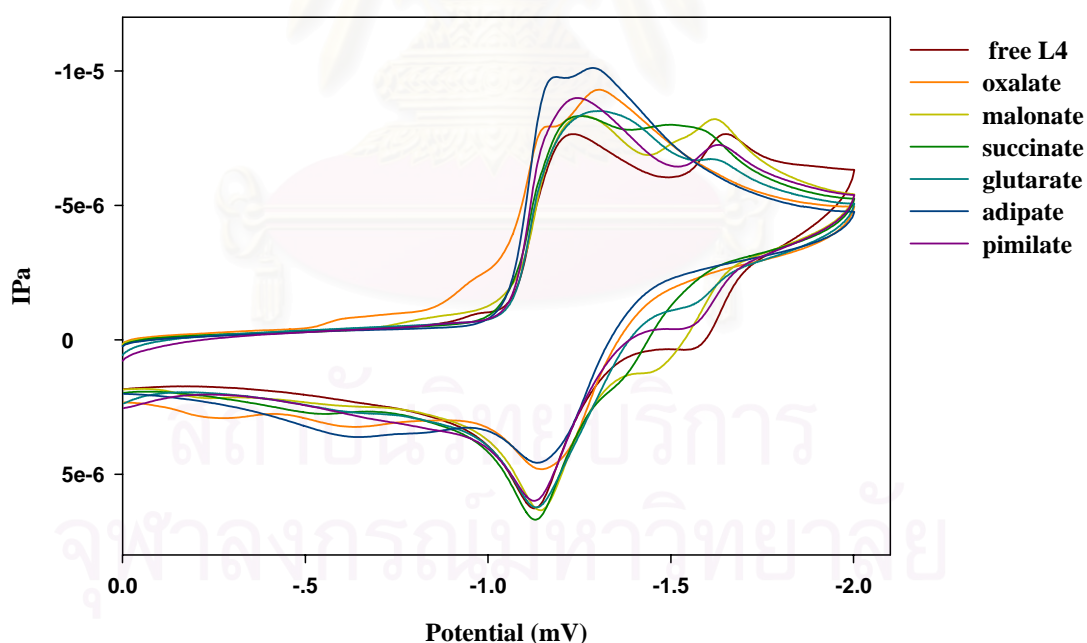


Figure 3.40 Cyclic voltammograms of compound **L4** upon addition 2 equiv of dicarboxylate anions

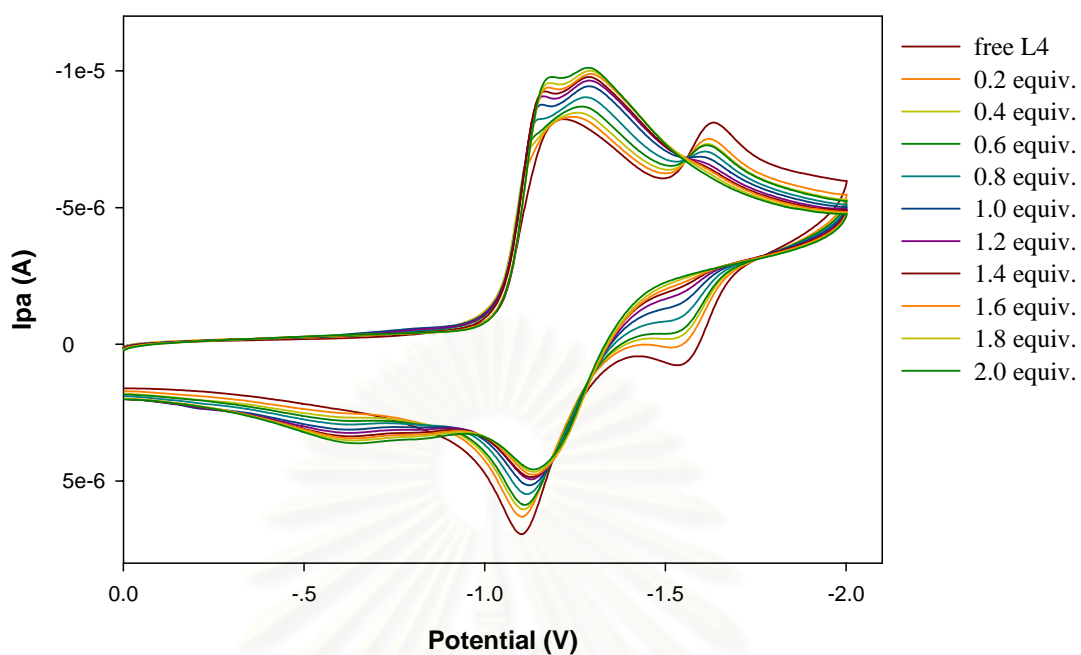
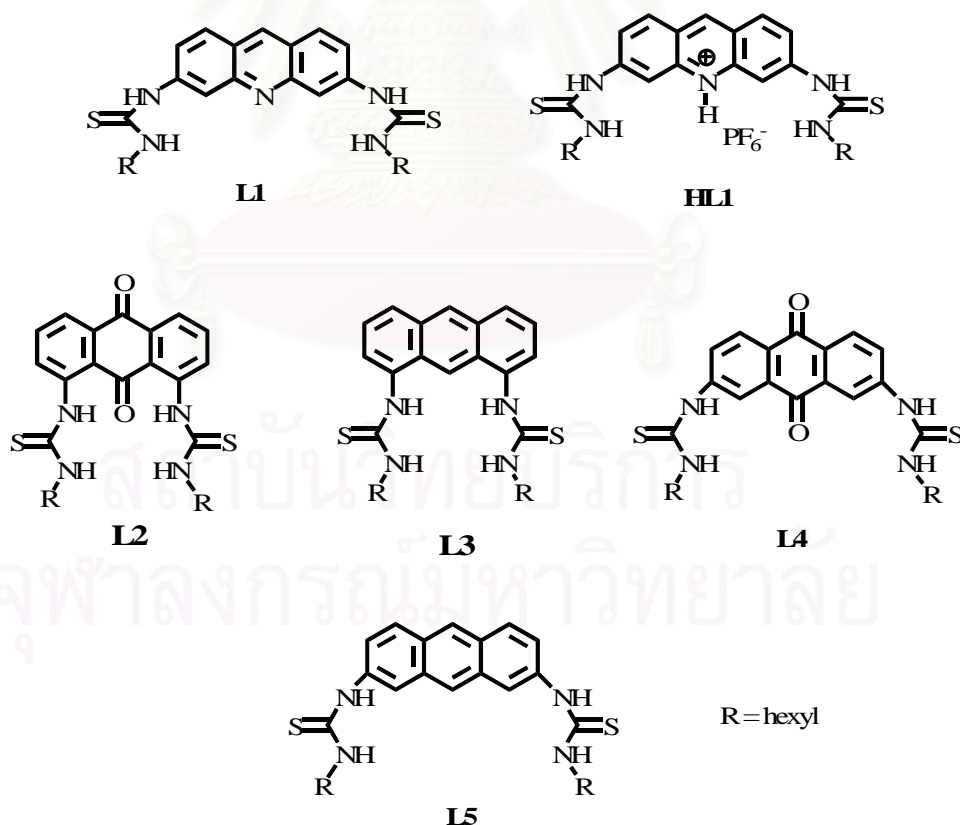


Figure 3.41 Cyclic voltammograms of compound **L4** upon addition of adipate

สถาบันวิทยบริการ
จุฬาลงกรณ์มหาวิทยาลัย

CHAPTER IV CONCLUSIONS

In conclusion, we have synthesized new colorimetric anthracene derivative-bisthiourea based anion chemosensors **L1**, **HL1**, **L2**, **L3**, **L4** and **L5**. Three structures of compounds **L1**, **HL1**, **L4** and **L5** conformers optimized at the B3LYP/6-31G(d) and two-layered ONIOM(B3LYP/6-31G(d):AM1) levels of theory were obtained. The single-point energies calculations were also obtained at the MP2(fc)/6-31G(d) level. The relative stabilities of compounds **L1**, **L4** and **L5** conformers are decreasing in orders: **L1a** > **L1b** > **L1c**, **L4a** > **L4b** > **L4c** and **L5a** > **L5b** > **L5c**, respectively. In contrast, the relative stabilities of compounds **HL1** are decreasing in orders: **HL1c**⁺ > **HL1b**⁺ > **HL1a**⁺. All the protonation reactions of compound **L1** conformers are spontaneously exothermic processes. The measured ¹H NMR chemical shifts and IR vibration modes of neutral and protonated structures compound **L1** were analyzed and compared to the computations.



The anion recognition *via* multi hydrogen bonding interactions were monitored by anion complexation induced change in ¹H-NMR chemical shifts, UV-vis absorption spectra and fluorescence emission intensities in DMSO. The cyclic

voltammetry was also used to studies complexed behavior of compounds **L2** and **L4**. For $^1\text{H-NMR}$ titration, the 1:1 complexations were confirmed by Job's plot. The binding constants (β_1) of dicarboxylate anions to the synthetic compounds (0.01 M) in $\text{DMSO-}d_6$ were obtained by the complexation induced shift (CIS) of the thiourea NH protons. Compounds **L1** and **L4** formed the most stable complexes with pimelate and the binding constant of compound **L4** with pimelate 3-fold higher than that of compound **L1**. Compounds **L3** and **L5** formed the most stable complexes with glutarate while compound **L2** formed the most stable complexes with succinate. All compounds form the least stable complexes with malonate. The binding constants were found to be strongly dependent on the chain length of dicarboxylate anion and the distance between thiourea groups. The optimizations of complexed structures were calculated and found the good agreement with experimental binding constants.

The UV-vis titration showed decreasing of maxima absorption intensity when successive addition of dicarboxylate anions in DMSO solution of all compounds (2×10^{-5} M). The binding constants from UV-vis titrations of all compounds toward anions were obtained by specfit32 program. The $\log\beta_1$ results indicate that compounds **L1** formed the highest selectivity and the most stable complexes with adipate. Compound **L5** showed strongest binding abilities with oxalate as well as pimilate. Compound **L2**, **L3**, and **L4** did not show must difference in binding abilities toward any anions.

The complexation between compound **L1**, **L3** and **L5** and anions also studied by fluorescence titration in DMSO and showed the decreasing of fluorescence emission upon successive addition of anions. The electrochemical studies of compounds **L2** and **L4** by cyclic voltammetry in DMF with NBu_4PF_6 as supporting electrolyte confirmed the occurring of complexation of synthetic compounds and dicarboxylate anions. The electrochemistry of compounds **L2** and **L4** in the presence and absence of various anions concentrations were studied. Upon successive addition of anions, cyclic wave corresponded to AQ^{2-} species were decreased in peak height and disappeared when more than one equivalent of anions were added. When complexations formed, the more difficult reduction reactions of semiquinone to dianion were found. Therefore the cyclic wave correspond to the AQ^{2-} species shifted significantly to potential more than 2 volt which is outside to window of the solvent and electrode or may be the AQ^{2-} species cannot promote. The data presented here

demonstrates that the electrochemistry of compound **L2** changes dramatically in the presence of succinate and the complexation between compound **L4** and adipate shows the most change in the cyclic voltammograms of compound **L4**.

Suggestion for future works

From all obtained results and discussion, future works should be focused on;

1. X-ray crystal structures of compound and their complexes with various anionic guests should be obtained in order to understand the structure of the synthetic receptors and their coordination chemistry.
2. Computational optimization of compound and their complexes with various anionic guests should be investigated to obtain complexation energies and physical properties upon complexation.
3. The possibility of using compound as a molecular device should be explored using many techniques such as membrane electrodes.



สถาบันวิทยบริการ
จุฬาลงกรณ์มหาวิทยาลัย

REFERENCES

- [1] Lehn, J.-M. Design of organic complexing agents Strategies towards properties. Struct. Bonding. 16(1973): 1-69.
- [2] Lehn, J.-M. Cryptates: inclusion complexes of macropolycyclic receptor molecules. Pure Appl. Chem. 50(1978): 871-892.
- [3] Lehn, J.-M. Cryptates: the chemistry of macropolycyclic inclusion complexes. Acc. Chem. Res. 11(1978): 49-57.
- [4] Lehn, J.-M. Supramolecular Chemistry - Scope and Perspectives Molecules, Supermolecules, and Molecular Devices (Nobel Lecture). Angew. Chem. Int. Ed. 27(1988): 89-112.
- [5] Lehn, J.-M. Supramolecular Chemistry, Concepts and Perspectives. VCH, Weinheim, 1995.
- [6] Beer, P. D.; Gale, P. A.; Smith, D. K. Supramolecular Chemistry. Oxford University Press, 1999.
- [7] Steed, J. W.; Atwood, J. L. Supramolecular Chemistry, Wiley & sons, 2000.
- [8] Smithrud, D. B.; Sanford, E. M. I. Chao, S. B. Ferguson, D. R. Carcanague, J. D. Evanseck, K. N. Houk, F. Diederich, Solvent effects in molecular recognition. Pure Appl. Chem. 62(1990): 2227-2236.
- [9] Beer, P. D.; Gale, P. A. Anion Recognition and Sensing: The State of the Art and Future Perspectives. Angew. Chem., Int. Ed. 40(2001): 486-516.
- [10] Shannon, R. D. Revised effective ionic radii and systematic studies of interatomic distances in halides and chalcogenides. Acta Crystallogr. Sect. A. 32(1976): 751-767.
- [11] Hofmeister, F. Zur Lehre von der Wirkung der Salze Zweite Mittheilung. Arch. Exp. Pathol. Pharmacol. 24(1888): 247-260.
- [12] Pedersen, C. J. The Discovery of Crown Ethers (Noble Lecture). Angew. Chem. Int. Ed. 27(1988): 1021-1027.
- [13] Dietrich, B.; Lehn, J.-M.; Sauvage, J. P. Diaza-polyoxa-macrocycles et macrobicycles. Tetrahedron Lett. (1969): 2885-2888.
- [14] Park, C. H.; Simmons, H. E. Macrobicyclic amines. III. Encapsulation of halide ions by in,in-1,(k + 2)-diazabicyclo[k.l.m.]alkane ammonium ions. J. Am. Chem. Soc. 90(1968): 2431-2432.

- [15] Bianchi, A.; Bowman-James, K.; García-España, E. Eds. Supramolecular Chemistry of Anions. Wiley-VCH, New York, 1997.
- [16] Gale, P. A. Anion and ion-pair receptor chemistry: highlights from 2000 and 2001. Coord. Chem. Rev. 240(2003): 191-221.
- [17] Gale, P. A. Anion receptor chemistry: highlights from 1999. Coord. Chem. Rev. 213(2001): 79-128.
- [18] Gale, P. A. Anion coordination and anion-directed assembly: highlights from 1997 and 1998. Coord. Chem. Rev. 199(2000): 181-233.
- [19] Chakrabarti, P. Anion Binding Sites in Protein Structures. J. Mol. Biol. 234(1993): 463-482.
- [20] Mangani, S.; Ferraroni, M. In; Bianchi, A.; Bowman-James, K.; García-España, E. Eds., Supramolecular Chemistry of Anions. Wiley-VCH, New York, 1997.
- [21] Holloway, J. M.; Dahlgren, R. A.; Hansen B.; Casey, W. H. Contribution of bedrock nitrogen to high nitrate concentrations in stream water. Nature. 395(1998): 785-787.
- [22] Scheele, J.; Timmerman P.; Reinhoudt, D. N. A significant effect of anion binding ureas on the product ratio in the palladium(II)-catalyzed hydrocarbonylation of alkenes. Chem. Commun. (1998): 2613-2614.
- [23] Sessler, J. L.; Sansom, P. I.; Andriersky, A.; Král, V. Supramolecular Chemistry of Anions. Wiley-VCH, New York, 1997.
- [24] Scheerder, J.; Engbersen, J. F. J.; Reinhoudt, D. N. Synthetic Receptors for Anion Complexation. Recl. Trav. Chim. Pays-Bas. 115(1996): 307-320.
- [25] Quioco, F. A., Sack, J. S.; Vyas, N. K. Stabilization of charges on isolated ionic groups sequestered in proteins by polarized peptide units. Nature. 329(1987): 561-564.
- [26] Pflugrath, J. W., Quioco, F. A. The 2 Å resolution structure of the sulfate-binding protein involved in active transport in *Salmonella typhimurium*. J. Biol. Chem. 263(1988): 163-180.
- [27] Pinkhassik, E.; Sidorov, V.; Stibor, I. Calix[4]arene-Based Receptors with Hydrogen-Bonding Groups Immersed into a Large Cavity. J. Org. Chem. 63(1998): 9644-9651.

- [28] Loll, P. J.; Bevivino, B. D.; Korty, B. D.; Axelsen, P. H. Simultaneous Recognition of a Carboxylate-Containing Ligand and an Intramolecular Surrogate Ligand in the Crystal Structure of an Asymmetric Vancomycin Dimer. J. Am. Chem. Soc. 119(1997): 1516-1522.
- [29] Sharman, G. J.; Williams, D. H. Common factors in the mode of action of vancomycin group antibiotics active against resistant bacteria. J. Chem. Soc., Chem. Commun. (1997): 723-724.
- [30] Linton, B. R.; Goodman, M. S.; Hamilton, A. D. Nitronate Anion Recognition and Modulation of Ambident Reactivity by Hydrogen-Bonding Receptors. Chem. Eur. J. 6(2000): 2449-2455.
- [31] Pernía, G. J.; Kilburn, J. D.; Essex, J. W.; Mortishire-Smith, R. J.; Rowley, M. Stabilization of a *Cis* Amide Bond in a Host-Guest Complex. J. Am. Chem. Soc. 118(1996): 10220-10227.
- [32] Bordwell, F. G.; Algrim, D. J.; Harrelson, J. A. The relative ease of removing a proton, a hydrogen atom, or an electron from carboxamides versus thiocarboxamides. J. Am. Chem. Soc. 110(1988): 5903-5904.
- [33] Molina, M. T.; Yáñez, M. O.; Mó, R.; Notario, A. The Chemistry of Double-Bonded Functional Groups, Part 2. John Wiley & Sons: Chichester, 1997.
- [34] Rienäcker, C. M.; Klapötke, T. The Chemistry of Double-Bonded Functional Groups, Part 1. John Wiley & Sons: Chichester, 1997.
- [35] Mogck, O.; Böhmer, V.; Vogt, W. Hydrogen bonded homo- and heterodimers of tetra urea derivatives of calix[4]arenes. Tetrahedron. 52(1996): 8489-8496.
- [36] Harmann, B. C.; Shimizu, K. D.; Rebek, J. Reversible Encapsulation of Guest Molecules in a Calixarene Dimer. Angew. Chem., Int. Ed. Engl. 35(1996): 1326-1329.
- [37] Zhao, X.; Chang, Y-L.; Fowler, F.W.; Lauher, J. W. An approach to the design of molecular solids. The ureylene dicarboxylic acids. J. Am. Chem. Soc. 112(1990): 6627-6634.
- [38] Kane, J. J.; Liao, R.-F.; Lauher, J. W.; Fowler, F. W. Preparation of layered diacetylenes as a demonstration of strategies for supramolecular synthesis. J. Am. Chem. Soc. 117(1995): 12003-12004.

- [39] Snowden, T. S.; Anslyn, E. V. Anion recognition: synthetic receptors for anions and their application in sensors. Current. Opinion in Chemical Biology. 3(1999): 740-747.
- [40] Beer, P. D. Anion selective recognition and optical/electrochemical sensing by novel transition metal receptor systems. Chem. Commun. 6(1996): 689-696.
- [41] Lee, D. H.; Lee, H. Y.; Lee, K. H.; Jong-In Hong, Selective anion sensing based on a dual-chromophore approach. Chem. Commun. 13(2001): 1188-1189.
- [42] Henrich, G.; Sonnenschein H.; Resch-Genger, U. Fluorescence anion receptors with iminoylthiourea binding sites-selective hydrogen bond mediated recognition of CO_3^{2-} , HCO_3^- and HPO_4^{2-} . Tetrahedron Lett. 15(2001): 2805-2808.
- [43] Kubo, Y.; Tsukahara, M.; Ishihara S.; Tokita, S. A simple anion chemosensor based on a naphthalene-thiouronium dyad. Chem. Commun. 4(2000): 653-654.
- [44] Raker, J.; Glass, T.E. Selective via cooperative interaction: detection of dicarboxylates in water by a pinwheel chemosensor. J. Org. Chem. 17(2002): 6113-6116.
- [45] Fabbrizzi, L.; Licchelli, M.; Rabaioli, G.; Taglietti, A. The design of luminescent sensors for anions and ionisable analytes. Coor. Chem. Rev. 205(2000): 85-108.
- [46] Stryer, L. Biochemistry 4th ed., W. H. Freeman, New York, 2000.
- [47] Fielding, L. Determination of Association Constants (K_a) from Solution NMR Data Tetrahedron. 56(2000): 6151-6170.
- [48] Macomber, R.S. An introduction to NMR titration for studying rapid reversible complexation. J. Chem., Ed., 69(1992): 375-378.
- [49] Wang, J. Analytical Electrochemistry. New York: Wiley-VCH Publishers, 1994.
- [50] Plambeck, J. A. Electroanalytical chemistry. New York: Wiley-VCH Publisher, 1982.
- [51] Clark, T. A Handbook of Computational Chemistry. Wiley, New York, 1985.
- [52] Cramer, C. J. Essentials of Computational Chemistry. John Wiley & Sons, 2002.
- [53] Jensen, F. Introduction to Computational Chemistry. John Wiley & Sons, 1999.

- [54] Young, D. Computational Chemistry: A Practical Guide for Applying Techniques to Real World Problems. John Wiley & Sons, 2001.
- [55] Cragg, P. J. A practical guide to supramolecular chemistry. John Wiley & Sons, 2005.
- [56] Valiyaveetil, S.; Engberson, J. F. J.; Verboom, W.; Reinhoudt, D. N. Synthesis and complexation studies of neutral anion receptors. Angew. Chem., Int. Ed. Engl. 32(1993): 900-901.
- [57] Kelly, T. R.; Kim, M. H. Relative binding affinity of carboxylate and its isosteres: nitro, phosphate, phosphonate, sulfonate and δ -lactone. J. Am. Chem. Soc. 116(1994): 7072-7080.
- [58] Buhlmann, P.; Nishizawa, S.; Xiao, K. P.; Umezawa, Y. Strong hydrogen bond-mediated complexation of H_2PO_4^- by neutral bis-thiourea hosts. Tetrahedron. 53(1997): 1647-1654.
- [59] Jeong, H.; Choi, E. M.; Kang, S. O.; Nam, K. C.; Jeon, S. Electrochemistry of a urea-functionalized calix[4]quinone sulfate-anion selective receptor. J. Electroanal. Chem. 485(2000): 154-160.
- [60] Mei, M. Wu, S. Fluorescent sensor for α,ω -dicarboxylate anion. New J. Chem. 25(2001): 471-475.
- [61] Lee, D. H.; Lee, K. H.; Hong, J. An azophenol-based chromogenic anion sensor. Org. Lett. 3(2001): 5-8.
- [62] Miyaji, H.; Satan, W.; Sessler, J. L. Naked-eye detection of anions in dichloromethane: colorimetric anion sensors based on calix[4]pyrrole. Angew. Chem. 112(2000): 1847-1850.
- [63] Miyaji, H.; Sessler, J. L. Off-the-shelf colorimetric anion sensors. Angew. Chem. Int. Ed. 40(2001): 154-157.
- [64] Lee, D. H.; Lee, H. Y.; Hong, J. Anion sensor based on the indoaniline-thiourea system. Tetrahedron Lett. 43(2002): 7273-7276.
- [65] Sabin, J. R.; Trickey, S. B.; Apell, S. P.; Oddershede, J. Molecular Shape, Capacitance, and Chemical Hardness. Int. J. Quantum Chem. 77(2000): 358-366.
- [66] Koopmans, T. Über die Zuordnung von Wellenfunktionen und Eigenwerten zu den Einzelnen Elektronen Eines Atoms. Physica. 1(1933): 104-113.

- [67] Wannoo, B.; Ruangpornvisuti, V. Tautomeric and rotameric transformations of 4-methyl-3,6-pyridazinedione isomers. Chem. Phys. Lett. 415(2005): 176-182.
- [68] Thipyapong, K.; Yasarawan, N.; Wannoo, B.; Arano, Y.; Ruangpornvisuti, V. Conformational investigation of N,N-propylene bis(benzohydroxamamide), its oxotechnetium(v) and oxorhenium (v) complexes and determination of their reaction energies. J. Mol. Struct. (Theochem). 755(2005): 45-53.
- [69] Wannoo, B.; Ruangpornvisuti, V. An investigation of molecular structures of sulfonylcalix[4]arene, mercaptosulfonylcalix[4]arene and aminosulfonylcalix [4]arene, their proton affinities and complexation with zinc(II). J. Mol. Struct. 787(2006): 76-89.
- [70] London, F. Quantum theory of interatomic currents in aromatic compounds. J. Phys. Radium. 8(1937): 3974-3976.
- [71] Ditchfield, R. Self-consistent perturbation theory of diamagnetism. I. A gauge-invariant LCAO method for N.M.R. chemical shifts. Mol. Phys. 27(1974): 789-807.
- [72] Wolinski, K.; Himton, J. F.; Pulay, P. Efficient implementation of the gauge-independent atomic orbital method for NMR chemical shift calculations. J. Am. Chem. Soc. 112(1990): 8251-8260.
- [73] Flükiger, P.; Lüthi, H. P.; Portmann, S.; Weber, J. MOLEKEL 4.3. Swiss Center for Scientific Computing, Manno, Switzerland, 2000.
- [74] Goldman, M. A.; Emerson, M. T. Hydrogen-bonded species of acetic acid in inert solvents. J. Phys. Chem. 77(1973): 2295-2299.
- [75] Scott, A.P.; Radom, L. Harmonic Vibrational Frequencies: An Evaluation of Hartree-Fock, Møller-Plesset, Quadratic Configuration Interaction, Density Functional Theory, and Semiempirical Scale Factors. J. Phys. Chem. 100(1996): 16502-16513.
- [76] Gupta, N.; Linschitz, H.; Hydrogen-Bonding and Protonation Effects in Electrochemistry of Quinones in Aprotic Solvents. J. Am. Chem. Soc. 119(1997): 6384 -6391.
- [77] Brooks, S. J.; Birkin, P. R., Gale, P. A. Electrochemical measurement of switchable hydrogen bonding in an anthraquinone-based anion receptor. Electrochemistry Communications. 7(2005): 1351–1356.

- [78] Mogharrab, N.; Ghourchian, H. Anthraquinone 2-carboxylic acid as an electron shuttling mediator and attached electron relay for horseradish peroxidase. Electrochemistry Communications. 7(2005): 466–471.



สถาบันวิทยบริการ
จุฬาลงกรณ์มหาวิทยาลัย



APPENDIX

สถาบันวิทยบริการ
จุฬาลงกรณ์มหาวิทยาลัย

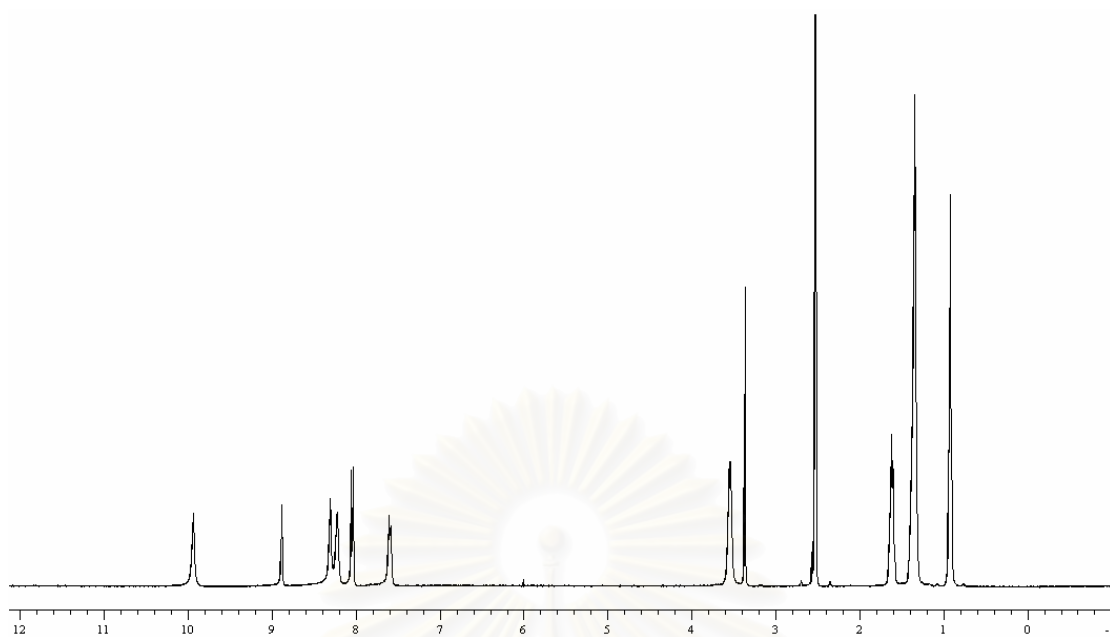


Figure 1 $^1\text{H-NMR}$ spectrum of **L1** in $\text{DMSO-}d_6$ with 400 MHz.

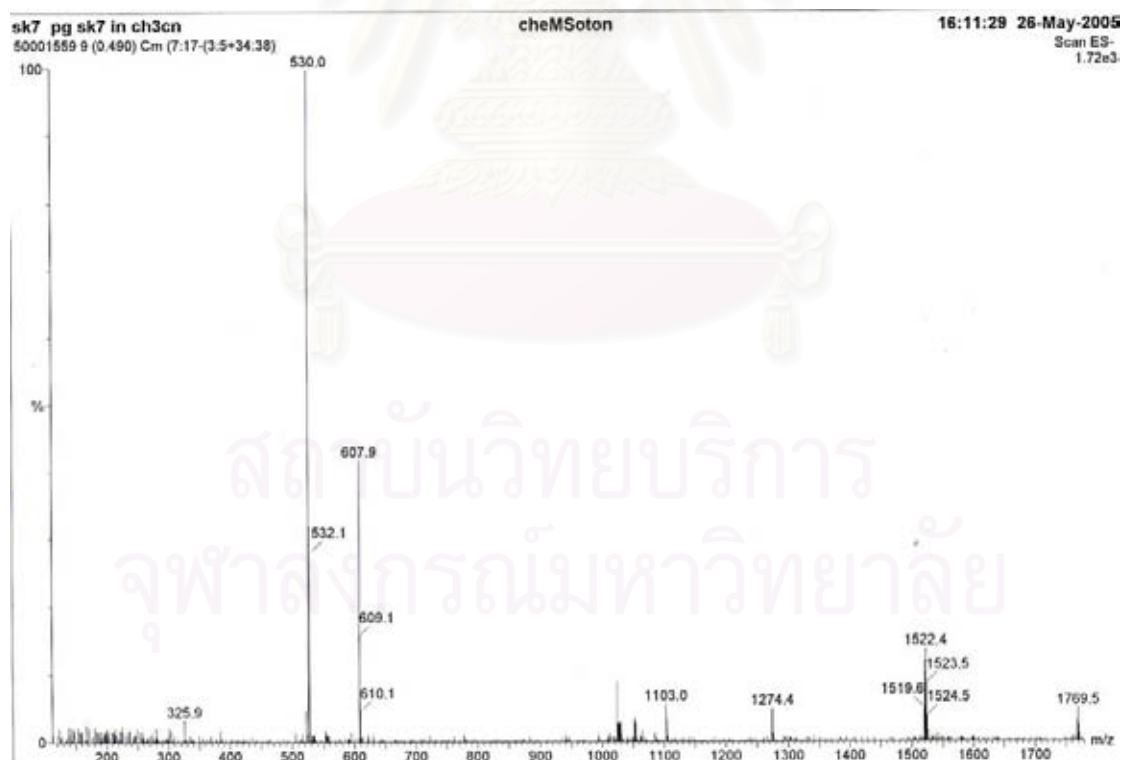


Figure 3 Mass spectrum of **L1** in acetonitrile.

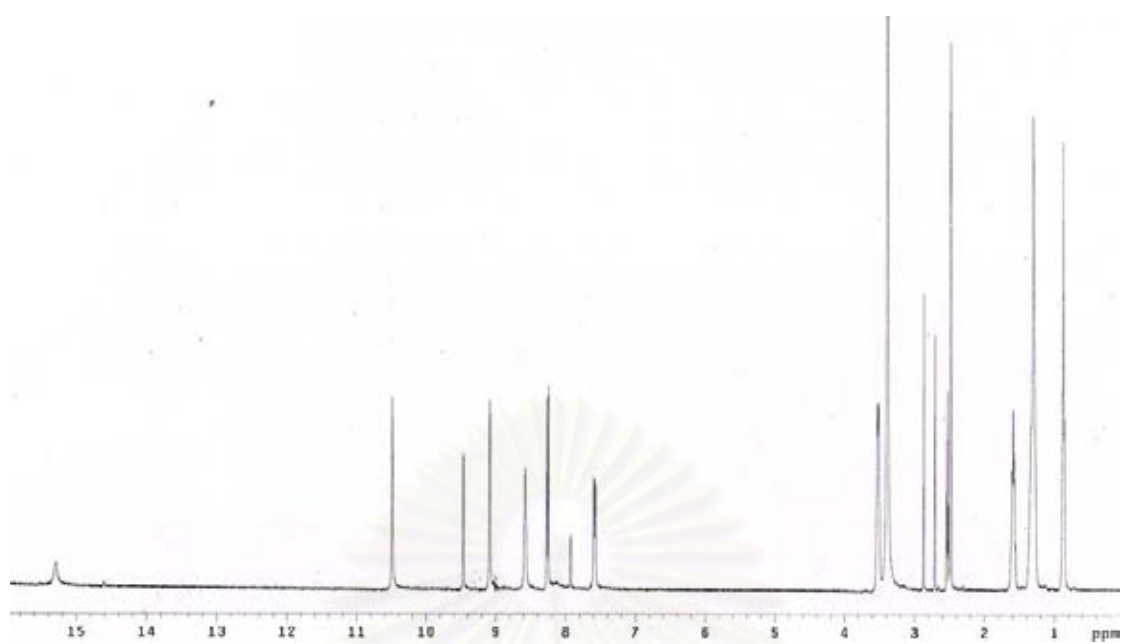


Figure 3 ¹H-NMR spectrum of **HL1** in DMSO-*d*₆ with 400 MHz.

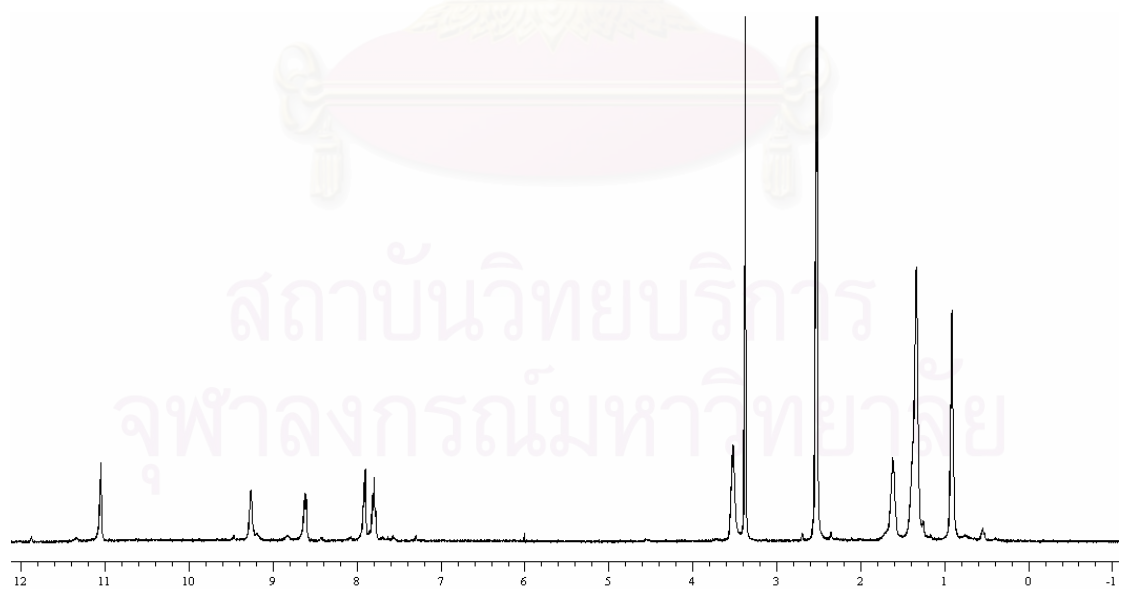


Figure 4 ¹H-NMR spectrum of **L2** in DMSO-*d*₆ with 400 MHz.

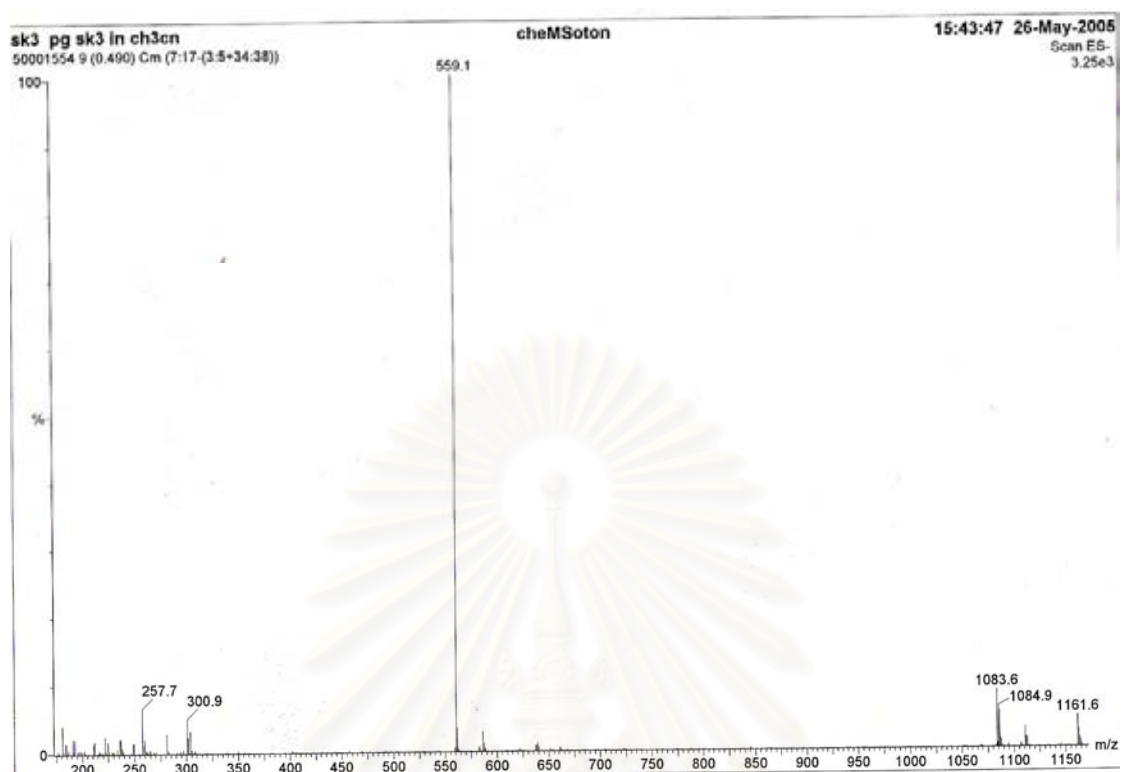


Figure 5 Mass spectrum of L2 in acetonitrile.

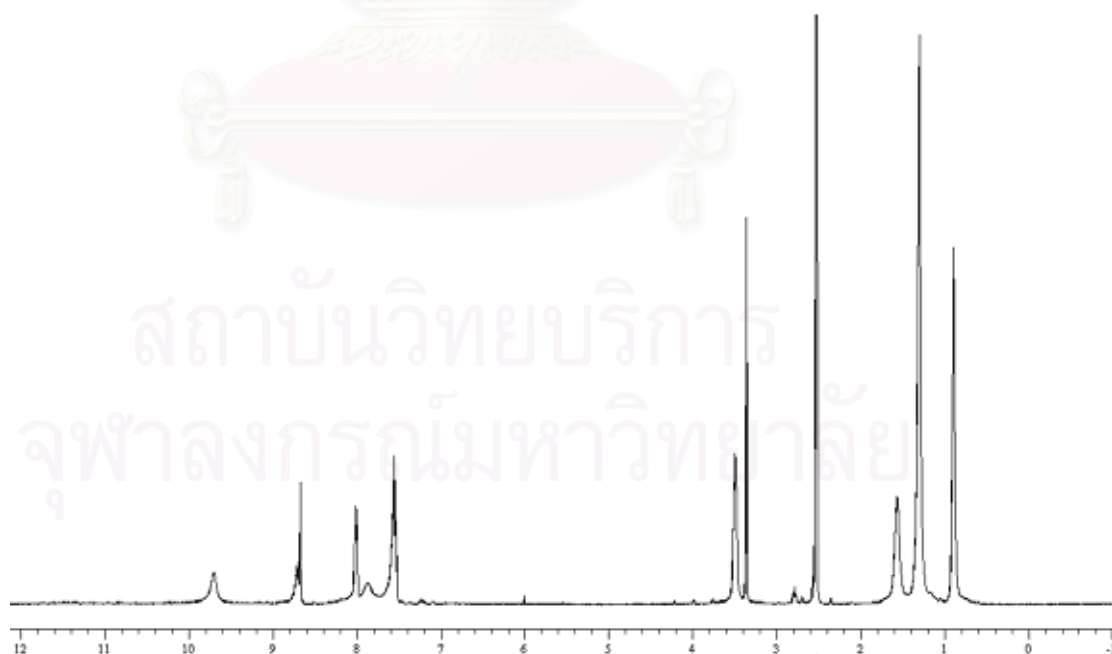


Figure 6 $^1\text{H-NMR}$ spectrum of L3 in $\text{DMSO-}d_6$ with 400 MHz.

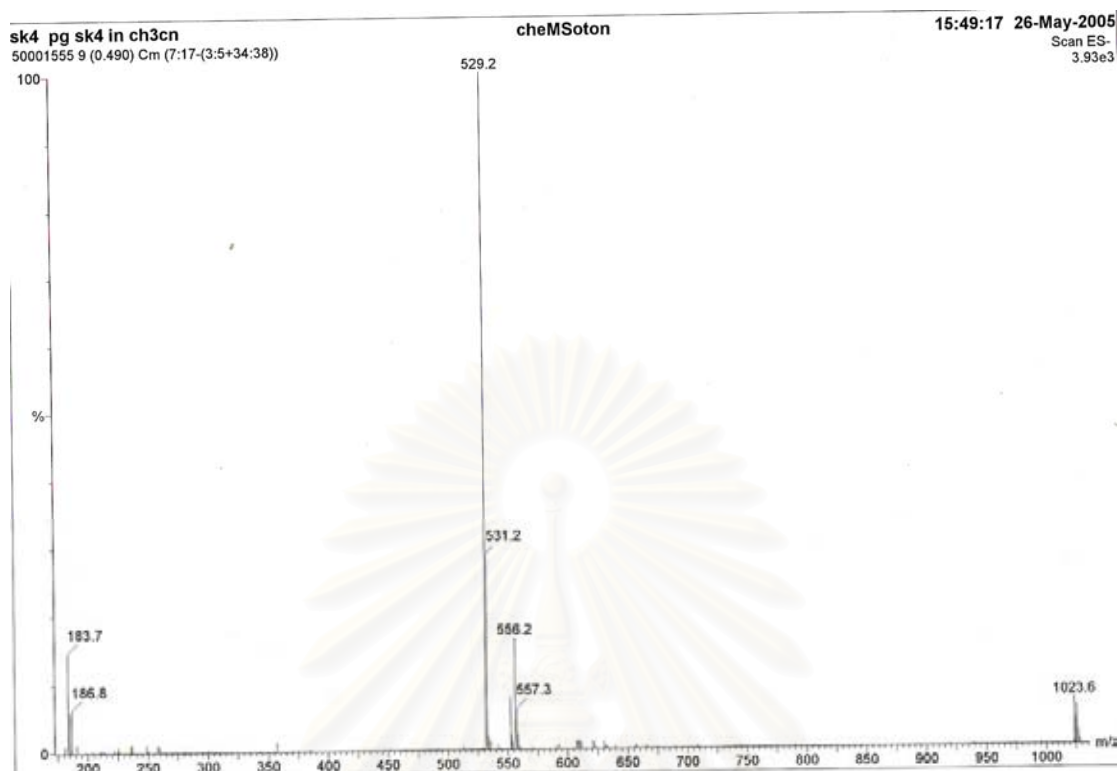


Figure 7 Mass spectrum of L3 in acetonitrile.

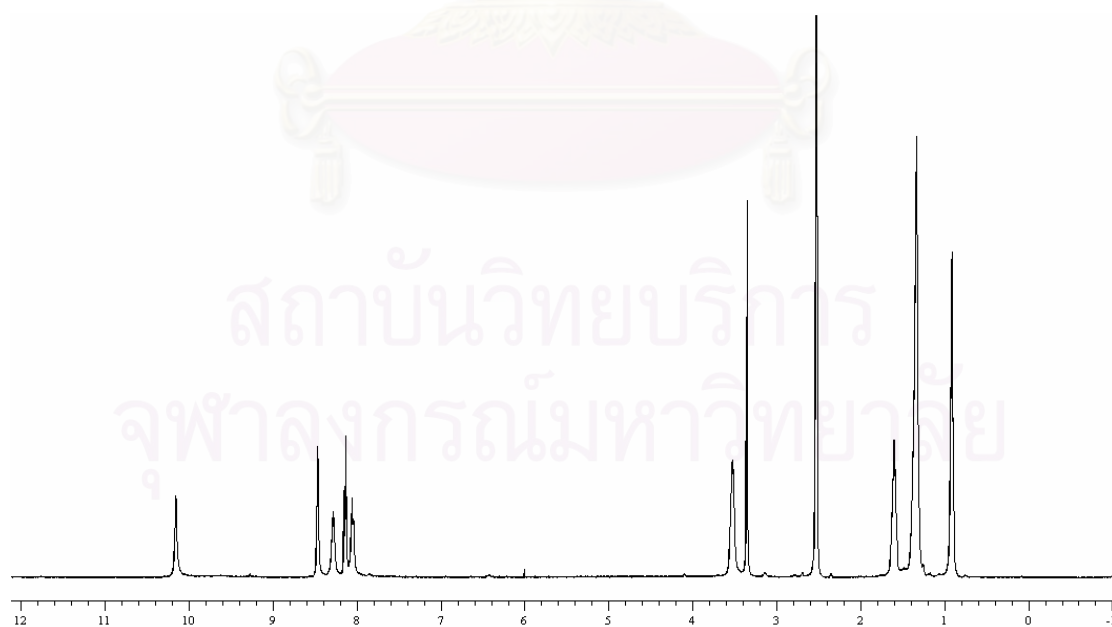


Figure 8 ^1H -NMR spectrum of L4 in $\text{DMSO-}d_6$ with 400 MHz.

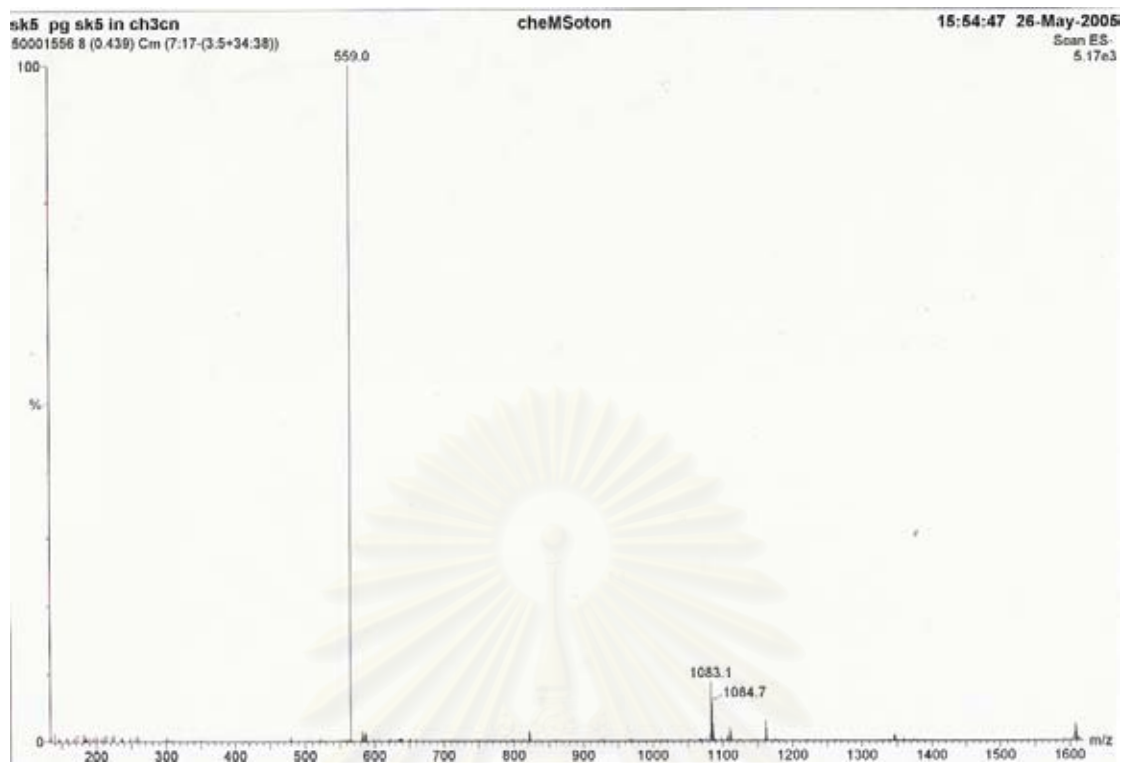


Figure 9 Mass spectrum of **L4** in acetonitrile.

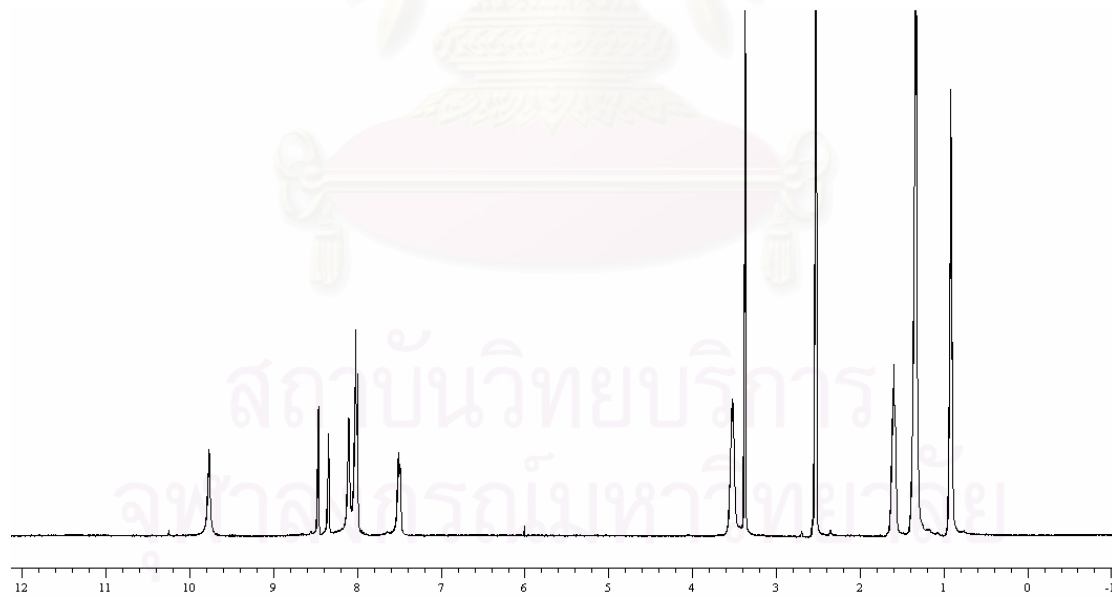


Figure 10 $^1\text{H-NMR}$ spectrum of **L5** in $\text{DMSO-}d_6$ with 400 MHz.

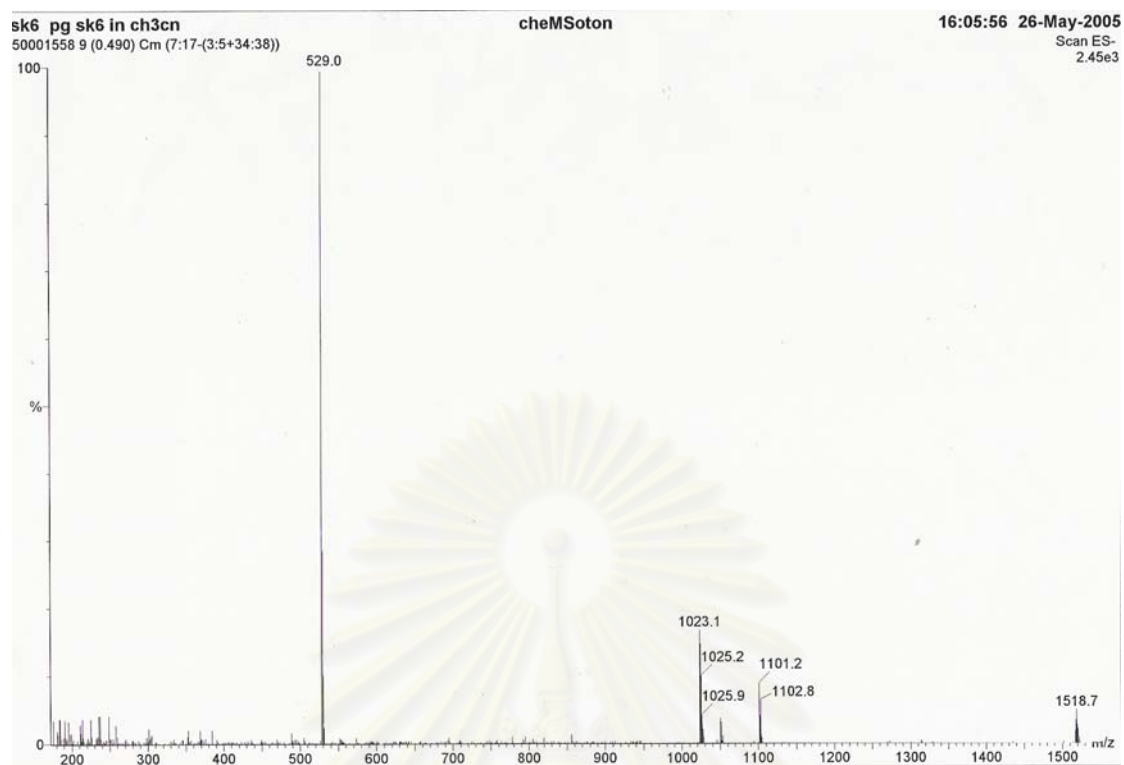


Figure 11 Mass spectrum of **L5** in acetonitrile.

สถาบันวิทยบริการ
จุฬาลงกรณ์มหาวิทยาลัย

Table 1 Geometrical parameters for the 3,9-di(hexylthioureido)acridine conformers and their protonated conformers computed at the B3LYP/6-31G(d) level of theory

System	L1a	L1b	L1c	HL1a ⁺	HL1b ⁺	HL1c ⁺
Bond length (Å)						
C(2)-N(1)	1.413	1.410	1.410	1.381	1.384	1.383
N(1)-C(4)	1.384	1.404	1.384	1.415	1.404	1.405
C(4)-N(2)	1.365	1.354	1.369	1.351	1.354	1.352
C(4)-S(1)	1.677	1.674	1.674	1.666	1.674	1.671
N(1)-H(1)	1.014	1.013	1.013	1.015	1.014	1.014
N(2)-H(2)	1.014	1.014	1.014	1.014	1.014	1.014
C(6)-N(3)	1.413	1.413	1.410	1.381	1.381	1.383
N(3)-C(8)	1.384	1.416	1.384	1.415	1.416	1.405
C(8)-N(4)	1.365	1.351	1.369	1.351	1.351	1.352
C(8)-S(2)	1.677	1.666	1.674	1.666	1.666	1.671
N(3)-H(3)	1.014	1.015	1.013	1.015	1.015	1.014
N(4)-H(4)	1.014	1.014	1.014	1.014	1.014	1.014
N(5)-H(5)	-	-	-	1.014	1.015	1.016
Angle (°)						
C(2)-N(1)-H(1)	113.3	112.9	113.1	114.8	112.7	113.0
C(1)-N(1)-H(1)	-	-	-	-	-	-
N(1)-C(4)-N(2)	111.5	111.1	111.0	110.7	111.1	111.2
C(4)-N(2)-H(2)	116.8	117.0	116.7	117.4	118.4	118.6
C(6)-N(3)-H(3)	113.3	113.2	113.1	114.8	114.8	113.0
N(3)-C(8)-N(4)	111.5	111.4	111.0	110.7	110.7	111.2
C(8)-N(4)-H(4)	116.8	116.8	116.7	117.4	117.4	118.5
Dihedral angle (°)						
C(1)-C(2)-N(1)-H(1)	155.8	-13.7	-15.0	166.1	0.3	-1.8
C(1)-C(2)-N(1)-C(4)	-42.8	153.2	152.6	-30.9	175.6	173.8
H(1)-N(1)-C(4)-S(1)	154.8	159.8	158.9	143.8	167.2	161.7
S(1)-C(4)-N(2)-H(2)	164.1	163.4	162.4	165.9	169.6	170.9
C(5)-C(6)-N(3)-H(3)	164.1	156.8	-15.0	166.1	166.5	-1.8
C(5)-C(6)-N(3)-C(8)	-42.8	-41.9	152.6	-30.9	-30.3	173.8
H(3)-N(3)-C(8)-S(2)	154.8	154.6	152.6	143.8	143.1	161.5
S(2)-C(8)-N(4)-H(4)	164.1	164.1	158.9	165.9	166.1	171.1

Molecular structures of 3,6-di(hexylthioureido)acridine conformers, their protonation, ^1H NMR and IR analyses: Theoretical and experimental studies

Somchai Keawwangchai, Thawatchai Tuntulani ^{*}, Vithaya Ruangpornvisuti ^{*}

Supramolecular Chemistry Research Unit, Department of Chemistry, Faculty of Science, Chulalongkorn University, Bangkok 10330, Thailand

Received 13 June 2006; received in revised form 25 July 2006; accepted 31 July 2006

Available online 14 September 2006

Abstract

The optimized structures of the 3,6-di(hexylthioureido)acridine conformers were obtained using density functional theory (DFT) and ONIOM methods. Three conformers of 3,6-di(hexylthioureido)acridine and their corresponding protonated forms were found. Single-point energies calculations were obtained using second-order Møller–Plesset at the MP2(fc)/6-31G(d) level. The computed ^1H NMR chemical shifts referenced to TMS in DMSO for all conformers were obtained. The presence of symmetrical conformers of the neutral and protonated structures were confirmed by the ^1H NMR measurement. The measured and computed IR spectra of the neutral and protonated species of 3,6-di(hexylthioureido)acridine were obtained and compared.

© 2006 Elsevier B.V. All rights reserved.

Keywords: 3,6-Di(hexylthioureido)acridine; Protonation; Proton NMR; IR; DFT; MP2; ONIOM

1. Introduction

As a result of the biological and environmental significance of anions, selective recognition and sensitivity of anions are of great importance in modern host-guest chemistry [1–5]. Neutral anion receptors incorporated with functional moieties such as urea or thiourea, [6–8] amide, [9–11] and calixpyrrole [12–15] groups have been explored in biotic and abiotic systems. Such neutral receptors possess advantages over the charged compounds such as host molecules incorporated with cationic guanidinium [16–18], polyammonium [19,20] and quaternary ammonium [21,22] moieties. Urea or thiourea groups incorporated receptors showed selective anion recognition in nonpolar [23] and polar [24,25] solvents through hydrogen bonding. Chromo- and fluorogenic urea/thiourea derivatives are of considerable interest in anion chemosensor because of

their potential application as optoelectronic devices (e.g. sensors, [26,27] information processing, [28] storage devices [29] and molecular switches [30]). Of particular interest in this regard are chromogenic anion chemosensors that can be used for direct “naked-eye” sensing of anions. [31–34] Acridine is one of the interesting chromogenic subunits because of not only it would act as optically sensitive indicator of anion binding but also it could serve as a “sink” for charge transfer involving bound anionic guest. The recognition of carboxylate and dicarboxylates by azophenolthiourea derivatives was theoretically studied [35]. A few acridine derivatives have been used in the development of some chromogenic chemosensor for cation and anion recognitions.

As amino hydrogen atoms of two thiourea groups of the 3,6-di(hexylthioureido)acridine have ability to bind to many anions [23–25], its structures, electronic and ^1H NMR properties should be investigated. The structures of the 3,6-di(hexylthioureido)acridine conformers and their protonated species, their relative stabilities have been investigated in this work.

^{*} Corresponding authors. Tel.: +66 2218 7644; fax: +66 2254 1309.
E-mail address: vithaya.r@chula.ac.th (V. Ruangpornvisuti).

2. Methodology

2.1. Experimental

Nuclear magnetic resonance (NMR) spectra were recorded on a Varian 400 MHz nuclear magnetic resonance spectrometers. In all cases, both ligands were dissolved in deuterated dimethylsulfoxide (DMSO- d_6). Elemental analysis were carried out on CHNS/O analyzer (Perkin-Elmer PE2400 series II). Electrospray mass spectra were determined on a Micromass Platform quadrupole mass analyser (HP1050) with an electrospray ion source using acetonitrile as solvent. Absorption spectra were measured by a Varian Cary 50 UV–vis spectrophotometer.

2.1.1. 3,6-Diisothiocyanatoacridine

To a solution of 3,6-diaminoacridine hemisulfate (0.5625 g, 1.02 mmol) in dichloromethane (50 mL) was added K_2CO_3 (2.79 g, 20 mmol) in water (50 mL) and stirred for 30 min. Thiophosgene (0.2 mL, 2.5 mmol) was added in to the mixture and refluxed for 2 h in a nitrogen atmosphere. The mixture was cooled to room temperature and organic layer was separated, washed with water and dried (anhydrous Na_2SO_4). The solvent was removed in vacuo. The resulting solid was purified by column chromatography over silica gel with 20% hexane/ CH_2Cl_2 as eluent yield 0.5286 g (90%) yellow solid. 1H NMR (400 MHz, $CDCl_3$, ppm) 7.353–7.375 (d, 2H, ArH, $J = 8.8$ Hz) 7.950–7.969 (d, 2H, ArH, $J = 7.6$ Hz) 8.690 (s, 1H, ArH).

2.1.2. 3,6-Di(hexylthioureido)acridine (L)

In a 50 mL two-necked round bottom flask equipped with a magnetic bar, 3,6-diisothiocyanatoacridine (0.5793 g, 1.97 mmol) was dissolved in dichloromethane (20 mL) and *n*-hexylamine (0.44 mL, 4.99 mmol) was then added. The mixture was stirred overnight at room temperature under nitrogen atmosphere. After the reaction was completed, the resulting solid was filtered off to obtain a yellow residue (0.4590 g, 94%). The product was dried *in vacuo* and kept in a desiccator. Anal. Calcd. for $C_{28}H_{36}N_4O_2S_2$: C, 65.41; H, 7.52; N, 14.13. Found: C, 65.267; H, 7.627; N, 14.151. m/z (%) = 530.0 (100) $[M + Cl]^-$. 1H NMR spectrum (400 MHz, DMSO- d_6 , ppm) δ 0.901–0.916 (bm, 6H, CH_2CH_3 , $J = 6.1$ Hz), 1.340 (bs, 12H, $CH_2CH_2CH_2CH_2CH_3$), 1.580–1.630 (m, 4H, $CH_2CH_2CH_2$, $J = 20.0$ Hz) 3.535–3.548 (bd, 4H, $NHCH_2CH_2$, $J = 4.8$ Hz) 7.580–7.602 (d, 2H, ArH, $J = 8.7$ Hz) 8.028–8.050 (d, 2H, ArH, $J = 8.8$ Hz) 8.220 (s, 2H, $CSNHCH_2$) 8.302 (s, 2H, ArH) 8.879 (s, 1H, ArH) 9.934 (s, 2H, ArNHCS).

2.1.3. 3,6-Di(hexylthioureido)acridinium triflate (HL)

In a 50 mL two-necked round bottom flask equipped with a magnetic bar, 3,6-di(hexylthioureido)acridine (0.2530 g, 0.51 mmol) was dissolved in dimethylformam-

ide (10 mL) and trifluoromethanesulfonic acid (0.12 mL, 1.70 mmol) was then added. The mixture was stirred 2 h at room temperature under nitrogen atmosphere. The solvent was removed in vacuo. The resulting solid was recrystallized in CH_2Cl_2 /hexane and the resulting solid was filtered off to obtain a orange residue (0.3234 g, 98%). 1H NMR spectrum (400 MHz, DMSO- d_6 , ppm) δ 0.854–0.887 (m, 6H, CH_2CH_3 , $J = 13.2$ Hz), 1.303 (bs, 12H, $CH_2CH_2CH_2CH_2CH_3$), 1.554–1.606 (m, 4H, $CH_2CH_2CH_2$, $J = 20.8$ Hz) 3.512–3.526 (bd, 4H, $NHCH_2CH_2$, $J = 5.6$ Hz) 7.575–7.597 (d, 2H, ArH, $J = 8.8$ Hz) 8.248–8.271 (d, 2H, ArH, $J = 9.2$ Hz) 8.580 (s, 2H, ArH) 9.087(s, 2H, $CSNHCH_2$) 9.464 (s, 1H, ArH) 10.490 (s, 2H, ArNHCS) 15.293 (s, 1H, ArNH).

2.2. Computations

Full geometry optimizations of all investigated molecules and complexes were computed by density functional theory (DFT) using the hybrid density functional B3LYP [36,37] methods and the two-layered ONIOM(MO:MO) approach [38,39] using B3LYP/6-31G(d) as high model and semiempirical AM1 [40] as low model. All geometry optimizations have been carried out using the B3LYP/6-31G(d) and two-layered ONIOM(B3LYP/6-31G(d):AM1) with zero-point vibration energy corrections. Energies obtained from single point calculations using the second-order Møller–Plesset [41] (frozen core), MP2(fc) method at the MP2(fc)/6-31G(d) level have been used for improvement of energy correction. All single-point calculations at the B3LYP/6-31G(d)//ONIOM(B3LYP/6-31G(d):AM1), MP2(fc)/6-31G(d)//ONIOM(B3LYP/6-31G(d):AM1) and MP2(fc)/6-31G(d)//B3LYP/6-31G(d) levels of theory have been also employed for the energy computations. For the two-layered ONIOM(B3LYP/6-31G(d):AM1), two *n*-hexyl terminals of the 3,6-di(hexylthioureido) acridine were treated as less important layer (low model) and the remaining part was treated as more important one (high model). The solvent effect was investigated by single-point computations on the B3LYP/6-31G(d)-optimized gas-phase structures using the conductor-like polarizable continuum model (CPCM) and [42,43].

All calculations were performed with the GAUSSIAN 03 program [44]. The MOLDEN 4.2 program [45] was utilized to display molecular structures and observed the geometry convergence via the Gaussian output files. The molecular graphics of all species were generated with the MOLEKEL 4.3 program [46].

The Mulliken electronegativity (χ), chemical hardness (η) and electronic chemical potential (μ) for all isomers of the 3,6-bis-*N*-(*n*-hexylthioureido) acridine conformers were computed using orbital energies of the highest occupied molecular orbital (HOMO) and the lowest unoccupied molecular orbital (LUMO) at the B3LYP/6-31G(d) level of theory. The chemical hardness, electronic chemical

potential and Mulliken electronegativity were derived from the first ionization potential (I) and electron affinity (A) of the N -electron molecular system with a total energy (E) and external potential ($v(\vec{r})$) using the relations: $\chi = -(\frac{\partial E}{\partial N})_{v(\vec{r})} = -\mu \approx \frac{1}{2}(I + A)$ and $\eta = -(\frac{\partial^2 E}{\partial N^2})_{v(\vec{r})} \approx \frac{1}{2}(I - A)$, and the first ionization potential and electron affinity are $I = E(N - 1) - E(N)$ and $A = E(N) - E(N + 1)$ [47]. According to the Koopmans theorem [48], I and A were computed from the HOMO and LUMO energies using the relations: $I = -E_{\text{HOMO}}$ and $A = -E_{\text{LUMO}}$. Therefore, $\eta = \Delta E_{\text{HOMO-LUMO}}/2$, $\mu = (E_{\text{HOMO}} + E_{\text{LUMO}})/2$ and $\chi = -(E_{\text{HOMO}} + E_{\text{LUMO}})/2$ were employed as the previous works [49–51].

The ^1H NMR chemical shifts were calculated with the IEFPCM/B3LYP/6-31G(d) computations using the gauge-invariant atomic orbitals (GIAO) method [52–54]. The ^1H NMR chemical shifts referenced to tetramethylsilane (TMS) of which the calculated absolute shift $\sigma(\text{H})$ is 31.1731 ppm were obtained from the single-point GIAO IEFPCM/B3LYP/6-31G(d) NMR calculations as in dimethyl sulphoxide (DMSO) solvent.

3. Results and discussion

3.1. Conformer, stability and protonation of 3,6-di(hexylthioureido)acridine

The structures of all conformers of 3,6-di(hexylthioureido)acridine and their protonated forms optimized at the B3LYP/6-31G(d) and two-layered ONIOM(B3LYP/6-31G(d):AM1) levels were obtained. The geometrical parameters for the B3LYP/6-31G(d)-optimized structures of 3,6-di(hexylthioureido)acridine conformers and their protonated conformers are listed in Table 1 and their atomic numbering is shown in Fig. 1. The B3LYP/6-31G(d)-optimized structures of 3,6-di(hexylthioureido)acridine conformers and their corresponding protonated structures are shown in Fig. 2.

Total energies of the 3,6-di(hexylthioureido)acridine conformers and their protonated conformers were computed at the ONIOM(B3LYP/6-31G(d):AM1), B3LYP/6-31G(d), B3LYP/6-31G(d)//ONIOM(B3LYP/6-31G(d):AM1), MP2(fc)/6-31G(d)//ONIOM(B3LYP/6-31G(d):AM1) and

Table 1
Geometrical parameters for the conformers of 3,6-di(hexylthioureido)acridine and their protonated forms computed at the B3LYP/6-31G(d) level of theory

Parameter	Neutral form			Protonated form		
	La ^a	Lb	Lc	HLa ⁺	HLb ⁺	HLc ⁺ ^b
<i>Bond length (Å)</i>						
C(2)–N(1)	1.413	1.410	1.410	1.381	1.384	1.383
N(1)–C(4)	1.384	1.404	1.384	1.415	1.404	1.405
C(4)–N(2)	1.365	1.354	1.369	1.351	1.354	1.352
C(4)–S(1)	1.677	1.674	1.674	1.666	1.674	1.671
N(1)–H(1)	1.014	1.013	1.013	1.015	1.014	1.014
N(2)–H(2)	1.014	1.014	1.014	1.014	1.014	1.014
C(6)–N(3)	1.413	1.413	1.410	1.381	1.381	1.383
N(3)–C(8)	1.384	1.416	1.384	1.415	1.416	1.405
C(8)–N(4)	1.365	1.351	1.369	1.351	1.351	1.352
C(8)–S(2)	1.677	1.666	1.674	1.666	1.666	1.671
N(3)–H(3)	1.014	1.015	1.013	1.015	1.015	1.014
N(4)–H(4)	1.014	1.014	1.014	1.014	1.014	1.014
N(5)–H(5)	–	–	–	1.014	1.015	1.016
<i>Angle (°)</i>						
C(2)–N(1)–H(1)	113.3	112.9	113.1	114.8	112.7	113.0
N(1)–C(4)–N(2)	111.5	111.1	111.0	110.7	111.1	111.2
C(4)–N(2)–H(2)	116.8	117.0	116.7	117.4	118.4	118.6
C(6)–N(3)–H(3)	113.3	113.2	113.1	114.8	114.8	113.0
N(3)–C(8)–N(4)	111.5	111.4	111.0	110.7	110.7	111.2
C(8)–N(4)–H(4)	116.8	116.8	116.7	117.4	117.4	118.5
<i>Dihedral angle (°)</i>						
C(1)–C(2)–N(1)–H(1)	155.8	–13.7	–15.0	166.1	0.3	–1.8
C(1)–C(2)–N(1)–C(4)	–42.8	153.2	152.6	–30.9	175.6	173.8
H(1)–N(1)–C(4)–S(1)	154.8	159.8	158.9	143.8	167.2	161.7
S(1)–C(4)–N(2)–H(2)	164.1	163.4	162.4	165.9	169.6	170.9
C(5)–C(6)–N(3)–H(3)	164.1	156.8	–15.0	166.1	166.5	–1.8
C(5)–C(6)–N(3)–C(8)	–42.8	–41.9	152.6	–30.9	–30.3	173.8
H(3)–N(3)–C(8)–S(2)	154.8	154.6	152.6	143.8	143.1	161.5
S(2)–C(8)–N(4)–H(4)	164.1	164.1	158.9	165.9	166.1	171.1

^a The most stable conformer of the neutral form.

^b The most stable conformer of the protonated form.

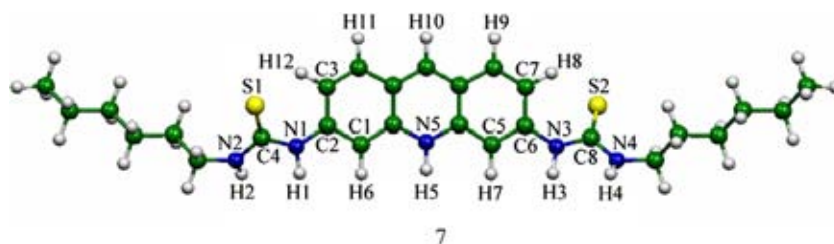


Fig. 1. Atomic labeling of the 3,6-di(hexylthioureido)acridine.

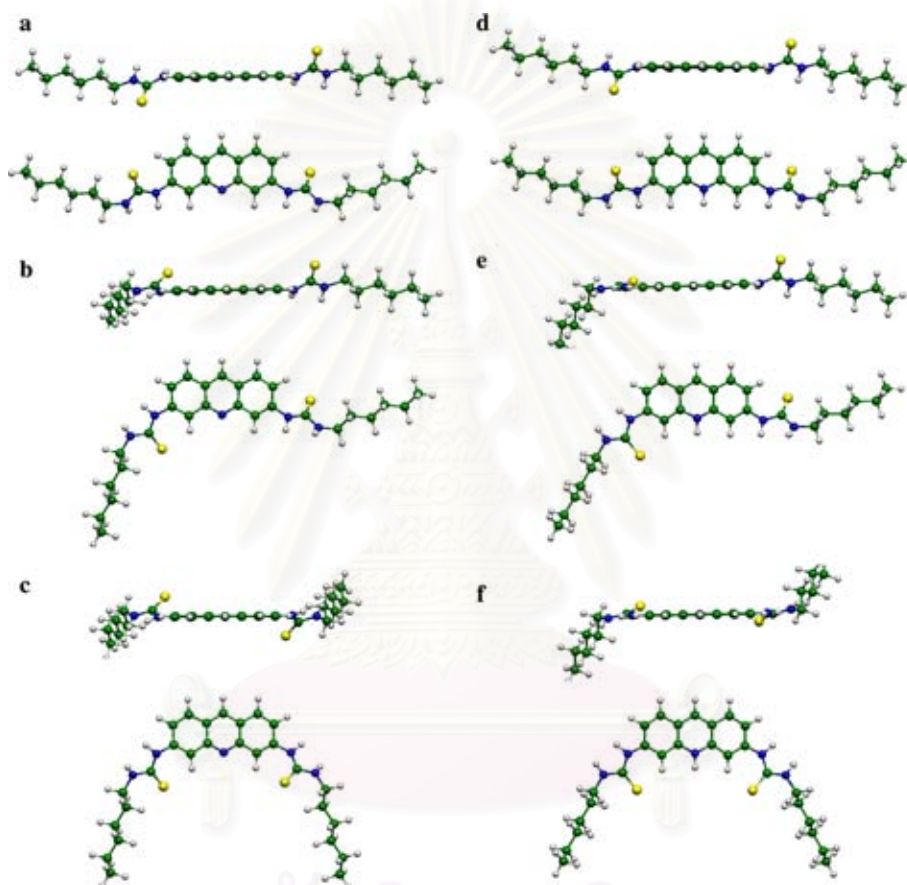


Fig. 2. B3LYP/6-31G(d)-optimized structures of 3,6-di(hexylthioureido)acridine conformers (a) La, (b) Lb and (c) Lc, and their protonated forms (d) HLa⁺, (e) HLb⁺ and (f) HLC⁺. Top and bottom figures are top and front views of their molecular structures, respectively.

MP2(fc)/6-31G(d)//B3LYP/6-31G(d) levels and their relative energies are tabulated in Table 2. Relative stabilities of the 3,6-di(hexylthioureido)acridine conformers and their protonated species are in decreasing orders: La > Lb > Lc and HLC⁺ > HLb⁺ > HLa⁺, respectively.

Based on the MP2(fc)/6-31G(d)//B3LYP/6-31G(d) calculations, the maximum ranges of relative energies for the neutral and protonated species of 3,6-di(hexylthioureido)acridine conformers are 3.58 and 3.78 kcal/mol, respectively. The protonation of 3,6-di(hexylthioureido)acridine conformers, their reaction energies, enthalpies and Gibbs free energies derived from vibration frequencies calculations at the ONIOM(B3LYP/6-31G(d):AM1) and B3LYP/6-31G(d) levels are shown in Table 3.

Protonation reactions of the 3,6-di(hexylthioureido)acridine conformers derived whether from various levels of theory are always exothermic and spontaneous processes. Based on the B3LYP/6-31G(d) method, the protonation enthalpies for conformers La, Lb and Lc are −248.07, −251.91 and −255.31 kcal/mol, respectively. The La conformer is the most stable species of the neutral form and more stable than that of Lb and Lc by 1.33 and 3.58 kcal/mol, respectively. On the other hand, the HLC⁺ conformer is the most stable species of the protonated form and more stable than that of HLb⁺ and HLa⁺ by 1.76 and 3.78 kcal/mol, respectively. In gas phase, the molecular energies of either neutral form or protonated forms are hardly ever different.

Table 2
Relative energies of 3,6-di(hexylthioureido)acridine conformers and their protonated conformers computed at various levels of theory

Conformer/system	ΔE (kcal/mol)					In DMSO ^b B3LYP/6-31G(d)
	In gas phase					
	ONIOM ^a	B3LYP/6-31G(d)	B3LYP/6-31G(d)// ONIOM ^a	MP2(fc)/6-31G(d)// ONIOM ^a	MP2(fc)/6-31G(d)// B3LYP/6-31G(d)	
Neutral form						
La	0.00	0.00	0.00	0.00	0.00	0.00
Lb	1.17	1.38	1.17	1.93	1.83	0.56
Lc	3.27	3.01	3.27	3.31	3.58	1.36
Protonated form						
HLa ⁺	4.18	4.15	4.18	3.53	3.78	1.65
HLb ⁺	1.59	1.81	1.59	1.69	1.76	0.75
HLC ⁺	0.00	0.00	0.00	0.00	0.00	0.00

^a The two-layered ONIOM(B3LYP/6-31G(d):AM1).

^b The single-point IEFPCM ($\epsilon = 46.7$, DMSO) at the B3LYP/6-31G(d) level.

Table 3
Reaction energies and thermodynamic properties of the protonation of 3,6-di(hexylthioureido)acridine conformers computed at two different levels of theory

Protonation	ONIOM (B3LYP/6-31G(d):AM1)			B3LYP/6-31G(d)		
	ΔE^a	ΔH^a	ΔG^a	ΔE^a	ΔH^a	ΔG^a
La + H ⁺ → HLa ⁺	−246.538	−246.401	−246.684	−248.248	−248.207	−248.082
Lb + H ⁺ → HLb ⁺	−250.262	−250.116	−251.135	−251.963	−251.907	−252.312
Lc + H ⁺ → HLC ⁺	−253.665	−253.489	−255.093	−255.408	−255.308	−257.066

^a In kcal/mol.

3.2. Electronic structure of 3,6-di(hexylthioureido)acridine

Energies of the highest occupied molecular orbital (HOMO), E_{HOMO} , the lowest unoccupied molecular orbital (LUMO), E_{LUMO} and the frontier molecular orbital energy gap, $\Delta E_{\text{HOMO-LUMO}}$ are shown in Table 4. Relative reactivities of the neutral and protonated species of 3,6-di(hexylthioureido)acridine conformers are in orders: Lc > Lb > La and HLa⁺ > HLb⁺ > HLC⁺, respectively. As the Lc conformer is the most active structure of the neutral species, its protonation is therefore the most favorable reaction and the most stable structure of the protonated species such as HLC⁺ is then formed. The HLC⁺ conformer is therefore the least active species of the protonated species. The chemical hardnesses of all species are in order: La > Lb > Lc > HLC⁺ > HLb⁺ > HLa⁺. Mulliken electronegativities of the neutral and protonated species of 3,6-di(hexylthioureido)acridine derived from their chemical potentials are within 3.547–3.662 and 6.981–7.010, respectively. The B3LYP/6-31G(d)-computed HOMOs and LUMOs for all species of 3,6-di(hexylthioureido)acridine are shown in Fig. 3. LUMOs of the neutral structures La, Lb and Lc shown in Fig. 3 are very similar to their corresponding orbitals of the protonated structures HLa⁺, HLb⁺ and HLC⁺, respectively. HOMOs of the neutral structures of 3,6-di(hexylthioureido)acridine are obviously situated on apex carbon and nitrogen atoms of the acridine ring but never situated on any atoms of the acridine ring of the protonated structures. This

phenomenon describes that a valence electron in their molecular orbitals transfer to amino-proton atom (H5) which is located at middle of the acridine ring to exert the protonated structure.

Electrostatic potential surfaces of the neutral and protonated structures of 3,6-di(hexylthioureido)acridine conformers were generated from the Gaussian output files of their B3LYP/6-31G(d) computation with GFPRINT and POP = FULL keywords using the Molekel 4.3 software [46]. Electrostatic potential surfaces (in a.u.) presented over electronic isodensity $\rho = 0.05 \text{ eA}^{-3}$ for La, $V_s = 31.5436$, Lb, $V_s = 87.5226$, Lc, $V_s = 63.9896$, HLa⁺, $V_s = 18.3433$, HLb⁺, $V_s = 45.3886$ and HLC⁺, $V_s = 101.865$ are shown in Fig. 4. The color maps of electronic isodensity surfaces in Fig. 4 show strong negative charge on the imino-nitrogen atom (N5 as shown in Fig. 1) for the neutral structures but show weak negative charge on the amino-nitrogen atoms (N1, N2, N3 and N4) for the protonated structures. Nevertheless, amino-hydrogen atoms of thiourea groups of either the neutral or protonated conformers show strong positive charges.

3.3. ¹H NMR chemical shifts of 3,6-di(hexylthioureido)acridine species

The B3LYP/6-31G(d)-computed proton chemical shifts for conformers of the neutral and protonated species of 3,6-di(hexylthioureido)acridine are shown in Table 5. The ¹H NMR spectra of 3,6-di(hexylthioureido)acridine con-

Table 4

The E_{HOMO} , E_{LUMO} and frontier molecular orbital energy gap, $\Delta E_{\text{HOMO-LUMO}}$ of the conformers 3,6-di(hexylthioureido)acridine and their corresponding protonated forms computed at the B3LYP/6-31G(d) level of theory

Species	$E_{\text{HOMO}}^{\text{a}}$	$E_{\text{LUMO}}^{\text{a}}$	$\Delta E_{\text{HOMO-LUMO}}^{\text{a}}$	$\eta^{\text{a,b}}$	$\mu^{\text{a,c}}$	$\chi^{\text{a,d}}$
La	-5.391	-1.933	3.458	1.729	-3.662	3.662
Lb	-5.303	-1.899	3.404	1.702	-3.601	3.601
Lc	-5.223	-1.872	3.351	1.675	-3.547	3.547
HLa ⁺	-8.192	-5.803	2.389	1.195	-6.997	6.997
HLb ⁺	-8.179	-5.783	2.396	1.198	-6.981	6.981
HLc ⁺	-8.264	-5.755	2.509	1.255	-7.010	7.010

^a In eV.

^b Chemical hardness, $\eta = \Delta E_{\text{HOMO-LUMO}}/2$.

^c Electronic chemical potential, $\mu = (E_{\text{HOMO}} + E_{\text{LUMO}})/2$.

^d The Mulliken electronegativity, $\chi = -(E_{\text{HOMO}} + E_{\text{LUMO}})/2$.

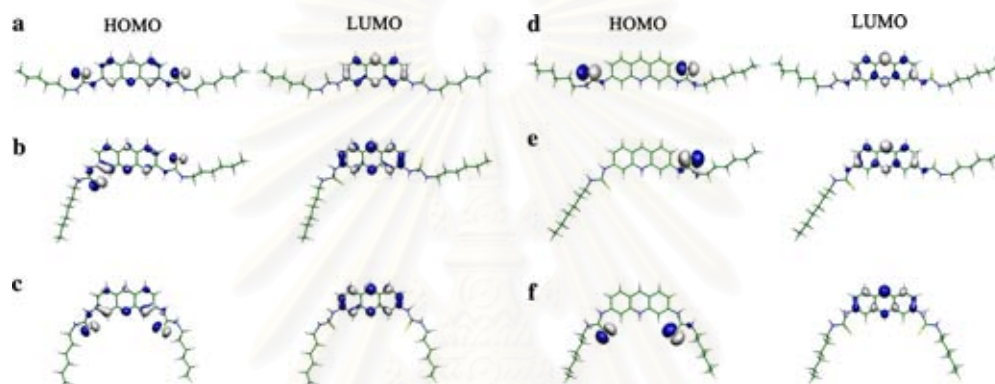


Fig. 3. The B3LYP/6-31G(d)-computed molecular orbitals contoured at an iso-surface value of 0.05 a.u. for LUMO and HOMO of conformers (a) La, (b) Lb, (c) Lc, (d) HLa⁺, (e) HLb⁺ and (f) HLc⁺.

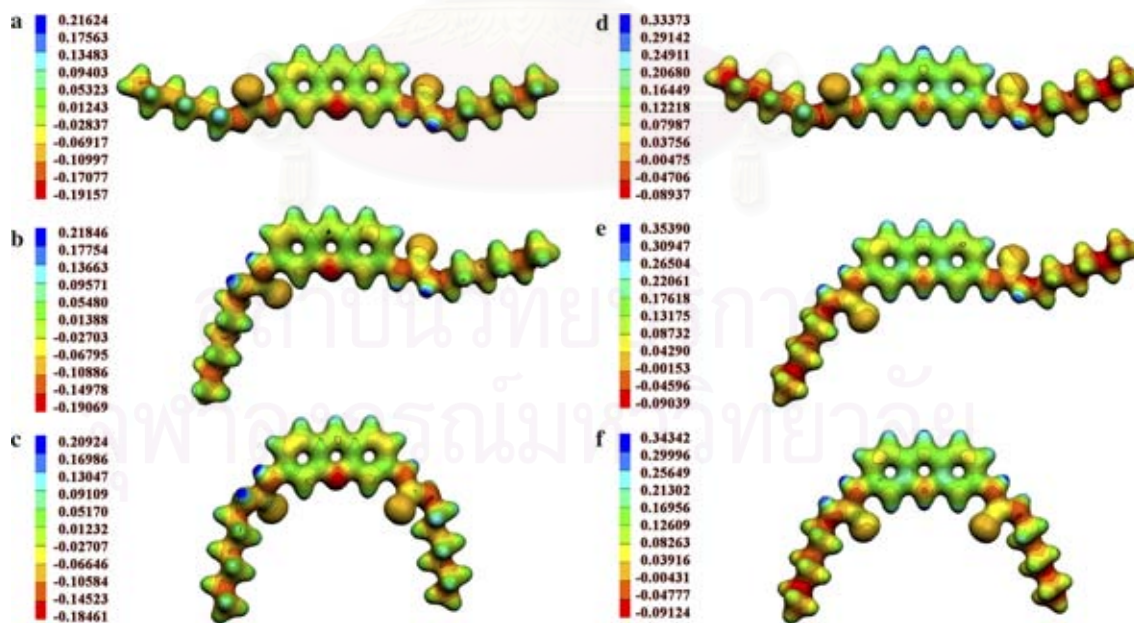


Fig. 4. Electrostatic potential surface (in a.u.) presented over electronic isodensity $\rho = 0.05 \text{ eA}^{-3}$ for (a) La, $V_s = 31.5436$, (b) Lb, $V_s = 87.5226$, (c) Lc, $V_s = 63.9896$, (d) HLa⁺, $V_s = 18.3433$, (e) HLb⁺, $V_s = 45.3886$ and (f) HLc⁺, $V_s = 101.865$.

formers and their corresponding protonated forms in DMSO referenced to TMS were obtained at 298.15 K. Based on the principle of weighted-average chemical shift

[55], a single peak of the observed ¹H NMR chemical shift is an average value of the corresponding protons of all present conformers. The single peak of H5 chemical shift

Table 5
¹H NMR chemical shifts for the 3,6-di(hexylthioureido)acridine conformers and their corresponding protonated forms

Species	¹ H NMR ^a							
	Computed ^b			Measured ^c	Computed ^b			Measured ^d
	La	Lb	Lc		HLa ⁺	HLb ⁺	HLC ⁺	
H1	7.94	7.74	7.80	9.93	8.07	8.08	8.02	10.49
H2	6.58	6.51	6.56	8.22	7.13	6.99	7.08	9.08
H3	7.94	7.88	7.80	9.93	8.07	8.08	8.02	10.49
H4	6.58	6.58	6.56	8.22	7.13	7.17	7.08	9.08
H5	–	–	–	–	9.47	10.24	10.34	15.29
H6	7.84	9.17	9.16	8.30	7.43	10.13	9.95	8.58
H7	7.84	7.79	9.16	8.30	7.43	7.45	9.95	8.58
H8	8.78	8.87	7.62	7.58–7.60	8.89	8.93	7.69	7.58–7.60
H9	8.58	8.56	8.56	8.036–8.05	8.74	8.72	8.77	8.25–8.27
H10	9.18	9.19	9.07	8.88	10.14	9.45	9.40	9.46
H11	8.58	8.68	8.56	8.036–8.05	8.74	8.78	8.77	8.25–8.27
H12	8.78	7.61	7.62	7.58–7.60	8.89	7.71	7.69	7.58–7.60

^a In ppm based on the tetramethylsilane (TMS, 32.1687 ppm) reference, computed at the B3LYP/6-31G(d) level with IEFPCM model in DMSO.

^b In DMSO using the IEFPCM model ($\epsilon = 46.7$) at the B3LYP/6-31G(d) level.

^c The values are expected to correspond the La conformer.

^d The values are expected to correspond the HLC⁺ conformer.

($\delta_{\text{observed}}^{\text{H5}}$) of the protonated species can be evaluated by the following weighted-average equation.

$$\delta_{\text{observed}}^{\text{H5}} = \delta_{\text{HLa}^+}^{\text{H5}} \cdot f_{\text{HLa}^+} + \delta_{\text{HLb}^+}^{\text{H5}} \cdot f_{\text{HLb}^+} + \delta_{\text{HLC}^+}^{\text{H5}} \cdot f_{\text{HLC}^+},$$

where $\delta_{\text{HLa}^+}^{\text{H5}}$, $\delta_{\text{HLb}^+}^{\text{H5}}$ and $\delta_{\text{HLC}^+}^{\text{H5}}$ are H5 chemical shifts of conformers HLa⁺, HLb⁺ and HLC⁺ and f_{HLa^+} , and f_{HLC^+} are their mole fractions, respectively. As the HLC⁺ is the most stable conformer, the mole fraction of HLC⁺ therefore approaches unity and others approach zero and $\delta_{\text{observed}}^{\text{H5}} = \delta_{\text{HLC}^+}^{\text{H5}}$ was possibly assumed. As the HLC⁺ is the most stable conformer of 3,6-di(hexylthioureido)acridine and its C_{2v} symmetry, the proton chemical shifts of its equivalent protons in which H1 and H3, H2 and H4, H6 and H7, H8 and H12, and H9 and H11 are equivalent, are therefore expected to correspond to the measured ¹H NMR spectrum, see Fig. 5 and Table 5. For the neutral system of the 3,6-di(hexylthioureido)acridine, its observed chemical shifts such as H1 ($\delta_{\text{observed}}^{\text{H1}}$) which is equivalent to H3, was expected to approach the H1 chemical shift of the La ($\delta_{\text{La}}^{\text{H1}}$) which is the most stable conformer. As the La is the most stable conformer of 3,6-di(hexylthioureido)acridine and its C_{2v} symmetry, the proton chemical shifts of its equivalent protons are therefore expected to correspond to the measured ¹H NMR spectrum, see Fig. 5 and Table 5.

3.4. FT-IR spectra of 3,6-di(hexylthioureido)acridine species

Vibration frequencies of the neutral and protonated species of 3,6-di(hexylthioureido)acridine were computed at the B3LYP/6-31G(d) level and obtained from the measurement prepared as a KBr pellet using Nicolet Impact 410 FT-IR spectrometer at room temperature. The measured and computed IR spectra are shown in Fig. 6 and their selected vibration modes are listed in Table 6. The

computed spectra in Fig. 6 are derived from the B3LYP/6-31G(d) vibration frequencies of which wave numbers were corrected using empirical scaling factor of 0.9641 determined by Scott and Radom [56]. This figure shows equivalences of N–H and C–H protons chemical shifts for the neutral species La and protonated HLC⁺ according to their C_2 – molecular symmetries. Table 6 shows the NH stretching of N–H5 (mode 17) of HLC⁺ species at 3426.5 cm⁻¹ which is combined with NH stretching of H2 and H4 at 3432.1 cm⁻¹ appearing as one peak as shown in Fig. 6(b). Nevertheless, these vibration modes are not possible to be certainly assigned for the experimental IR spectra. Difference between IR spectral peaks of protonated (HLC⁺) and neutral (La) structures appearing within 1430–1300 cm⁻¹ are able to be observed, see experimental IR spectra in Fig. 6. This region contains at least three vibration modes of NH bending of H5 proton.

Based on the computed vibration spectra, the N–H stretching absorption bands, ν_{NH} are at 3430.0 cm⁻¹ for the neutral form and 3432.1 with 3426.5 cm⁻¹ for the protonated form. The absorption peaks at 3441.7 and 3387.9 cm⁻¹ of the protonated structure possess the thiourea NH groups (N–H1, N–H2, N–H3 and N–H4) and imino NH, respectively. Peak at ~3400 cm⁻¹ of the protonated structure of which band is the combination bands of 3441.7 and 3387.9 cm⁻¹ is obviously higher than that of the neutral species. The N–H bending absorption bands, δ_{NH} are at 1513.6 cm⁻¹ for the neutral form and 1576 cm⁻¹ for the protonated species Scheme 1.

4. Conclusions

Three structures of 3,6-di(hexylthioureido)acridine conformers and their corresponding protonated forms optimized at the B3LYP/6-31G(d) and two-layered

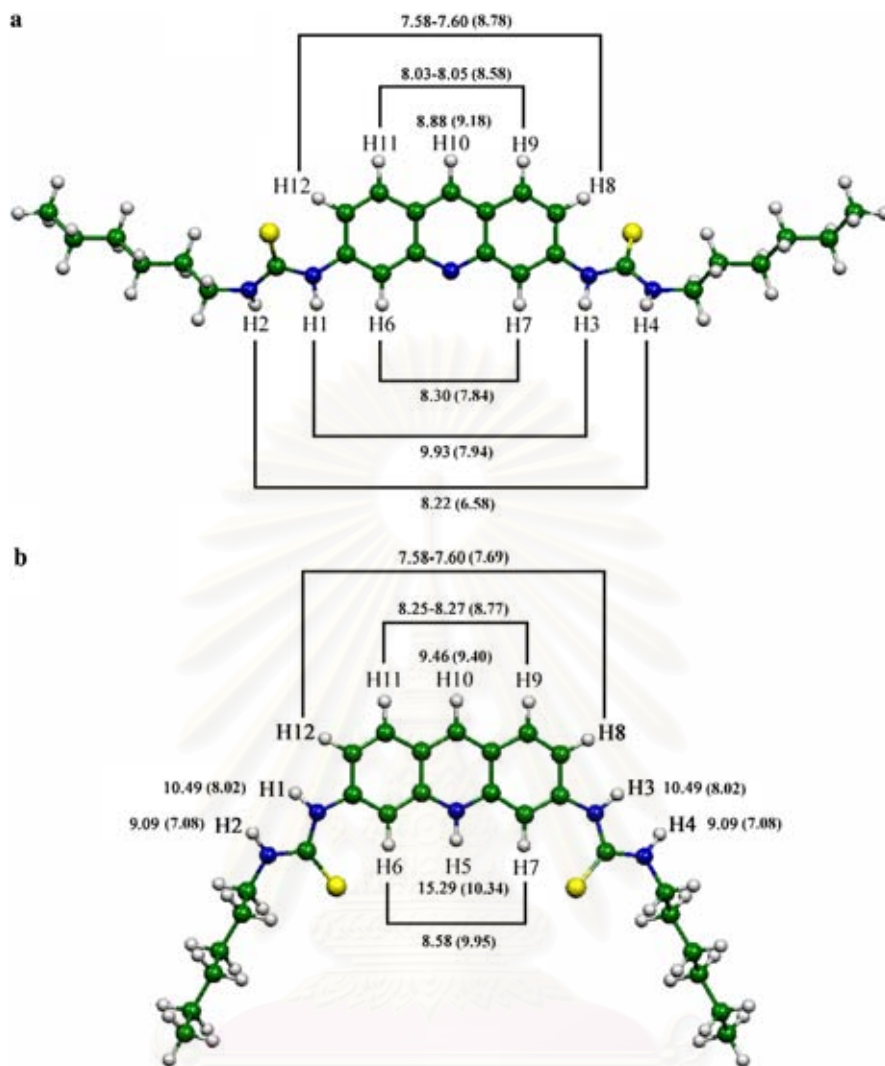


Fig. 5. Proton chemical shifts of the measured and B3LYP/6-31G(d)-computed $^1\text{H-NMR}$ (in parenthesis) of the most stable structure of (a) the neutral and (b) protonated forms of 3,6-di(hexylthioureido) acridine conformers. The chemical shifts are in ppm referenced to the TMS standard.

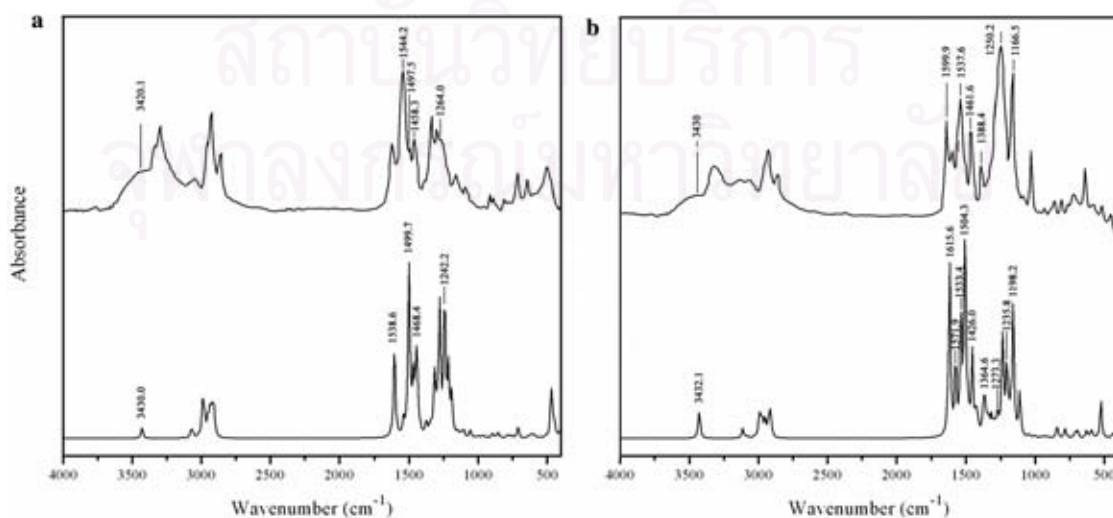


Fig. 6. FT-IR spectra of the (a) neutral and (b) protonated forms of 3,6-di(hexylthioureido) acridine. Top and bottom are the measured and computed infrared spectra, respectively. The computed IR spectra are of the most stable species, La and HLC^+ .

Table 6
Selected wave numbers (cm^{-1}) and their corresponding intensities of the B3LYP/6-31G(d)-computed and observed IR vibration modes for the neutral and protonated species of 3,6-di(hexylthioureido)acridine. The computed IR vibration frequencies were scaled by 0.9614

Mode/species	Computed frequency ^a	IR intensities ^b	Observed Frequency ^a	Assignment ^c
<i>Neutral form^d</i>				
1	1242.2	731	1264.0	NH _(1,2,3,4) bending + CH bending
2	1468.4	253	1458.3	NH _(1,2,3,4) bending
3	1499.7	837	1497.5	NH _(2,4) bending + CH bending
4	1538.6	82	1544.2	NH _(1,3) bending
5	3430.0	28	3420.1	NH _(1,2,3,4) stretching
<i>Protonated form^e</i>				
6	1198.2	149	1166.5	NH ₍₅₎ bending + CH bending
7	1235.8	688	1250.2	NH _(1,3) bending + CH bending
8	1273.3	144	– ^f	NH ₍₅₎ bending + CH bending
9	1364.6	192	1388.4	NH ₍₅₎ bending + CC bending
10	1426.0	143	1461.6	NH ₍₅₎ bending + CH bending
11	1504.3	1259	– ^f	NH _(2,4) bending
12	1533.4	761	1537.6	NH _(1,2,3,4) stretching
13	1571.9	360	1599.9	NH _(1,3) bending
14	1615.6	1086	1640.0	NH ₍₅₎ bending + CH bending
15	3418.9	23	– ^g	NH _(3,4) stretching
16	3419.1	17	– ^g	NH _(1,2) stretching
17	3426.5	31	– ^g	NH ₍₅₎ stretching
18	3432.1	129	~3430	NH _(2,4) stretching

^a In cm^{-1} .

^b In km/mol .

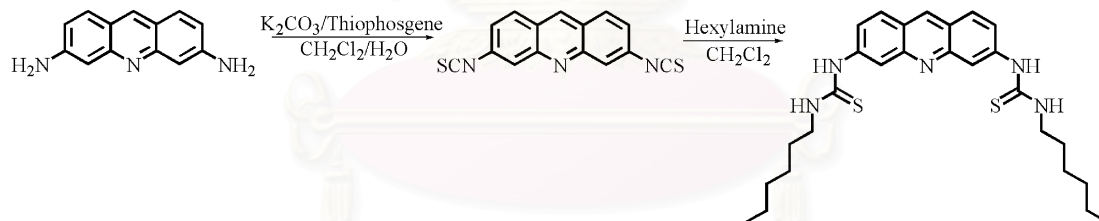
^c The numbers in parentheses refer to hydrogen atoms of which numbers are defined in Fig. 1.

^d Based on La structure.

^e Based on HLc⁺ structure.

^f No assignment.

^g They are combined to broaden peak at $\sim 3500 \text{ cm}^{-1}$.



Scheme 1. Synthesis of bisthiourea.

ONIOM(B3LYP/6-31G(d):AM1) levels of theory are obtained. The single-point energies calculations were also obtained at the MP2(fc)/6-31G(d) level. The relative stabilities of the 3,6-di(hexylthioureido) acridine conformers and their protonated conformers are in decreasing orders: La > Lb > Lc and HLc⁺ > HLb⁺ > HLa⁺, respectively. All the protonation reactions of 3,6-di(hexylthioureido) acridine conformers are spontaneously exothermic processes. The measured ¹H NMR chemical shifts and IR vibration modes of neutral and protonated structures of 3,6-di(hexylthioureido)acridine were analyzed and compared to the computations.

Acknowledgements

This work was financially supported by the Thailand Research Fund (TRF). The Royal Golden Jubilee (RGJ)

grant, No. PHD/00900/2544 supported by TRF to S.K. was acknowledged. The Rachadapisek Sompoch Endowment Fund, Chulalongkorn University is gratefully acknowledged for partially financial supported our research unit. We also thank Mr. Banchob Wannoo for his helps and valuable suggestions and Ms. Duangruthai Sri-daeng for the FTIR spectra.

References

- [1] M.M.G. Antonisse, D.N. Reinhoudt, Chem. Commun. (1998) 443.
- [2] P.A. Gale, Coord. Chem. Rev. 199 (2000) 181.
- [3] P.A. Gale, Coord. Chem. Rev. 213 (2001) 79.
- [4] P.D. Beer, P.A. Gale, Angew. Chem. Int. Ed. 40 (2001) 486.
- [5] P.A. Gale, Coord. Chem. Rev. 240 (2003) 191.
- [6] J. Scheerder, M. Fochi, J.F.J. Engbersen, D.N. Reinhoudt, J. Org. Chem. 59 (1994) 7815.
- [7] J. Scheerder, J.F.J. Engbersen, A. Casnati, R. Ungaro, D.N. Reinhoudt, J. Org. Chem. 60 (1995) 6448.

- [8] T. Hayashita, T. Onodera, R. Kato, S. Nishizawa, N. Teramae, *Chem. Commun.* (2000) 755.
- [9] C.A. Hunter, *J. Chem. Soc. Chem. Commun.* (1991) 749.
- [10] K. Kavallieratos, C.M. Bertao, R.H. Crabtree, *J. Org. Chem.* 64 (1999) 1675.
- [11] M.A. Hossain, J.M. Llinares, D. Powell, K. Bowman-James, *Inorg. Chem.* 40 (2001) 2936.
- [12] P.A. Gale, J.L. Sessler, V. Kral, V. Lynch, *J. Am. Chem. Soc.* 118 (1996) 5140.
- [13] L. Bonomo, E. Solari, G. Toraman, R. Scopelliti, M. Latronico, C. Floriani, *Chem. Commun.* (1999) 2413.
- [14] S. Camiolo, P.A. Gale, *Chem. Commun.* (2000) 1129.
- [15] J.L. Sessler, H. Maeda, T. Mizuno, V.M. Lynch, H. Furuta, *Chem. Commun.* (2002) 862.
- [16] B. Dietrich, T.M. Fyles, J.-M. Lehn, L.G. Pease, D.L. Fyles, *J. Chem. Soc. Chem. Commun.* (1978) 934.
- [17] D.M. Kneeland, K. Ariga, V.M. Lynch, C.-Y. Huang, E.V. Anslyn, *J. Am. Chem. Soc.* 115 (1993) 10042.
- [18] P.D. Beer, M.G.B. Drew, D.K. Smith, *J. Organomet. Chem.* 543 (1997) 259.
- [19] M.W. Hosseini, A.J. Blacker, J.-M. Lehn, *J. Am. Chem. Soc.* 112 (1990) 3896.
- [20] B. Hinzen, P. Seiler, F. Diederich, *Helv. Chim. Acta* 79 (1996) 942.
- [21] F.P. Schmidtchen, *Angew. Chem. Int. Ed. Engl.* 16 (1977) 720.
- [22] P.D. Beer, J.W. Wheeler, A. Grieve, C. Moore, T. Wear, *J. Chem. Soc. Chem. Commun.* (1992) 1225.
- [23] H. Boerrigter, L. Grave, J.W.M. Nissink, L.A.J. Christoffels, J.H. van der Maas, W. Verboom, F. de Jong, D.N. Reinhoudt, *J. Org. Chem.* 63 (1998) 4174.
- [24] E. Fan, S.A. Van Arman, S. Kincaid, A.D. Hamilton, *J. Am. Chem. Soc.* 115 (1993) 369.
- [25] K.H. Lee, J. Hong, *Tetrahedron Lett.* 41 (2000) 6083.
- [26] T. Tuntulani, C. Suksai, *Chem. Soc. Rev.* 32 (2003) 192.
- [27] R. Martínez-Máñez, F. Sancenón, *Chem. Rev.* 103 (2003) 4419.
- [28] Y. Kobuke, A. Ohgoshi, *Colloids Surf. A* 169 (2000) 187.
- [29] M. Miguel Clemente-León, F. Marchioni, S. Silvi, A. Credi, *Synthetic Metals* 139 (2003) 773.
- [30] O.J. Jeppesen, J. Perkins, J. Becher, J.F. Stoddart, *Angew. Chem. Int. Ed.* 40 (2001) 1216.
- [31] D.H. Lee, H.Y. Lee, J. Hong, *Org. Lett.* 3 (2001) 5.
- [32] H. Miyaji, J.L. Sessler, *Angew. Chem. Int. Ed.* 40 (2001) 154.
- [33] D.H. Lee, H.Y. Lee, J. Hong, *Chem. Commun.* (2001) 1188.
- [34] D.H. Lee, H.Y. Lee, J. Hong, *Tetrahedron Lett.* 43 (2002) 7273.
- [35] V. Ruangpornvisuti, *J. Mol. Struct. (Theochem)* 686 (2004) 47.
- [36] A.D. Becke, *Phys. Rev. A* 38 (1988) 3098.
- [37] C. Lee, W. Yang, R.G. Parr, *Phys. Rev. B* 37 (1988) 785.
- [38] F. Maseras, K. Morokuma, *J. Comp. Chem.* 16 (1995) 1170.
- [39] S. Humbel, S. Sieber, K. Morokuma, *J. Chem. Phys.* 105 (1996) 1959.
- [40] M.J.S. Dewar, C.H. Reynolds, *J. Comp. Chem.* 2 (1986) 140.
- [41] C. Moller, M.S. Plesset, *Phys. Rev.* 46 (1934) 618.
- [42] V. Barone, M. Cossi, J. Tomasi, *J. Comput. Chem.* 19 (1998) 404.
- [43] M. Cossi, V. Barone, *J. Chem. Phys.* 109 (1998) 6246.
- [44] M.J. Frisch, G.W. Trucks, H.B. Schlegel, G.E. Scuseria, M.A. Robb, J.R. Cheeseman, J.A. Montgomery, Jr., T. Vreven, K.N. Kudin, J.C. Burant, J.M. Millam, S.S. Iyengar, J. Tomasi, V. Barone, B. Mennucci, M. Cossi, G. Scalmani, N. Rega, G.A. Petersson, H. Nakatsuji, M. Hada, M. Ehara, K. Toyota, R. Fukuda, J. Hasegawa, M. Ishida, T. Nakajima, Y. Honda, O. Kitao, H. Nakai, M. Klene, X. Li, J.E. Knox, H.P. Hratchian, J.B. Cross, V. Bakken, C. Adamo, J. Jaramillo, R. Gomperts, R.E. Stratmann, O. Yazyev, A.J. Austin, R. Cammi, C. Pomelli, J.W. Ochterski, P.Y. Ayala, K. Morokuma, G.A. Voth, P. Salvador, J.J. Dannenberg, V.G. Zakrzewski, S. Dapprich, A.D. Daniels, M.C. Strain, O. Farkas, D.K. Malick, A.D. Rabuck, K. Raghavachari, J.B. Foresman, J.V. Ortiz, Q. Cui, A.G. Baboul, S. Clifford, J. Cioslowski, B.B. Stefanov, G. Liu, A. Liashenko, P. Piskorz, I. Komaromi, R.L. Martin, D.J. Fox, T. Keith, M.A. Al-Laham, C.Y. Peng, A. Nanayakkara, M. Challacombe, P.M.W. Gill, B. Johnson, W. Chen, M.W. Wong, C. Gonzalez, and J.A. Pople, *Gaussian 03*, revision B.3; Gaussian, Inc., Wallingford CT, 2004.
- [45] MOLDEN 4.2: G. Schaftenaar, CAOS/CAMM Center Nijmegen, Toernooiveld, Nijmegen, The Netherlands, 1991.
- [46] P. Flükiger, H.P. Lüthi, S. Portmann, J. Weber, *MOLEKEL 4.3: Swiss Center for Scientific Computing*, Manno, Switzerland, 2000.
- [47] J.R. Sabin, S.B. Trickey, S.P. Apell, J. Oddershede, *Int. J. Quantum Chem.* 77 (2000) 358.
- [48] T. Koopmans, *Physica* 1 (1933) 104.
- [49] B. Wann, V. Ruangpornvisuti, *Chem. Phys. Lett.* 415 (2005) 176.
- [50] K. Thipyapong, N. Yasarawan, B. Wann, Y. Arano, V. Ruangpornvisuti, *J. Mol. Struct. (Theochem.)* 755 (2005) 45.
- [51] B. Wann, V. Ruangpornvisuti, *J. Mol. Struct.* 787 (2006) 76.
- [52] F. London, *J. Phys. Radium.* 8 (1937) 3974.
- [53] R. Ditchfield, *Mol. Phys.* 27 (1974) 789.
- [54] K. Wolinski, J.F. Himton, P. Pulay, *J. Am. Chem. Soc.* 112 (1990) 8251.
- [55] M.A. Goldman, M.T. Emerson, *J. Phys. Chem.* 77 (1973) 2295.
- [56] A.P. Scott, L. Radom, *J. Phys. Chem.* 100 (1996) 16502.

VITAE

Mr. Somchai Keawwangchai was born on April 18, 1976 in Nongbualumpoo, Thailand. He received his Bachelor's degree of Science in Chemistry from Maharakham University in 1999. Since 2000, he has been a graduate student at the Department of Chemistry, Chulalongkorn University and become a member of the Supramolecular Chemistry Research Unit under the supervision of Associate Professor Dr. Thawatchai Tuntulani. He had an opportunity to do the research in Dr. Philip A. Gale group at Southampton University in 2005 under the financial support from the Thailand Research fund. He graduated with a Ph.D. Degree in Chemistry in the academic year 2006.

Publications

Keawwangchai, S.; Tuntulani, T.; Ruangpornvisuti, V. "Molecular structures of 3,6-di(hexylthioureido)acridine conformers, their protonation, ^1H NMR and IR analyses: Theoretical and experimental studies" *J. Mol. Struct.* **2007**, 832, 16–25.

สถาบันวิทยบริการ
จุฬาลงกรณ์มหาวิทยาลัย